Assembly of Optically-Active Nanocomponents with DNA

Tao Zhang

München 2017

Assembly of Optically-Active Nanocomponents with DNA

Tao Zhang

Dissertation
an der Fakultät für Physik
der Ludwig–Maximilians–Universität
München

vorgelegt von
Tao Zhang
aus Shandong, China

München, den February 17th 2017

Erstgutachter: Prof. Dr. Tim Liedl
Zweitgutachter: Prof. Dr. Alexander Högele
Tag der mündlichen Prüfung: March 30th 2017

Contents

List of Figures

List of Tables

Zusammenfassung

DNA-basierte Selbstorganisation bietet hohe Genauigkeit und Robustheit für die Anordnung optisch aktiver Nanokomponenten in komplexe photonische Strukturen. Nanokomponenten mit unterschiedlicher Zusammensetzung, Größe und Form können zu wohldefinierten geometrischen Strukturen mit kontrollierten Orientierungen und Abständen zusammengebaut werden. Untersuchungen der Eigenschaften von selbstorganisierten photonischen Nanostrukturen können neue Einsichten in die physikalischen Mechanismen der Licht-Materie-Wechselwirkung liefern oder sogar neue Phänomene offenbaren.

In dieser Arbeit demonstriere ich die Platzierung von optisch-aktiven Nanokomponenten auf DNA-Vorlagen, reichend von individuellen DNA-Strukturen zu komplexeren dreidimensionalen DNA-Matrizen. Nanodiamanten (mit eingeschlossenen Stickstofffehlstellen-Farb-Zentren), kolloidale Quantenpunkte und Goldnanopartikel wurden in verschiedenen Konfigurationen - Homodimere, Heterodimere, Heterotrimere und andere hybride Strukturen - zusammengebaut. Um dies zu erreichen habe ich neue Funktionalisierungsmethoden entwickelt und existierende, effiziente Methoden optimiert, was eine hohe Anbindungsgenauigkeit ergab und gleichzeitig die optischen Eigenschaften der optischen Komponenten erhielt. Um Nanopartikel in regulären Mustern in drei Dimensionen räumlich anzuordnen, wurde eine dreieckige DNA-Origami-Struktur entworfen, die in ein rhomboedrisches Gitter der Größenordnung von 10 Mikrometern polymerisieren kann. Die große Einheitszelle von $1.8 \times 10^5\ nm^3$ erlaubt die Ko-Kristallisation von großen Gastkomponenten. Elektronenmikroskopie und Kleinwinkelröntgenstreuung bestätigten den kristallinen Zusammenbau der DNA-Origami-Strukturen und die erfolgreiche Inkorporation von Goldnanopartikeln verschiedener Größen.

Im Großen und Ganzen bietet der Zusammenbau mit Hilfe von DNA-Vorlagen neue Möglichkeiten um optische Komponenten im Nanobereich zu steuern. Weiter verbesserte Zusammenbauqualität und Komplexität wird uns erlauben Energieübertragungsereignisse die in nanophotonischen Netzwerken auftreten systematisch zu studieren und wird möglicherweise zu Anwendungen in Energie-“Harvesting”-Geräten und aktiven plasmonischen Schaltkreisen führen.

Abstract

DNA-based self-assembly offers high accuracy and robustness to arrange optically active nanocomponents into complex photonic structures. Nanocomponents of different compositions, sizes, and shapes can be assembled into defined geometries with controlled orientations and separations. Investigating the properties of self-assembled photonic nanostructures can provide new insights into the physical mechanisms of the light-matter interactions or even reveal new phenomena.

In this thesis, I demonstrate the placement of optically-active nanocomponents on DNA templates, from individual DNA structures to more complex three dimensional DNA matrices. Nanodiamonds (with enclosed nitrogen-vacancy color centers), colloidal quantum dots, and gold nanoparticles were assembled into different configurations such as homodimers, heterodimers, heterotrimers, and other hybrid structures. To achieve this, I developed new and optimized existing efficient functionalization methods which result in high binding accuracy and at the same time preserve the optical properties of the optical components. To spatially arrange nanoparticles in regular patterns in three dimensions, a triangular DNA origami structure was designed that can polymerize into a rhombohedral lattices of tens of micrometers in size. The large unit cell of 1.8×10^5 nm^3 allows co-crystalization of large guest components. Electron microscopy and small-angle X-ray scattering confirmed the crystalline assembly of DNA origamis and the successful incorporation of gold nanoparticles of various sizes.

Overall, DNA-templated assembly provides new opportunities to operate optical components in the nano-realm. Further improved assembly quality and complexity will allow to systematically study energy transfer events occurring in nanophotonic networks and will potentially lead to applications in energy harvesting devices and active plasmonics circuits.

Chapter 1

Nanomaterial fabrication

1.1 Introduction to nanotechnology

One nanometer (nm) is a unit length that equals to 1×10^{-9} m. One nanometer introduces a length of approximately three gold atoms being arranged together.

Nanotechnology aims for devices miniaturization and new functions exploration using nanoscale materials. It is a research subject containing two subjects: 1) the designing, manufacturing and application of nanomaterials, and 2) the fundamental understanding of the correlation of nanomaterial physical properties and material dimensions.[1]

Such a generalized description of nanotechnology indicates that nanotechnology is a very interdisciplinary area, including - but not limited to - synthesis of semiconductor nanoparticles, surface science, self-assembly, organic chemistry, polymer science, molecular biology, biomacromolecules, as well as optical physics of nanoscale materials.

Nanotechnology is a recently developed research topic. People often attribute the conceptual idea of nanotechnology to the lecture given by physicist Richard Feynman, "There's Plenty of Room at the Bottom", at Caltech on December 29th 1959. In this talk, Richard Feynman said, "I would like to describe a field, in which little has been done, but in which an enormous amount can be done in principle....What I want to talk about is the problem of manipulating and controlling things on a small scale."[2]

However, the time of people using nanomaterials dates back to a long time ago. For example, the Lycurgus cup, a 4th-century Roman glass cage cup (Figure 1.1), shows different color under different illumination. The cup exhibits a reddish color when light is transmitted and greenish color when light is reflected from the glass. Further investigation found that such dichroic effects is caused by gold and silver nanoparticles inside the glass.[3]

Nonetheless, the determination of the term Nanotechnology has helped people to specify the research topics in the field, which facilitates the field development. Another accelerator for the nanotechnology field is the improvement of analysis and measurement technologies. In particular, there is a great advancement for the instrument for nanomaterial characterization, with better and better resolution and accuracy. For example, Scanning Tunneling

Figure 1.1: The Lycurgus Cup in the British Museum frontlit (left) revealing reflected greenish light and backlit (right) showing transmitted reddish light.

Microscope can have a 0.1 nm lateral resolution and 0.01 nm depth resolution. State-of-the-art Transmission Electron Microscope (TEM) can reach atomic resolution, while the resolution of Scanning Electron Microscope (SEM) can easily go down to 5 nm. Equipped with cutting-edge instruments, researchers then can observe, measure, and manipulate the materials on nanoscale and have a better understanding of corresponding effects and mechanisms.

The next questions will be, how to obtain nanomaterials in order to investigate their properties. Such as the size effects in the absorption and emission of photonic nanocrystals, the distance dependent coupling of gold nanoparticles pairs, and the collective effects in a periodic assembly of photonic nanocrystals arrays. To date, mainly there are two approaches, top-down and bottom-up, to prepare nanoscale materials. In the following sections, these two approaches are introduced with several representative examples.

1.2 Top-down approaches

Top-down approach is a widely-used method for nanomaterial fabrication which relies on the division of bulk materials, on the miniaturization of bulk fabrication processes, or using external equipment assisted manipulation to create nanoscale materials or surface patterns. In this section, using examples of ball-milling, atomic manipulation with STM tip, and top-down lithography, a brief introduction of their basic ideas, working process, advantages and disadvantages will be given.

1.2.1 Ball-milling

A representative method of top-down approach is mechanical attrition, for example, ball-milling which uses the high-energy collision from the balls either to crush the bulk solids or induce phase transition to produce nanostructured materials with an average particle size down to several nm.[4] Mechanical attrition based ball milling have been a popular method to prepare nanocrystalline materials because of its simplicity, the relatively inexpensive equipment, and the possibility to scale up the production. However, sample prepared from ball milling can be easily contaminated from the milling media. And it can only be applicable for solid materials, mainly metal materials, metal oxides, and alloys and is impossible to create materials of heterogeneity and complexity.

1.2.2 Scanning tunneling microscope

The invention of STM makes it possible to visualize the world down to its molecules and atoms, and to directly observe the surface roughtness, defects, surface reactions, as well as to manipulate atoms one by one. An extraordinary example is that in 1990, IBM (International Business Machines Corporation) scientists used STM tips to move 35 xenon atoms on nickel surface and spelled out the company logo, IBM.[5] However, for STM, high resolution images often require stable setup and high technical skills, as the vibrations from pumps, machinery, building movements may bring significantly background signal. Sometimes ultra high vacuum and low temperature are also essential. Moreover, the STM does not measure material nuclear position directly but the electron density clouds on the conductive sample surface. The electron clouds can represent the atom locations accurately but not always. As the STM tip can manipulate atoms or molecules one by one, it also means to scale up the surface patterning will be time-consuming.

1.2.3 Lithography

To date, semiconductor lithography is the main process to create integrated circuits for device miniaturization. The lithography process in integrated circuit fabrication can be approximated in three steps. First, deposition of a uniform film of material on the wafer, which includes chemical vapor deposition of insulating films, plasma deposited and sput-

tered deposited films, and evaporated metal films. Second, lithography to create an image of the pattern. And third, etch to transfer the pattern to the wafer.

One particular application of lithography is to create noble metal nanostructures to investigate the phenomenon like coupling or field enhancement of localized surface plasmon resonance (LSPR). LSPR is highly dependent on the size, shape, and dielectric properties of the metamaterials and the surrounding environment. Using lithography, the ability to prepare different metamaterial assembly allows to exploit the theoretical predictions and experimental realizations on plasmon-enhanced single molecular sensing, plasmon-exciton interaction, Fano resonance, and plasmonic lens.[6][7][8][9]

In short, modern lithography provides a fast, low-cost approach for micro- and nanoscale surface patterning. However, diffraction-limited resolution is a big barrier for smaller nanostructures fabrication. In addition, lithography has a better control at planar nanostructures but it remains challenging for three dimensional heterostructure manufacturing. Also, lithography technique requires expensive setup, clean room, vacuum condition, and critical working process. To study size- and distance- dependent effect within a range of one to ten nanometer, it is difficult to achieve if using top-down lithography.

1.2.4 Challenges

In this section, three examples are given to briefly show how top-down methods are used for nanomaterials fabrication. In general, top-down methods requires proper setup to complete the fabrication. The engineering process in general are complicated, expensive, and time-consuming. However, despite of many disadvantages, top-down methods represent frontier techniques and common used fabrication methods in industry.

It is believed that top-down method equipped with cutting-edge setup will keep increasing their accuracy and resolution in industrial production and applications. For the particular goal of this thesis to arrange nanocomponents to investigate light-mater interaction and energy transfer events, top-down methods has their limitation to build corresponding photonic nanostructures and networks of nanodiamonds, quantum dots and gold nanoparticles. An ideal method we aimed for should be simple, without external manipulation, inexpensive, and accurate at single molecular level.

1.3 Bottom-up approaches

In comparison to top-down, bottom-up methods serve as an alternative for nanomaterials production starting from single atoms or molecules. Bottom-up methods have molecular-level control of material compositions and structures thus hold possibilities to engineer material functions at the molecular level. Materials construction process in bottom-up manner is completed in a spontaneous reaction of atoms or molecules which allows to produce finely tuned nanomaterials. Though sometimes external temperature control is essential, bottom up methods usually do not require complicated setups. However, it does require deep understanding of the individual molecular structures, stability, dynamic behaviors, interactions (covalent or non-covalent), bonding strength, and molecular responses to environmental stimuli.

This section uses three examples to introduce bottom-up methods: colloidal nanoparticles synthesis, nanoparticles (for example gold nanoparticles) self-assembly, and DNA nanotechnology. Similar to the top-down approaches section, the basic ideas, working process, advantages and disadvantages will be given. Because in this thesis DNA-based self assembly are the main technique that used for templated assembly of nanoparticles, DNA nanotechnology is listed as an independent section and some details of DNA-based assembly will be introduced.

1.3.1 Colloidal gold nanoparticles

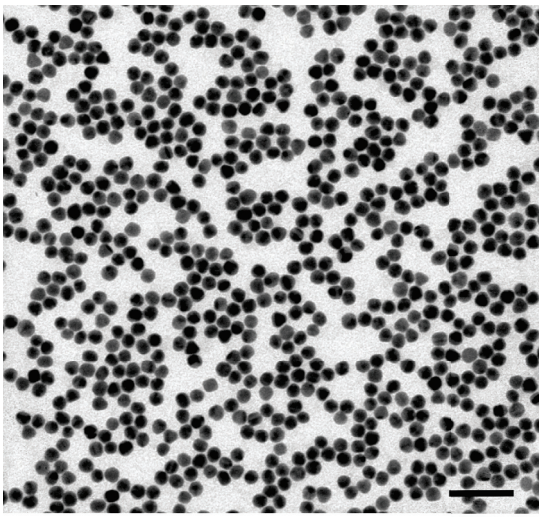

Figure 1.2: TEM images of lab synthesized spherical gold nanoparticles[10] with average diameter 11.4 nm (STD: 1.3 nm). Figure repoduced from bachelor thesis of T. Fetter from T. Liedl's group. Scale bar is 50 nm.

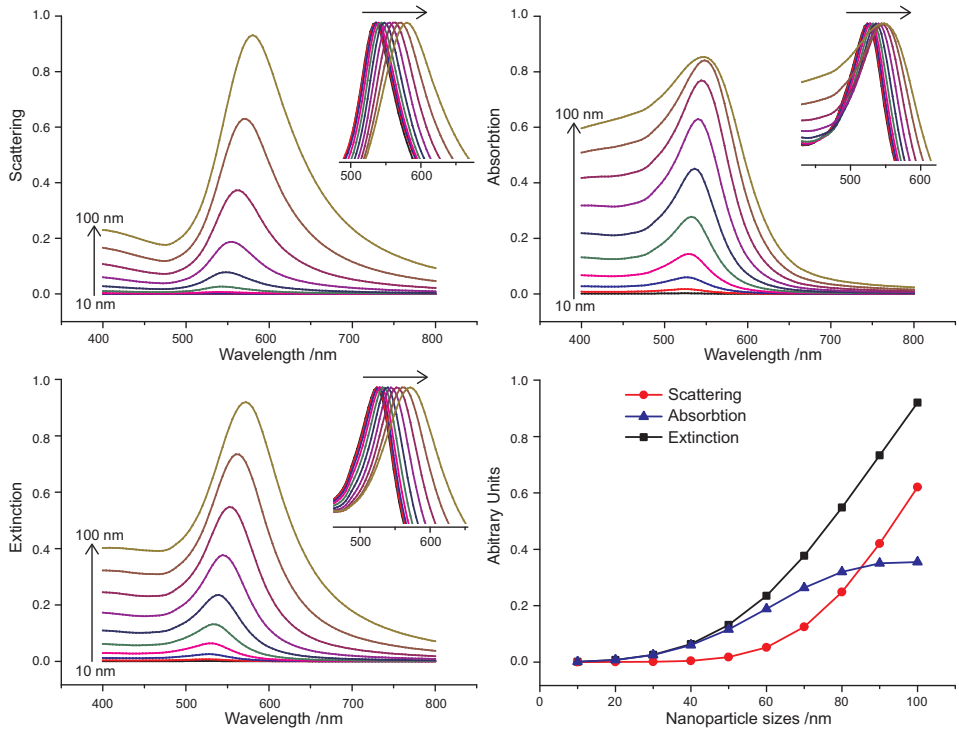

Figure 1.3: The theoretical prediction of scattering, absorption and extinction intensities of different sizes of gold spherical nanoparticles. Data were generated from online (visited date: 1st, Feb. 2017) tool at `http://nanocomposix.eu`

So far chemical synthesis of different sizes of gold nanoparticles are very well-established. Protocols of gold nanoparticles synthesis can be easily found, such as citrate based two solution methods for 10-15 nm gold nanoparticles (Figure 1.2) synthesis[11][10], seed mediated nanorods synthesis in the surfactant cetyltrimethylammonium bromide (CTAB) solution[12][13]. Using the method of the citrate stabilized spherical gold nanoparticles, it can produce about $150\,\mathrm{mL} \times 10\,\mathrm{nmol\,L^{-1}}$ colloidal nanoparticles solution in one-shot synthesis. In contrast, top down methods like ball-milling or lithography are not able to achieve this scale with mass production. In addition, different sizes of spherical gold nanoparticles (from 5 to 100 nm) and aspect ratios of gold nanorods are commercially available from Sigma-Aldrich and Nanoseedz. In fact, wet chemistry methods are now also able to synthesize other typed nanoparticles with good quality like triangular gold nanoplates[14], silver nanocubes[15], and spherical or rod-shaped quantum dots[16][17][18].

Due to the facile synthesis and modification and the tunable optical properties, gold nanoparticles are the most accessible nanomaterials for chemical, optical, biological, and self-assembly studies. Figure 1.3 shows a theoretical prediction of scattering and absorption values of different sizes of spherical gold nanoparticles. Such plasmonic properties is due to the interaction of incident light with surface electrons of the gold nanoparticles, a dual effect of light absorption and scattering on nanoparticles. According to Mie theory[19][20][21],

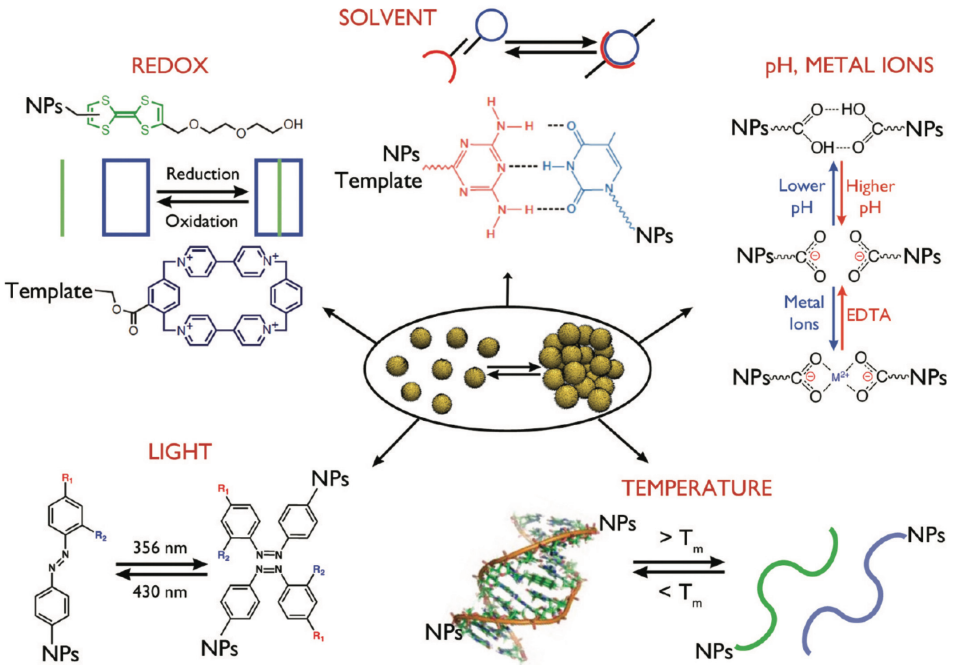

Figure 1.4: Nanoparticles assembly with different ligands interaction and stimuli. Reprinted with permission from American Chemical Society.[33]

both absorption and scattering values will increase when sizes become larger. For particles less than 40 nm, absorption is the main contribution to extinction. When sizes get larger, scattering begins to show up. When sizes are larger than 80 nm, the extinction value is dominated mainly by scattering. Other shaped gold nanoparticles, like rod- or triangle-shaped, have similar phenomenon but become complicated as it has several size parameters.

For spherical gold nanoparticles, their surface plasmon oscillation generates an enhanced local field in a small volume. In a particular case, when two spherical gold nanoparticles are placed in close proximity, it creates a significantly enhanced field between two particles, in terms of "hotspot". This nanoparticles size and distance dependent[22] effect or phenomenon results in series of theoretical and experimental studies[23] like photothermal effect[24], sensing[25], plasmon exciton interactions[26][27][28], enhancement or quenching effect to fluorescent molecule placed in hotspot[29], and plasmonic chirality[30][31][32]. More detailed description can be found in section 2.3.

1.3.2 Nanoparticles self-assembly

Spontaneous organization of individual components into ordered structures defines an ubiquitous nanotechnology technique of self-assembly. Several factors influence the self-assembly process. First, one or different kinds of components exist in the self-assembling system. The components have the potential to interact with each other through a balance of attractive and repulsive forces. To generate ordered structures, the interactions must

be weak enough for reversible binding and strong enough to against the disruption forces which prevent the assembly. In addition, the self-assembly environment, in solution or at the interface, should allow required motion of the components to self-adjust the orientation and complete the self-assembly process.[34]

When using nanoparticles as components, the nanoparticle-nanoparticle interactions are defined by the surface ligands.[35][36] First of all, during wet chemistry synthesis of colloidal nanoparticles, ligands molecules are essential reactants. As when particle dimensions reduce to nanoscale, small-size effects associated with nanoparticles become more pronounced and particles begin to have an increased surface energy, which render surface atoms reactive and unstable. The important functions of ligands are to reduce the surface energy by introducing steric or electrostatic repulsion effect to prevent aggregation. More importantly, if the introduced surface ligands have desired binding interactions, nanoparticles then can be organized in certain assemblies, in a spontaneous way.[33][37]

Nanoparticles self-assembly enables the transition from amorphous aggregates to a periodic organized geometries. The periodic arranged nanoparticles then can exhibit distinct collective effects, which is different from single nanoparticles and amorphous aggregates. Figure 1.4 shows nanoparticles self-assembly based on different interactions *via* different ligands. In principle, any kinds of interactive molecular pairs can be employed to mediate nanoparticles assembly, as long as the molecular pairs can be functionalized to nanoparticles in order to transfer the interaction between molecules to nanoparticles. Interactions (Figure 1.4) that can be adopted include, but not limited to, host-guest recognition, hydrogen bonds, charge-charge attraction, coordinate bonds (by forming chelation using metal ions and chelating molecules), dipole-dipole interaction, or complementary DNA strands hybridization.

The key feature of these interactions is that they are all non-covalent weak bonds. Nanoparticles functionalized with these molecular pairs can proceed the self-assembly under thermodynamic equilibrium conditions. As mentioned above, the constant binding and unbinding of free species to precursor allows new components to self-adjust their orientations and positions. Effective collision happens only when new components bind through a certain number of cooperative non-covalent interactions. Eventually, the system free energy is minimized and the self-assembly event is completed (Figure 1.5).[38][39][40][41]

To introduce directional interactions to surface isotropic nanoparticles, one kind of ligands that attracted much attention is DNA.[25][42] The simple rule of complementary DNA strands hybridize, tunable hybridizing strength *via* temperature, strands length and sequence allows to introduce highly specific, orthogonal interactions design. The thiol-gold bond has high bond energy and the chemistry of thiol residue labeled DNA oligos is very-well developed and commercially available. DNA capped gold nanoparticles then serve as basic building blocks that can crystallize into highly-ordered macroscopic assemblies.

Typically, spherical gold nanoparticles are fully covered with DNA oligonucleotides *via* the covalent thiol-gold bonds. Different bases of DNA spacers can be introduced to vary the linkers length between the functional thiol group and the recognition sequences. The sequence dependent hybridization of the DNA oligonucleotides at the recognition sections then leads to the formation of densely-packed, 3D gold nanoparticle crystals. Using

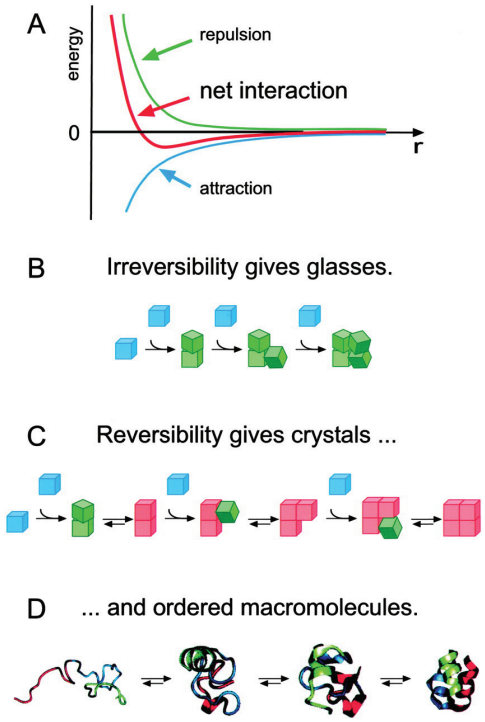

Figure 1.5: Weak interaction permits reversible association to self-adjust components positions. A, successful self-assembly requires a balance between attraction and repulsion. B&C, schematic illustration of the essential differences between irreversible aggregation and ordered self-assembly. D, ordered macromolecules assembly represents one complicated self-assembly process in biological system. Copyright (2002) National Academy of Sciences.[38]

this method, mainly Gang group and Mirkin group have developed different nanoparticle lattices with control over the particle-to-particle spacing and the lattice geometry.[43][44]

Usually, synchrotron-based small-angle X-ray scattering (SAXS) is used to monitor the *in situ* phase behavior of the nanoparticles crystalline assembly (Figure 1.6). SAXS specifies on the small angles of 0.1 to 10° (2θ). According to Bragg's law (Equation 1.1), given an incident X-ray beam with certain wavelength of λ, lower angles allow to determine larger d values.

$$2d \sin\theta = n\lambda \tag{1.1}$$

In the nanoparticles crystal system, nanoparticles act as programmable atom equivalents. The directional bonding interactions between nanoparticles are realized with DNA base-pairing. The periodic arranged nanoparticles can have well defined small-angle peaks analogous to the diffraction peaks observed at wide angles for atomic crystals. The reconstruction from the diffraction pattern to three dimensional model can determine the positions and geometries of spatially arranged nanoparticles. In addition, SAXS technique

allows to analyze real time spacings in the nanoparticles assemblies *in situ* and is also possible to characterize the reaction kinetics based time-resolved crystallography.[45][46]

The power of DNA-nanoparticles crystallization is that the parameters of building blocks and the interactions among the building blocks are fully tunable (Figure 1.7). The building blocks of nanoparticles can have different sizes, shapes, and compositions. So far, gold nanoparticles of various sizes, quantum dots, magnetic nanoparticles, proteins, and hollow spherical nucleic acids spacers have been used as building blocks in lattice self-assembly. DNA molecules that are attached to nanoparticles surface can have different length and binding energies. The fine tuning of these parameters allow for more control over the types of crystal lattice.[47][48][49][50][51]

Recently, Gang group reported lattices engineering through the nanoparticle-DNA origami interactions, using DNA origami structures as spacers and nanoparticles as joints.[52][53][54][55] Gold nanoparticles with corresponding shaped DNA origami structures were mixed and slowly cooled down from 50 °C to room temperature. Here, the lattice geometries were mainly determined by the shape of the DNA origami structures. As shown in Figure 1.8, gold nanoparticle face-centred-cubic (FCC), body-centred-tetragonal (BCT), simple cubic, and hexagonal lattices are generated by using origami structures of octahedra, elongated square bipyramid, cubes, and prisms respectively.

One feature of surface ligands mediated assembly is that the building blocks are densely packed *via* the ligand-ligand interactions. The connectivity inside the lattices is provided by the building blocks and the surface ligands. Lattice engineering with several kinds of nanocomponents have to be realized with different surface ligands design. Nevertheless, such precisely engineered nanoparticles superlattices can possess unique optical properties due to the collective effects of nanoparticles assembly.[56]

Besides DNA, diblock copolymer-mediated nanoparticles assembly can be another suitable substitution.[57] DNA-based assembly are carried out in aqueous solution, however, polymer-mediated assembly can be in almost any kind of solvent from polar to non-polar. The bonding interactions listed above like electrostatic, π-effects, van der Waals forces, and hydrophobic effects can be all applied. Although polymer-mediated assembly has less programmability than DNA, the polymer price is cheaper. Using plasmonic components and playing with solvent polarity can imitate the assembly of amphiphilic copolymers[58][59] which can have further development and applications.

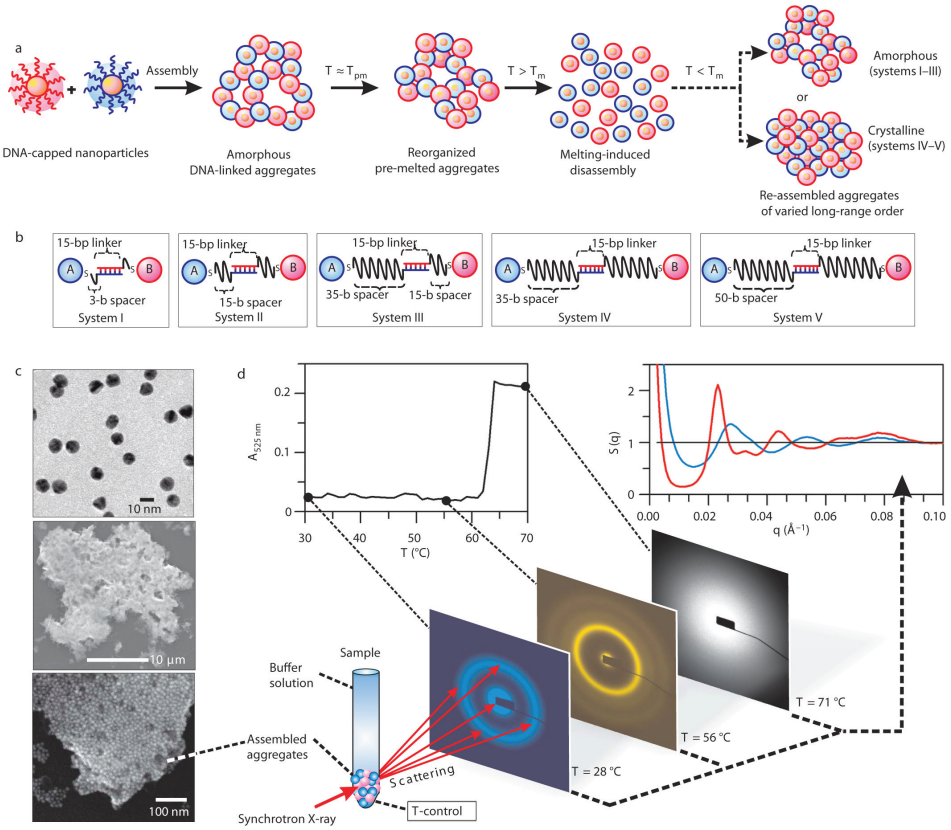

Figure 1.6: Schematic illustration of the gold nanoparticles lattices preparation and the SAXS measurement. a, the assembly of DNA modified gold nanoparticles under a variety of thermal conditions. b, detailed design of DNA linkages between nanoparticles. c, representative electron microscopy images of nanoparticles and nanoparticles assemblies. d, typical experimental measurement of the correlation between the melting profile of the aggregates and the internal structures as probed by *in situ* SAXS measurement. Reprinted with permission from Nature Publishing Group.[43]

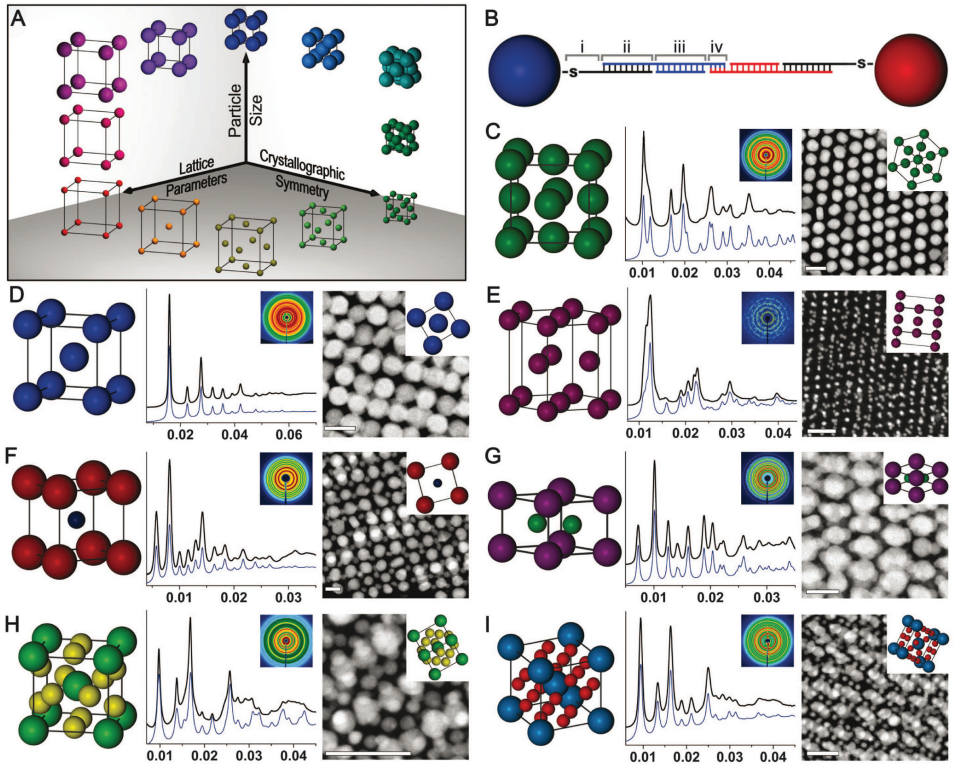

Figure 1.7: Nanoparticle superlattice engineered with DNA. A, DNA mediated nanoparticle superlattice with independent control of design parameters: particle size, lattice paramters, and crystallographic symmetry. B, DNA linkage details. C-I, nanoparticle lattice of different geometries: fcc (C), bcc (D), hcp (E), CsCl (F), AlB_2 (G), Cr_3Si (H), and Cs_6C_{60} (I). Reprinted with permission from the American Association for the Advancement of Science.[47]

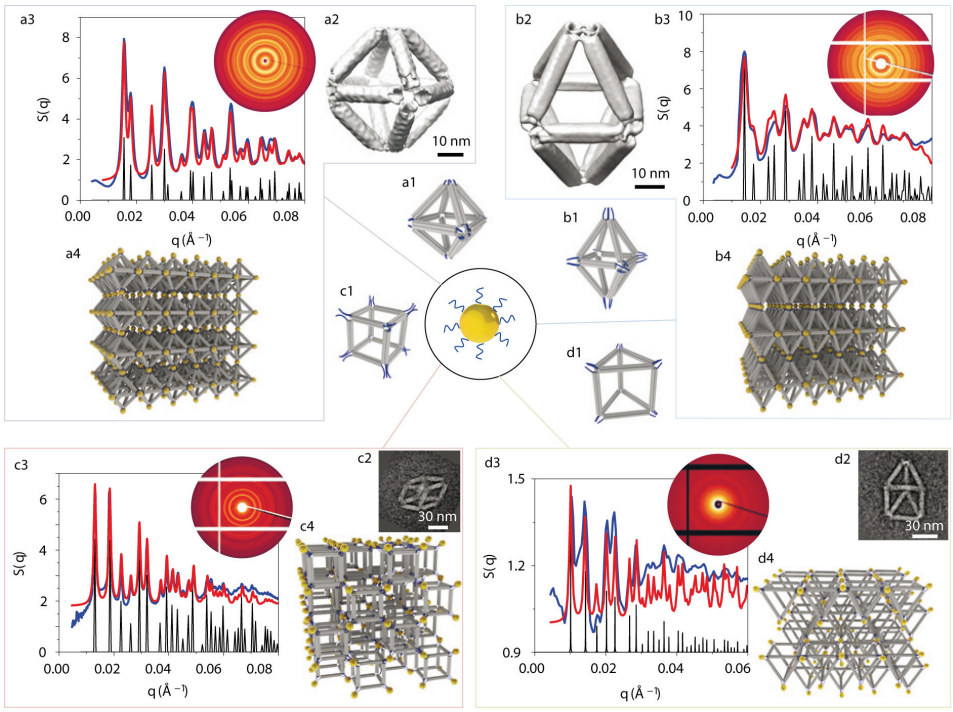

Figure 1.8: DNA origami mediated nanoparticle lattices. a-d, DNA functionalized 10 nm gold nanoparticles bind different types of DNA origamis at their respective vertices *via* strands hybridization. For each lattice structure, X-ray scattering structure factor, extracted from the 2D SAXS pattern and the proposed superlattice structures were given. The experimental scattering profile is in blue and the model fitting is in red. The black peaks mark the standard peak positions of the proposed lattice: face-centred-cubic (FCC) by the octahedra (a3), body-centred-tetragonal (BCT) by elongated square bipyramid (b3), simple cubic by the cubes (c3) and hexagonal by the prisms (d3). Reprinted with permission from Nature Publishing Group.[55]

1.3.3 DNA nanotechnology

In this section, a brief information of DNA double helix (duplex) will be given, followed by an introduction to DNA nanotechnology, mainly on structural DNA nanotechnology and their applications for templated assembly.

The double helix

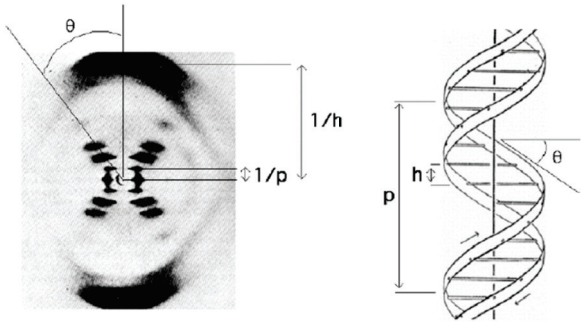

Figure 1.9: X-ray diffraction photograph of a DNA fiber at high humidity and the Watson-Crick model of B-DNA.[60]

A key element in the race towards the structure of DNA was the availability of the X-ray diffraction photography of DNA fibres.[61] Figure 1.9 shows the photograph 51 of B-form DNA and the Watson-Crick model of DNA double helix. The photograph 51 of the X-ray diffraction pattern contains most of the double helix makeup of natural DNA.[62][63][64]

In detail, the natural DNA is a double helical (duplex) structure (showing the **X** shape in the diffraction pattern) formed by two hybridized complementary single strands. The two strands in duplex are antiparallel, which means two strands run in opposite direction. The base at the 5' end of one strand is paired with the base at the 3' end of the other. In the most common B-form DNA, the duplex has a radius of 10 Å and a pitch of 34 Å containing 10.5 bases per helical turn. The stability forces are from both hydrogen bonds of base-pairs (A to T, G to C) across the axis and the base-pairs stacking interactions along the axis. As GC base-pair has three hydrogen bonds and AT has two, under same conditions, DNA duplex with higher GC content have a higher melting temperature (T_m) to dissociate two strands. In addition, higher salt concentrations (sodium or magnesium) tend to stabilize the duplex and increase the T_m values. For other conformations of DNA duplex of A-form and Z-form, the parameters can be found in *Ref.* [65].

DNA in a material world

The application of DNA in a material world is based on the specific interaction of DNA base complementarity. Originally it is Ned Seeman who pioneered this field. Back to 1980s, Ned Seeman found it is difficult to crystalize some proteins for structural analysis.

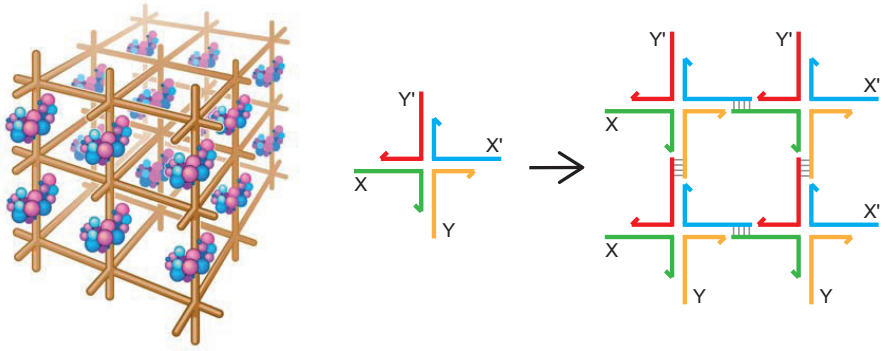

Figure 1.10: Left, an array of six-arm junctions connected together to form a three-dimensional framework for guest molecules co-crystalization. Figure adapted from [66]. Right, self-assembly of branched DNA molecules into a two-dimensional framework.

He was inspired by a woodcut *Depth* to orient the guest proteins on a pre-assembled periodic scaffold(Figure 1.10). At that time, Ned Seeman thought to use DNA to build the framework.[66][67] As mentioned above, many features of DNA indicate that DNA is indeed a suitable self-assembling material. For example, the specific interaction based on the simple rule of complementary strands hybridizaition, the robust chemical modification at bases, 5' or 3' end, and phosphate backbones allowing to introduce functional residues to render DNA to be conjugatable to other materials thus expand the research scope of DNA-based assembly.[68]

The early efforts from Ned Seeman's lab include the branched DNA motifs which are floppy but in principle can polymerize to different directions[67][69][70], two double-crossover motifs which aims to improve the bundle rigidity[71], and so on. In 1991, Ned Seeman reported conceptually the first three dimensional DNA cube structure.[72] The later development of using unusual DNA motifs to build defined shapes and arrangements determines a new research field in terms of *Structural DNA Nanotechnology*.[73][74][75][76]

In last three decades, DNA-based self-assembly has proven to be the most powerful approach to assemble single DNA molecules to intricate objects.[77][78][79][80][81][82] The assembling techniques for *Structural DNA Nanotechnology* mainly include DNA-tile, single-stranded DNA bricks, and DNA origami (Figure 1.11). DNA-tile represents the earlier efforts in DNA nanotechnology. In detail, it preassembles several short DNA oligonucleotides into DNA-tile structures with defined shape. The tile-tile interactions lead to a further assembly of DNA-tiles to large structures. Very similar to the idea of DNA-tile based assembly, single-stranded DNA bricks assemble complex structures directly from each single stranded DNA strands. Instead of using only short stranded DNA oligonucleotides, DNA origami is a molecular self-assembly technique in which a long single strand scaffold DNA of thousands bases long (7k-8k bases), folds upon itself to a designed 2D or 3D nanoscale structure in the range of several ten to several hundred nanometers. This is accomplished by introducing interactions between different segments of the scaffold with the help of hundreds of short oligonucleotides. From the design perspective, one notable feature of

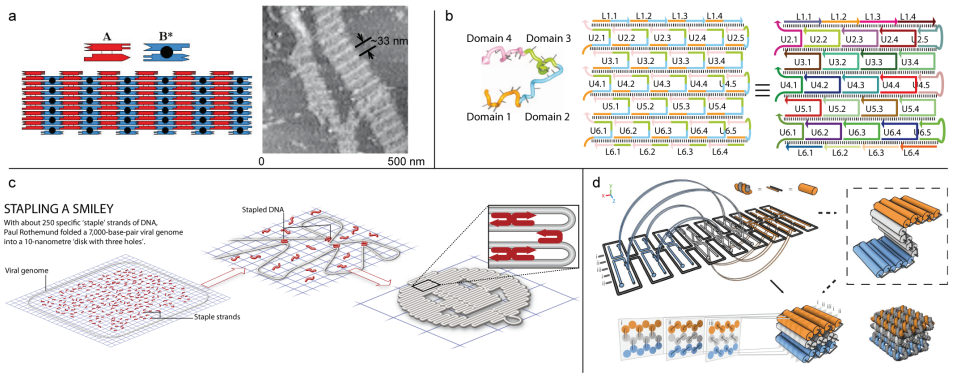

Figure 1.11: An overview of three kinds of DNA assembling technique. a, DNA tile based assembly. Several DNA strands are firstly assembled into DNA tiles with designed shapes. The pre-assembled DNA tiles serve as basic building blocks for further assembly.[77] b, Single-stranded DNA bricks. Here, each single-stranded DNA serve as one assembling unit and assemble into complex two- or three dimensional DNA nanostructures.[82] c&d, DNA origami. DNA origami assembly using several hundreds of short staple oligonucleotides to introduce binding interactions between different segments of a virus-based 7K-8K bases long scaffolded DNA. The introduced interactions fold the scaffolded DNA to defined two- or three dimensional structures.[79][83][80] Reprinted with permission from Nature Publishing Group.

single-stranded DNA bricks assembly is that it usually has one crossover instead of double crossover to connect the neighbouring helix. As DNA origami is the main structure used in this thesis, a detailed description will be given in the following section.

DNA origami

As the epitome of structural DNA nanotechnology, scaffolded-DNA origami has a fine explanation for specific interaction of complementary DNA strands, as well as the co-operative, programmable and the site-specific assembly.[79][80][84] The first example of this technique was shown in 2004 when William Shih *et al.* folded a 1669-bases long, single-stranded DNA, accompanied by five 40-mer oligonucleotides, into a 20 nm diameter octahedron structure.[85] In 2006, Paul Rothemund developed a versatile and simple "one-pot"method for creating 2D nanoscale shapes, which is now known as scaffolded DNA origami, by directly folding of a bacteriophage 7249-bases long single strand DNA with help of over 200 short synthetic single strands of DNA to hold the scaffold in place.[79] The generality of this method was further demonstrated by assembling different shapes such as squares, triangles, five-pointed stars and smiley faces. William Shih's lab extended this method to engineer 3D multi-layer DNA solid structures with precisely specified shapes and greater complexity.[80] The latest report of reconfigurable DNA devices and assemblies is a new binding design by shape-complementary as an alternative to base pairing.[86]

There are several advantages to choose DNA origami based nanostructures. First,

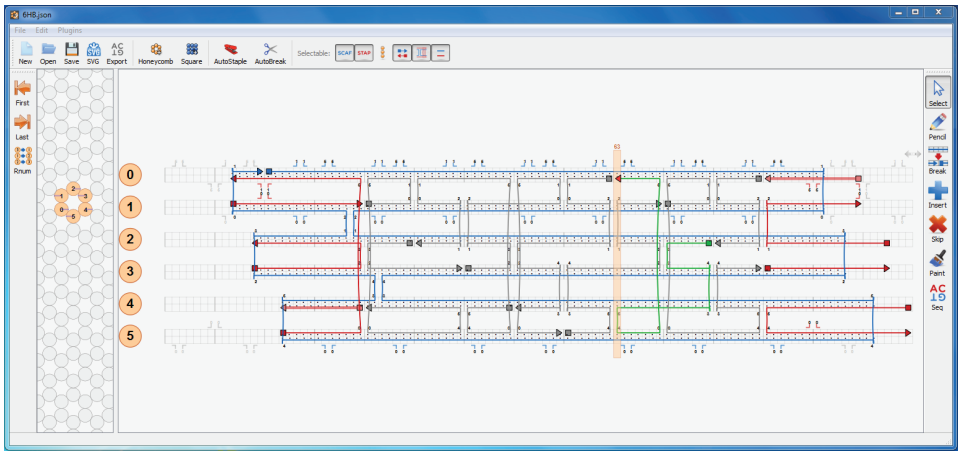

Figure 1.12: A screenshot of six helices bundle design on caDNAno. Left window shows the cross section of the six helices bunldes. Right window shows the two dimensional layout of the scaffold and staple strands. The sequences and positions of each staple strands are pre-defined by the design.[89]

design principle and folding pathways of scaffolded-DNA origami has been well-understood. Most likely, it is the cooperative assembly or synergistic effect of hundred short staple oligos that forces the 7k-8k virus-based single stranded DNA scaffold to predetermined monomeric DNA nanostructures. The sequence and position of each staple strands are specifically defined for guest components addressable assembly. Second, scaffold-guided assembly with densely packed helix create solid DNA structure with great rigidity.[87][88] Third, up to date, researchers have developed computer-aided design software caDNAno[89] and online tool CanDo for design feedback[90], as well as an optimized set of work flow, folding programs[91], purification protocols[92], and characterization methods for monomeric DNA origami structures design and folding. Fourth, DNA origami polymerization towards bigger structures has the potential to manufacture macroscopic functional devices while keeping the precision from individual structures.[93][94] In addition, the modular assembly of DNA origami polymerization enables designable interaction style and strength among single objects. For example, previous reports have shown DNA origami polymerization on two-dimensional level using sticky ends base-pairing or stacking interactions.[93][86]

The DNA origami structure design process can be carried out on the software caDNAno (Figure 1.12).[89] Here, honeycomb lattice will be used as an example to introduce a general workflow on caDNAno.

First, the target shape (here for example the six helices bundle) is approximated by selecting only the scaffold path. If only aiming for monomeric structure without further interests for origami polymerization, the “end”shape can be designed as shape non-complementable. Second, the scaffold has to be interconnected as one circular strand as currently most of scaffold strands are circular single stranded DNA. To check if the applied scaffold is circular, one can add the scaffold sequence to check if the sequence can

be applied to all segments of scaffold, and if the scaffold is long enough for the whole structure. Third, staples need to be broken manually into short staple strands with 18 to 50 bases. The staple strands can be generated accordingly on caDNAno. One suggested rule for staple strands cutting is that, if it has two crossovers, the length of each segment are better to be designed in a way of short-*crossover*-long-*crossover*-short(SLS), but not long-*crossover*-short-*crossover*-long(LSL). This is based on one hypothesis that during the annealing (often it is a ramp program), longer segments will bind first. If LSL style is used, the shorter middle segment might not hybridize properly to the scaffold.[95] In addition, one can try to use less crossovers for each staple, especially in the three dimensional origami design. Staple strands at different sections of the structure can be highlighted in different colors, which would help to sort them to different groups. Fifth, leaving scaffold loop empty (free of staple strands) or extending the sticky ends of the staples strands at both ends can sufficiently avoid blunt ends stacking induced aggregation. Finally, scaffold sequence can be added again to export the excel file which contains the information of staple strands such as sequence, length, oligo position.

Templated assemby

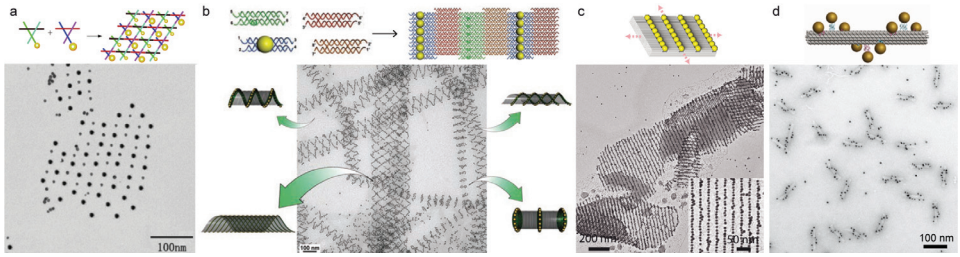

Figure 1.13: Templated assembly of gold nanoparticles on DNA nanostructures. a, DNA tile based templated assembly for 5 nm and 10 nm gold nanoparticles.[96] b, tubular assembly of gold nanoparticles on DNA tiles. The steric repulsion force among the nanoparticles drive the DNA templates forming tubular structures with different curvatures.[97] c, gold nanoparticles row assembly on DNA bricks templates.[98] d, left-handed gold nanoparticles chiral assemblies on 24 helices bundles.[32] Reprinted with permission from American Chemical Society, the American Association for the Advancement of Science, and Nature Publishing Group.

The realization of programmable DNA self-assembly permits the folding of designed DNA nanostructures. In addition, DNA oligonuleotides that modified with different chemical groups enable the DNA nanostructures to be functionalized with other chemical residues. These chemical residues can work as specific docking sites to attach functional groups for various applications. So far, the functionalized DNA structures have been used in super-resolution imaging[101], synthetic biological nanodevices[102][103][104], single molecular biophysical studies[105], or as cargo carriers for biological and nanomedical applications[106].

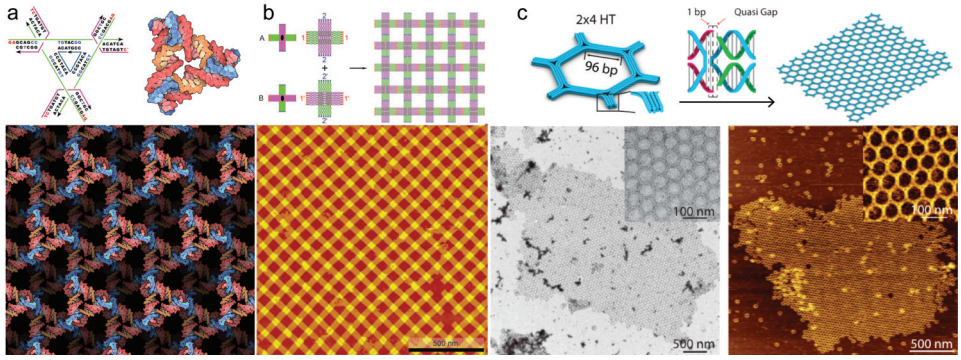

Figure 1.14: DNA motifs polymerization. a, DNA duplex based triangular motifs crystallize to a rhombohedral lattice purely made of DNA.[99] Figure adapted from the 3D rendering of DNA crystal (PDB entry 3gbi) at `https://pdb101.rcsb.org/motm/119`. b, cross-shaped DNA origami motifs polymerize to two dimensional lattices.[93] c, hexagonal DNA origami motifs polymerize to two dimensional hexagonal pattern.[100] Reprinted with permission from Nature Publishing Group, John Wiley and Sons, and American Chemical Society.

The templated-assembly for metallic nanoparticles is one important research topic in DNA nanotechnology.[32][96][97][98][107] Different from packing nanoparticles into three dimensional lattices, the site-specific positioning of nanoparticles on pre-assembled DNA nanostructures have different features. First, it is DNA template that provides the structural rigidity and connectivity. Nanoparticles are placed at selected positions on the DNA structures. Direct nanoparticle-nanoparticle interactions are not necessary. Second, the size of nanoparticles assemblies relies on size of the DNA templates. Also, the structural quality and morphology of the templates are crucial to determine the nature of nanoparticles assemblies. Third, the assembly of guest nanoparticles on DNA templates may bring new driving forces to assemble the DNA templates to new kinds shapes. As shown in Figure 1.13 b, the steric repulsion effects of the self-assembled gold nanoparticles force the DNA tile based structures forming tubular assemblies. Figure 1.13 a&c give other examples of templated-assembly of gold nanoparticles with different configurations. In addition to the various assembly, Figure 1.13 d also gives a particular example of left-handed assembly of gold nanoparticles on 24 helices bundle structures. Such chiral arranged gold nanoparticles exhibit plasmonic chiral response at the visible range.[32]

On one hand, template-assembly gives more freedom to nanoparticles assembly. Several kinds of nanoparticles can be spontaneously placed on the same DNA structures. On the other hand, large scale arrangement of guest nanocomponents requires large DNA templates of high quality. To date, DNA self-assembly allows 1) the rational design of perfectly defined monomeric DNA nanostructures and 2) the precise tuning of monomer-monomer interaction strenghs.[86][108][109] Polymerized individual DNA motifs in principle can create large templates for the accommodation of guest components with high accuracy.

Figure 1.14 gives three examples of polymerized DNA motifs. Figure 1.14 a shows the

three dimensional polymerization of duplex based triangular motif, while Figure 1.14 b&c show two kinds of DNA origami design that can polymerize to micrometer-sized two dimensional patterns. Here, the duplex DNA motif can polymerize into three dimensional crystal but its limited cavity size prevents the templated assembly of guest nanocomponents. For DNA origamis, they has enough space to accommodate nanoparticls but can grow to only two-dimensional lattice. To achieve three dimensional arrangement of nanoparticles, the individual DNA motifs should offer enough space and can polymerize to three dimensions. Aim for this, two different origami designs are demonstrated in chapter 3.

1.3.4 Challenges

Bottom-up approaches create nanomaterials from even smaller building blocks, as shown here the colloidal nanoparticles synthesized from the precursors of corresponding metal ion, colloidal nanoparticles assembly from the building blocks of single nanoparticles, and DNA nanostructures built from individual DNA oligonucleotides. Potentially bottom-up approaches are able to produce large amount of uniform nanomaterials in parallel and can be cheaper than top-down approaches.

However, it is still difficult to synthesize nanoparticles with outstanding quality control. For gold nanoparticles, although synthesis protocol of 10 to 15 nm spherical gold nanoparticles are very standard, gold nanoparticles of other sizes, gold nanorods with perfect shape control are challenging. For other kinds of optically-active nanoparticles like quantum dots, the optical properties are very sensitive to surface defects, material types, and precursor purities. The method to arrange nanoparticle *via* self-assembly requires ligands modification. Low bond energy of ligands to nanoparticle, or low surface coverage of ligands on nanoparticle surface lead to low assembly yield or even nanoparticles cluster. To solve these problems, nanoparticles surface chemistry and ligands chemistry are needed to be systemically studied. In addition, ligands exchange induced surface defects may also change the nanoparticles optical properties.[110] A better understanding of structure-property correlation and ligands design can benefit the nanoparticles assembly.

DNA nanostructures templated-assembly has been proven to be an accurate and controllable assembling method. However, in order to position nanocomponents on DNA nanostructures, they have to be modified with complementary DNA oligos (which can hybridize to docking oligos on DNA nanostructures) or other dual-linkers to place them at target positions. At the same time, these nanoobjects should also survive in the ionic solution (like 11 mM Mg^{2+}) which is required to stabilize DNA nanostructures. In chapter 2, more technical details will be described using the example of nanodiamonds, quantum dots, and gold nanoparticles.

1.4 Top-down meets bottom-up

If bottom-up methods can be combined wth top-down ones, it can integrate the advantages of both methods. Therefore the fabrication could have molecular level accuracy and macroscopic control. One recent example comes from Paul Rothemund group. They positioned discrete numbers of origami nanostructure carrying defined numbers of subcomponents (here Cy5) at the lithographically patterned binding sites. Top-down lithography can prepare micrometer sized microcavities arrays. Bottom-up origami technique can position fluorescent molecules at molecular resolution. The power of this method was demonstrated by reprinting Van Gogh's The Starry Night which was approximated with 65,536 cavities each having from zero to seven binding sites.[111]

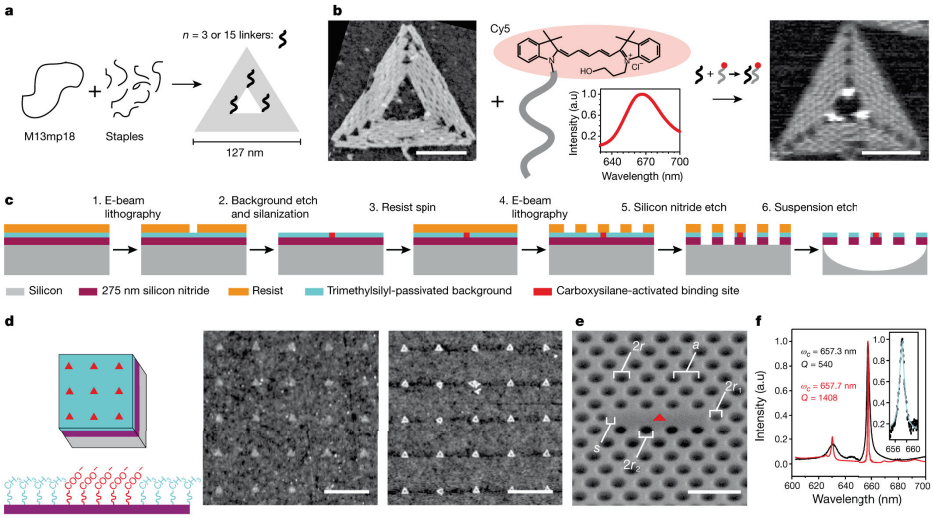

Figure 1.15: DNA origami, binding sites for placement, and photonic crystal cavities (PCC). a&b, triangular DNA origami folding with precisely positioned subcomponents (Cy5). c, fabrication of a single binding site (red), within a passivation layer (blue), followed by construction of a photonic crystal cavity (PCC) around it. d, diagram shows test substrate for placement fidelity (without PCCs), and the groups which mediate binding (carboxylate), and non-binding (methyl). AFM images show binding sites before (left) and after (right) placement. e, SEM of a PCC; a = 256 nm, r/a = 0.3, r1/a = 0.2, r2/a = 0.25, s = 0.22a. f, Low resolution PCC reflectance spectra (black) is compared to FDTD prediction (red). Scale bars: b, 50 nm; d, 400 nm; e, 500 nm. Reprinted by permission from Nature Publishing Group.[111]

Another example is from Peng Yin group. They used metallized DNA nanostructures (more details in subsection 1.3.3) as lithographic masks to pattern two-dimensional nanomaterials.[112] Self-assembled DNA nanostructures serve as mask templates with defined shape, size and curvatures. Jin *et. al.* demonstrated the shape transfer from complex DNA structures to graphene. Typically, hydrophilic DNA templates were first deposited

on graphene with the help of 1-pyrenemethylamine. Then DNA nanostructures were selectively metallized with silver and gold. This metallization of the DNA template allows the DNA template to survive the subsequent etching. After Ar/O_2 plasma reactive ion etching (RIE), unprotected region of graphene were removed and the spatial information from self-assembled DNA templates were transferred to final etched graphene products after metal dissolution. Self-assembled DNA nanostructures can be designed and folded with precisely prescribed shape. Using DNA nanostructures as masks allows to increase the shape complexity of traditional lithographic processing. One of the key steps is to metallize the DNA to survive the plasma etching. Given the unique electronic properties of graphene, DNA masked fabrication strategy could help researchers to build electronic circuits made of graphene.

For combined techniques of top-down and bottom-up, the difficulty is to find a joint where top-down and bottom up methods can meet and match. In this case, the placement of self-assmbled nanostructures on a lithographically produced patterns is the most promising option for large scale fabrication but with molecular level precision.

Chapter 2

Nanoparticles self-assembly with DNA

Structural DNA nanotechnology provides nanometre-scale control for bottom-up assembly of nanocomponents, e.g. gold nanoparticles, with tailored physical properties.[32][107] Using DNA, we aim to construct nanophotonic networks using fluorescent and plasmonic units (such as fluorescent nanodiamonds, colloidal quantum dots and gold nanoparticles). With these assemblies we aim to study light-matter interactions, in particular energy transfer along photonic networks.[113]

This chapter introduces the research work of surface modification of nanodiamonds (with exhibiting nitrogen-vacancy colour centres), colloidal quantum dots (CdSeS/ZnS), and gold nanoparticles, as well as their self-assembly into defined geometries on DNA templates.

2.1 Nanodiamonds

Due to their peculiar fluorescence properties, nanodiamonds with enclosed nitrogen-vacancy centers (N-V centers) represent a promising material for future developments in quantum information processing such as magnetometry, sensing, quantum computing, quantum cryptography and spintronics.[114] So far, however, research has focused on the properties of individual N-V centers or groups of two centers that randomly gathered or gold nanoparticles-nanodiamonds hybrid structure using AFM (atomic force microscope) tip.[115][116] This project aims at the precise spatial organization of nanodiamonds on DNA nanostructures. Such assemblies would allow for the systematic investigation of spin-state exchange mechanisms of N-V centers arranged in complex patterns and pave the way for quantum state simulator applications.

2.1.1 Introduction

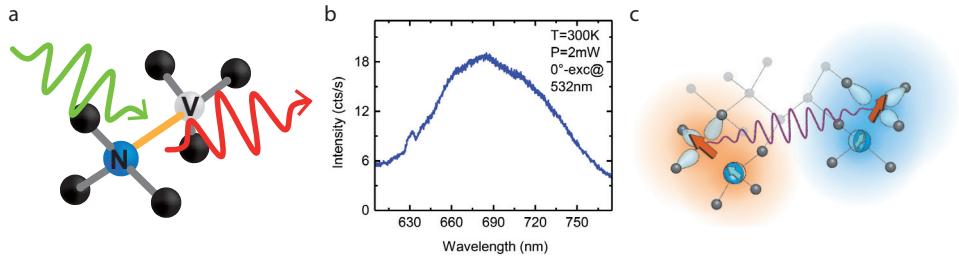

Figure 2.1: a, schematic figure of nitrogen-vacancy(N-V) center. b, excited with 532 nm laser, N-V center emit a characteristic zero-phonon line at 637nm accompanied by Stokes and anti-Stokes phonon-sidebands. Measured by J. Lindlau from Alexander Högele group. c, N-V pairs for room-temperature electron spins entanglement studies. Reprinted with permission from Nature Publishing Group.[117]

Nanodiamonds are allotropes (sp^3) of carbon and possess a series of distinct properties compared to other carbon-based materials. Their outstanding characteristics include extreme hardness, high thermal conductivity, transparency at all optical wavelengths, biocompatibility, and chemical robustness.[118]

Pure diamond is an electric insulator while a doped diamond becomes a semiconductor with a large bandgap (5.5 eV at room temperature). Doped impurities can additionally create optically active defects - also called color centers - within the diamonds, a process that usually involves ion implantation and annealing treatment at high temperature. Up to 500 different color centers associated with specific impurities have been identified and many have been extensively studied with optical spectroscopy techniques.[119] In particular, if two adjacent positions in the atomic lattice of a nanodiamond are replaced, one with nitrogen atom while the other with a vacancy, a nitrogen-vacancy (N-V) center is formed (Figure 2.1). Under excitation with appropriate light sources, N-V centers can act

as reliable single-photon sources where the emitted photons carry defined spin information related to the spin state of the N-V center. Owing to the relatively long coherence times, N-V centers can be employed as optically addressable single spin storage and processing entities which in turn provides the basis for quantum bit information processing.[117][120] Due to the large bandgap of the surrounding crystalline diamond lattice, the excited photons can escape the nanodiamond without further scattering-related losses.

Because of these features, nanodiamonds, which were synthesized by detonation in the 1960s, has come into focus again.[121] The widely used nanodiamonds production method has been by detonation of TNT-hexogene mixtures during which nitrogen defects are introduced.[122] Currently, researchers focus on nanodiamonds with enclosed N-V centers are exploring their potential in applications such as spintronics and quantum computation but also bio-imaging, drug delivery, gene transfer, and cancer therapy.[123]

For many of these applications a key question is: How can the surface of a nanodiamond be tuned to realize its envisioned function? If the goal is to use nanodiamonds as drug carriers, the drug of interest must be loaded onto the nanodiamonds by non-covalent or covalent linkage. For nanodiamonds self-assembly on DNA nanostructures, functional ligands need to attach to nanodiamonds. Because an effective and reliable nanodiamond surface modification would help to manipulate and position it precisely, which would allow to overcome a critical challenge in research dedicated to the optical characterization of coupled N-V centers: the lack of control over their spatial arrangement.

State-of-the-art of nanodiamonds surface modification

In this section, the preexisting methods for nanodiamond surface modification and DNA-nanodiamond conjugation are summarized. Nanodiamonds are sp^3 allotrope of carbon materials, due to their high surface energy, many residual groups such as hydroxyl, carboxyl, lactone, and ketone exist at the nanodiamonds surface and these groups provided initial functional sites for further modification (Figure 2.2).[124] The surface modification procedures can be divided in two main categories: dry methods and wet methods. The dry methods usually employ gas plasma or high temperatures to remove the surface impurities and embed functional radicals. On the other hand, the wet methods use mineral acids to oxidize the surface and then further conjugate the oxidized surfaces with other groups by non-covalent or covalent interaction.

The gas plasma that is used to active the nanodiamond surfaces in dry surroundings is generally composed of hydrogen or halogens such as fluoride or chloride.[125] Fluorines groups can then be displaced by alkyl-lithium reagents, diamines, and amino acids. Others have used ammonia or hydrogen sulfide to directly modify the surface. Takahashi *et al.*[126] prepared hydrogen-terminated diamond by exposing the diamonds to microwave hydrogen plasma and then aminated the surface using ammonia gas after chlorination. The aminated sample was then immersed in a solution containing chloroform, succinyl chloride and triethyl amine for carboxylation. The resulting carboxyl groups on the diamond surface allows for a direact modification with amide DNA. The Hamers group[127][128] used a similar strategy but added a 10-carbon-spacer before attaching DNA. In their experi-

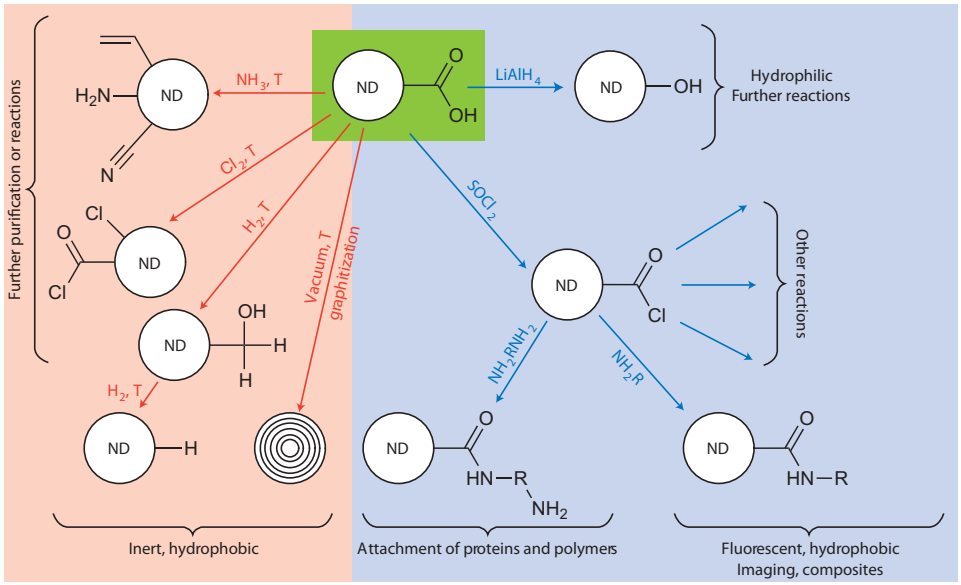

Figure 2.2: Carboxylic groups presented on nanodiamonds surface (ND-COOH; green region) are starting groups for further ligands chemistry. Reprinted with permission from Nature Publishing Group.[124]

ments, hydrogen terminated nanodiamonds were firstly photochemically reacted with a 10-aminodec-1-ene whose amino were protected with trifluoroacetamide functional group. After amino deprotected, primary amine was conjugated with a heterobifunctional crosslinker (sulphosuccinimidyl-4-(N-maleimidomethyl)cyclohexane-1-carboxylate) and finally reacted with thiol-modified DNA to produce the DNA-modified diamond surface.

In most wet chemical methods, the nanodiamond surfaces were oxidized by liquid mineral acid or reduced by lithium aluminium hydride. Ushizawa *et al.*[129] oxidized the diamond with a heated mixture of sulfuric acid and nitric acid (9:1) to achieve a carboxylated diamond surface. The resulting samples were successively treated with sodium hydroxide, hydrogen chloride and washed with water. Then thionyl chloride was added to prepare chlorocarbonyl-diamond. Finally, DNA was covalently immobilized onto the diamond through esterified linkage. Chang group[130][131] used the same acid bath to treat the nanodiamonds followed by coating with poly-L-lysine by charge interaction. To these coatings, it was then possible to covalently attach proteins using heterobifunctional crosslinker or to adsorb DNA *via* electrostatic coupling. Another kind of wet chemical method to conjugate DNA and diamond was developed by the Kruger group.[132] They treated nanodiamonds with reduction compounds, such as lithium aluminium hydride or borane in tetrahydrofuran to reduce the carbonyl to hydroxyl. Then the hydroxylated diamond surface was siliconized by (3-aminopropyl)trimethoxysilane (APS) to introduce primary amino group. The aminoalkyl-terminated siliconized diamond was then suitable for many reactions with amino acids, ester molecules, carboxylic molecules and alike reagents.

To summarize, nanodiamond surface modification, gas plasma or acid oxidization or

reductant reduction all aim to introduce versatile groups such as amino group, carboxylic group for further functionalisation. Most reports used infrared, elements analysis to characterize the products, which very few have showed TEM images of monodispersed nanodiamonds. Therefore a method to produce monodispersed nanodiamonds is very important before positioning single nanodiamonds.

2.1.2 Modification and assembly

The surface modification of nanodiamonds was realized by "wrapping"the nanodiamonds with denatured bovine serum albumin (BSA) that was functionalised with maleimide-PEG3000-biotin (PEG: polyethylene glycol). The stabilizing forces include charge-charge and hydrophobic interaction between negatively charged nanodiamonds surface and positively charged BSA backbones. Due to the steric effect of PEG, the nanodiamonds become highly dispersible in pH 8.4 TBE buffer even with 10 mM magnesium salt concentration. The surface modification was characterized by TEM, DLS (dynamic light scattering) and zeta potential measurement. By choosing biotin-modified ends of DNA structures, the assembly of biotin-nanodiamonds and DNA nanostructures was achieved with the help with neutravidin. Neutravidin can bind four biotin molecules per molecule with high affinity and selectivity. Their multiple binding sites permits the avidin-biotin conjugation can be used to bridge two biotinylated reagents.

Materials and methods

We received the nanodiamonds (ND) from our collaborating groups of Fedor Jelezko and Tanja Weil at University of Ulm. The NDs were originally purchased from Van Moppes SA, Switzerland which were produced by high pressure/high temperature method (HPHT). This material contains approximately 200 ppm nitrogen, resulting 1-2 N-V centers per nanodiamond. To remove graphitic and organic impurities from the surface, NDs were boiled in triacid mixture (sulfuric, hydrochloric and perchloric acids with volume ratio of 1:1:1). The cleaning step to neutralize the surface was carried out *via* repeated centrifugation (8×30 min at 5590 rcf). After each centrifugation step, the supernatant was discarded and the sedimented pellet was resuspended in deionized water. After purification, the carboxylated NDs were lyophilised for further use.

In a typical experiment, $100\,\mu L \times 100\,\mu mol\,L^{-1}$ native BSA solution in 0.5×TBE buffer (pH 8.4) were mixed with $100\,\mu L \times 10\,mol\,L^{-1}$ urea and stirred for 10-15min in a 2 mL Eppendorf tube to prepare denatured bovine serum albumin (dBSA). Then, tris (2-carboxyethyl) phosphine hydrochloride (TCEP, $50\,\mu L \times 100\,mmol\,L^{-1}$) were added to break the dual thiol bonds and stirred for another 30 min. Subsequently, the mixture was transferred into a big falcon tube with TBE buffer filled up to 10 mL. 12 mg maleimide-PEG3000-biotin (PEG: polyethylene glycol) or 3 mg of maleimide-PEG750-methoxy (the ratio of maleimide groups per thiol groups is >10) was added to cap the thiol groups (stiring for 3h). Then 0.5 mg N-(2-aminoethyl)maleimide trifluoroacetate was applied to consume the un-reacted thiol residues. Subsequently, $100\,\mu L$ NDs ($0.5\,mg\,mL^{-1}$, average size: 50 nm)

were added and stirred overnight. dBSA-PEG modified NDs were purified by high speed centrifugation at 4600 rcf for 30 min followed by two times washing with TBE buffer. NDs labeled with functional groups like biotin were obtained.

Four kinds of DNA origami structures, 24 helix bundle (24HB), 14 helix bundle (14HB), 6 helix bundle (6HB), and two-layers sheet (2LS) labeled with biotin oigos at different positions were folded and purified *via* agarose gel. In detail, 5 nM of scaffold strand (7560 base-long scaffold for 2 layers sheet (2LS), 6HB and 24HB and 8634 base-long scaffold for 14HB) with 50 nM of each staple oligonucleotide including 100 nM of biotin-labeled anchor strands were mixed and folded in a 500 µL buffer containing 14 mmol L^{-1} $MgCl_2$ and 1×TE buffer (pH 8.2). The folding program is about 27 h: 15 min at 65 °C, cooling to 58 °C with a cooling rate of −1 °C per 5 min followed by cooling from 58 °C to 35 °C with rate of −1 °C per 1 h and from 35 °C to 4 °C with rate of −1 °C per 5 min.

Directly after folding without further purification, excessive amounts of neutravidin (10 times more than biotin oligos) were added to prevent aggregation of the biotin-modified ends of the DNA origami structures. Biotin-labeled oligonucleotides extending from the DNA structures either at their ends or their sides served as anchor sites for neutravidin molecules, each of which offered four binding sites to biotin. The remaining unoccupied biotin pockets were then used to conjugate biotin residues of the biotin-functionalised FNDs (dBSA-PEG3000-biotin modified FNDs). To remove both excessive staple strands and neutravidin, the modified 6HB/14HB/24HB/2LS were purified by 0.7 % agarose gel electrophoresis after one day incubation at room temperature.

Results and dicussion

Figure 2.3 shows the surface modification process and TEM images of nanodiamonds (NDs) before and after surface modification. Before surface functionalisation, nanodiamonds gathered together in different groups on the TEM grids (Figure 2.3 b). After surface functionalisation, due to the steric repulsion effect of the grafted PEG(polyethylene glycol) chains, the dBSA-PEG coated NDs were fully dispersed (Figure 2.3 c&d). When the grids fully covered with functionalised nanodiamonds using different PEG(either PEG750 or PEG3000), we observed different surface-to-surface distances. NDs grafted with PEG3000 revealed a surface-to-surface distance of 149 ± 37 nm while NDs modified with the shorter PEG750 molecules exhibited a shorter separation distance of 48 ± 12 nm. Dispersed NDs allowed to measure the average diameter of NDs of 49 ± 14 nm. NDs were made from graphite using high pressure high temperature technique with local condition of temperature at approx.5000 K and pressure at approx. 2000 atm. The produced NDs thus have no defined shape but do have rough uniform size distribution.[133]

Dynamic light scattering and Zeta potential measurement revealed size and surface charge changes according to the surface modification (Figure 2.4). The measurement was carried out using a Malvern Zetasizer setup with picomolar concentrations of bare NDs and dBSA-PEG3000-biotin-NDs in TBE buffer, respectively. DLS measurements were carried out with NDs concentration of 0.2-0.3 nmol L^{-1} because low concentration is required for light scattering measurement. We found that the hydrodynamic diameter of the NDs

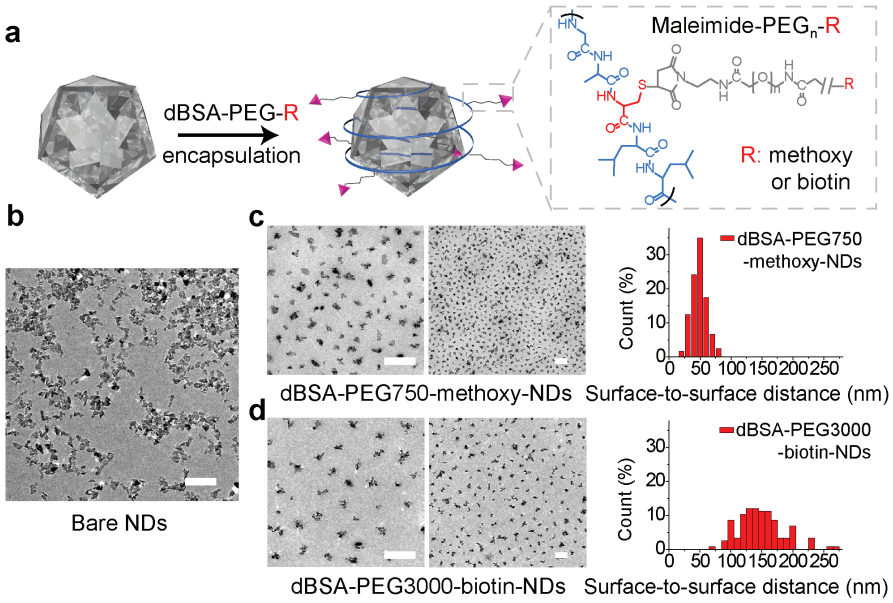

Figure 2.3: Nanodiamonds surface modification using denatured bovine serum albumin. a, dBSA-PEG-R (PEG: Polyethylene glycol, R: methoxy or biotin) is conjugated to the nanodiamonds *via* charge and hydrophobic interactions. b, TEM images of bare nanodiamonds. Mainly clusters are observed before coating. c, TEM images of nanodiamonds modified with dBSA-PEG750-methoxy. This coating results in perfect dispersion of the nanodiamonds and an average surface-to-surface distance of 48 ± 12 nm. d, TEM images of nanodiamonds modified with dBSA-PEG3000-biotin. The longer PEG chains increase the observed average surface-to-surface distance to 149 ± 37 nm. Scale bars are 200 nm. Reprinted with permission from American Chemical Society.

increased from 97.5 nm to 120.4 nm while the size distribution decreased from 124 nm to 107 nm (Full Width at Half Maximum, FWHM). Note that the hydrodynamic diameter of the bare NDs or the dBSA-PEG3000-biotin-NDs shown here is not the actual size of the particles alone. For example, the hydrodynamic diameter of dBSA-PEG3000-biotin-NDs is rather the size of NDs plus the length of attached (coiled) PEG3000 and layers of solvent molecules (here TBE buffer) adhered to the surface of the particles. The surface potential increased from -28.2 mV to -7.8 mV with modification using dBSA-PEG3000-biotin, which indicates that charge interactions contribute to the surface modification with the positively charged BSA backbone partially neutralizing the negatively charged ND surface. Also hydrophobic interactions between the lipophilic amino acid sequences of dBSA and the surface of the NDs are likely to stabilize the conjugates.

The FT-IR measurement of NDs further supported our successful functionalisation (Figure 2.5). The FT-IR spectra of the KBr pellets were recorded with a FT-IR spectrometer Perkin Elmer Spectrum 2000. The dried bare and modified NDs were mixed with KBr powder and pressed into pellets, which were then placed in an IR cell. After background

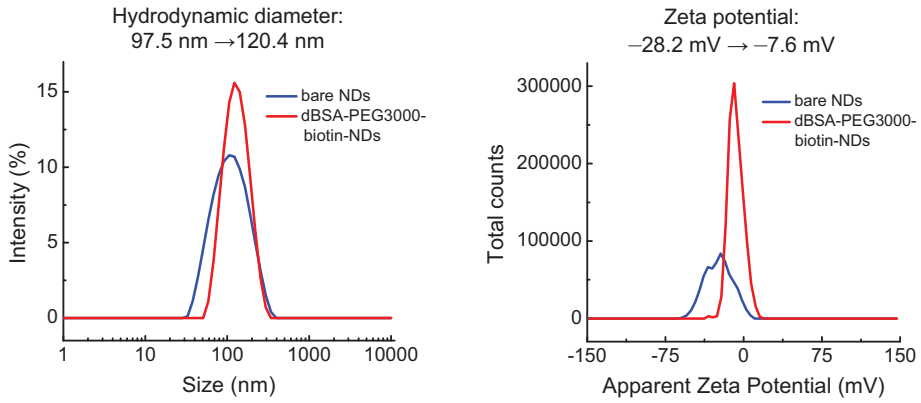

Figure 2.4: Dynamic light scattering measurement of size and surface charge changes according to ND modification.

substraction using pure KBr pellet, compare to unmodified NDs, the dBSA-PEG-NDs showed significant signal at 2916 cm^{-1}, 2849 cm^{-1} and 2351 cm^{-1} corresponding to the symmetric, non-symmetric stretching and scissoring vibration mode of C-H from methylene (-CH2-) of PEG molecules, respectively, 1653 cm^{-1} and 1541 cm^{-1} corresponding to the amide I and amide II modes of the polypeptide backbone and 1101 cm^{-1} corresponding to the C-N stretch vibration of peptide backbones and C-O stretch vibration of PEG.

Before the spatial arrangement of functionalised NDs on DNA origami, a crucial question is to obtain the nanoparticles concentrations of NDs. Because proper stoichiometric ratio of NDs to DNA origami is essential to avoid cluster and error assemblies. Figure 2.6 shows the UV-Vis absorption measurement of non-fluorescent NDs (black) and fluorescent NDs (red) using Nanodrop (ND-1000 spectrophotometer). The inserted photo shows two tubes, one with non-fluorescent and the other one with fluorescent NDs at same concentration of 0.25 $mg\,mL^{-1}$ (size 50 nm). Under daylight, the non-fluorescent NDs are much darker than the fluorescent NDs. The absorption curve (measured with a NanoDrop) shows that in the ultraviolet range, the non-fluorescent NDs have a higher absorption intensities than the fluorescent NDs. For fluorescent NDs, due to the low absorption intensities and absence of a specific absorption peak, it is difficult to determine the concentration of fluorescent NDs. Therefore for each batch of fluorescent NDs, orthogonal experimental design are needed to optimize the ratio of FNDs and DNA origami structures for a better assembly yield.

First, 6HB with neutravidin attached at both ends were chosen. Varying morphologies were observed dependent on the ratio of the mixed components. When excessive DNA origami were added to functionalised NDs (Figure 2.7), star like assembly with NDs at the center, 6HB sticking out were formed. Dimer assemblies of multiple 6HB linked two NDs were also observed on TEM grids. In contrast, if an excess of FNDs was added, many unbound FNDs were found on the TEM grids. By fine-tuning the ratio of biotin-FNDs and DNA origami structures for each batch of FNDs, I was able to approximate the rough

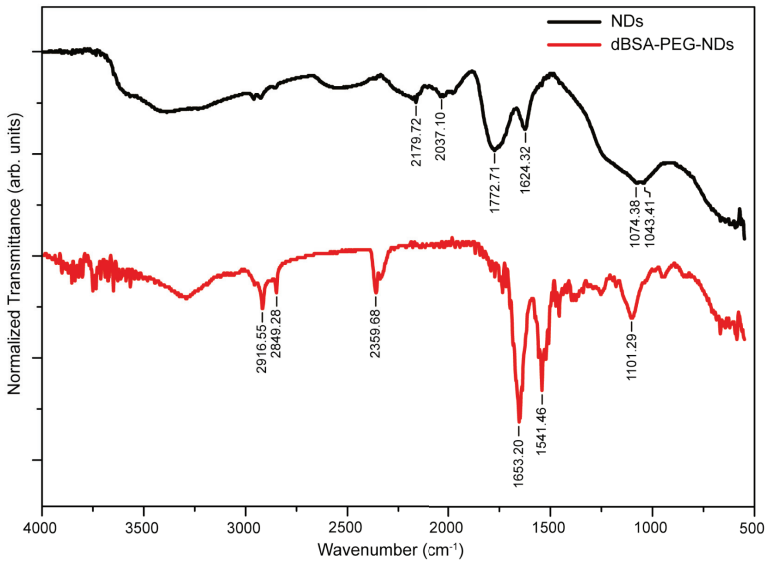

Figure 2.5: The FT-IR spectra of NDs and dBSA-PEG modified NDs.

concentration of NDs for each single batch. I then performed the general assembly of NDs on four effective DNA origami structures: 6HB (428 nm long), 14HB (210 nm long), 24HB (100 nm long), and a 2-layered sheet (50 nm × 50 nm) (Figure 2.8). TEM analysis confirmed the efficient control over the separation distances of FNDs dimers: 96 ± 45 nm for 24HB, 208 ± 59 nm for 14HB, and 361 ± 84 nm for 6HB. Especially for the relatively flexible 6HB that consist only of six parallel helix and exhibits a persistence length of only 2 µm[87], the deviation of the measured separation distance from the nominal length is striking. As a result of the flexibility, many of these DNA tubes adsorb on the TEM grid in bent configurations that have shorter end-to-end distances than a fully stretched bundle. Another factor that may contribute to the deviations is the flexible PEG-linkage that connects the FNDs to the DNA constructs.

As DNA origami allows the formation of virtually any 3D geometry, the spatial organization of FNDs is not limited to dimer assemblies. Figure 2.8 also shows FNDs arranged in a triangle and an irregular tetrahedron, respectively. For these geometries, either three or four binding sites were offered at the edges of the 2-layered sheet. Electron microscopy revealed the successful assembly of the desired clusters. Note that the three-dimensionality of the tetrahedron is lost due to the flattening of the structures during adsorption to the EM grid.

To confirm surface modification will not influence the photolumenescent properties of N-V color centers, we explored the optical properties of the self-assembled FND dimers containing N-V centers in a confocal micro-fluorescence spectroscopy setup under ambient conditions. A representative color-coded fluorescence intensity map of spatially dispersed FND dimer nanostructures (6HBs) on quartz is shown in Figure 2.9. The map was recorded with diffraction-limited confocal excitation at 532 nm and collection above 575 nm by raster

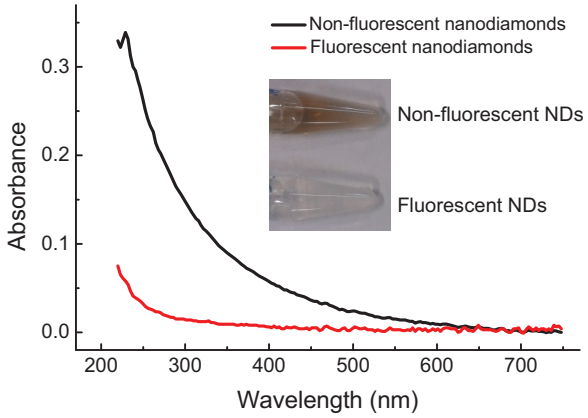

Figure 2.6: UV-Vis absorption measurement of non-fluorescent NDs (black) and fluorescent NDs (red) at the same concentration of 0.25 mg mL^{-1}.

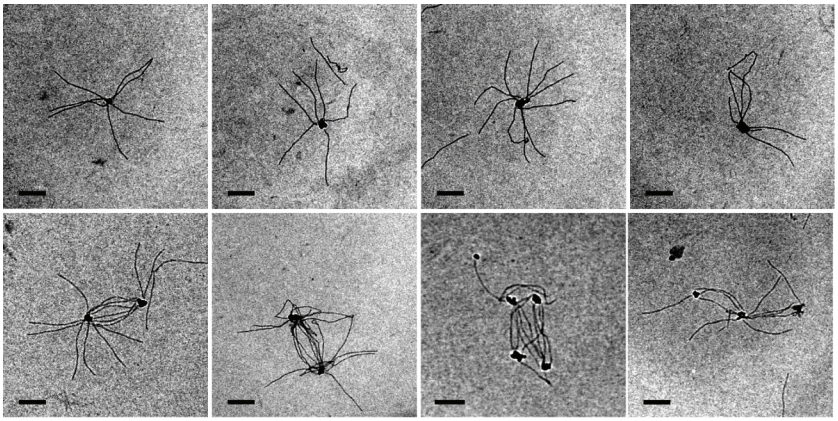

Figure 2.7: TEM images of dBSA-PEG3000-biotin modified FNDs assembled with excessive 6HB origami. Scale bars are 200 nm.

scanning the sample with respect to the focal spot (FWHM spot size of about 370 nm). Several FND dimer assemblies appear as fluorescence hotspots pairs in the map. Separate FND constituents were resolved as shown in Figure 2.9 b&c. High-resolution maps of FND dimers exhibited a separation distance of 451 and 406 nm, which is well within the limits of an expected maximum center-to-center distance of 476 nm: length of 6HB plus radius of coated FND (428+48 nm).

Figure 2.9 d shows a typical spectrum of an FND assembled on DNA origami (red trace). It exhibits spectral characteristics of negatively charged NV color centers in diamond with a noticeable zero-photon line at 637 nm (NV^-) accompanied by Stokes and anti-Stokes phononsidebands. For comparison, we also present typical spectra of a bare (upper gray trace) and a dBSA-PEG3000-biotin-modified (lower gray trace) FND. All spectra exhibit the same features indicating that the fluorescence properties of FNDs are robust against

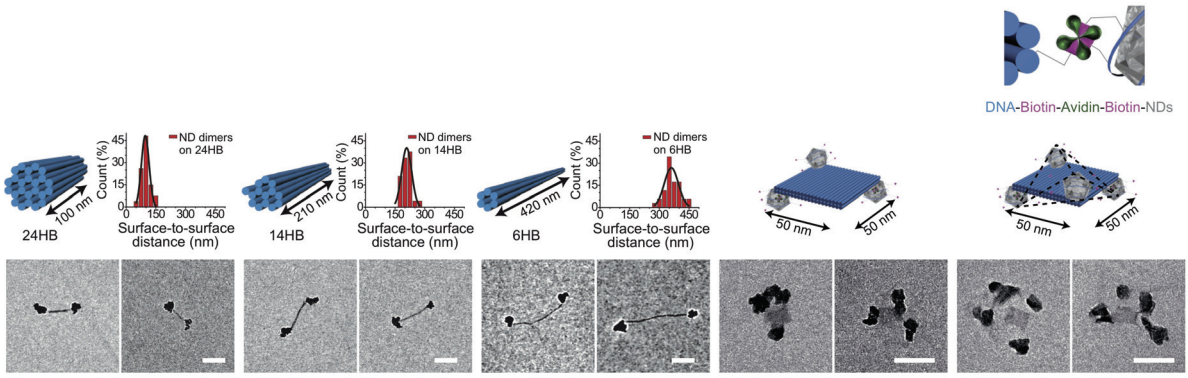

Figure 2.8: Self-assembly of nanodiamonds with DNA origami of 24 helix bundle(24HB), 14 helix bundle(14HB), 6 helix bundle(6HB), and two-layers sheet(2LS). Scale bars are 100 nm. Reprinted with permission from American Chemical Society.

the dBSA-PEG modification and the DNA assembly procedures. Extra measurement of the time trace of the multi-channel fluorescence spectrum shows no significant fluctuations in the fluorescence intensity or in the spectral profile over 150 s.[134]

2.1.3 Summary

In conclusion, we have successfully realized nanoscale positioning of NDs containing fluorescent N-V centers by DNA self-assembly in different geometries. Bioconjugation betweeen FNDs and DNA could be accomplished by a biotin-labeled biopolymer surface coating derived from the plasma protein BSA that imparts high colloidal stability to the FND. This approach offers the possibility to introduce many different modifications at the same time by attaching the desired end groups to the PEG molecules, as demonstrated herein for biotin. Moreover, using DNA origami, FNDs could be arranged in nanoscale geometries with other optically active nanoparticles. Fluorescence measurement certified that our method does not alter the optical properties of the N-V centers. Since these lattice defects exhibit excellent photostability and remarkably long electron spin coherence times for efficient spin manipulation by optical means, site-specific arrangement of FNDs would ultimately allow investigating the coherent coupling of N-V centers assembled in pairs and extended arrays or lattices, which is a step towards the realization of scalable quantum processors and simulators. Before this goal can be approached with the method presented here, however, thinner coating layers for the FNDS have to be developed and the positioning accuracy has to be improved.

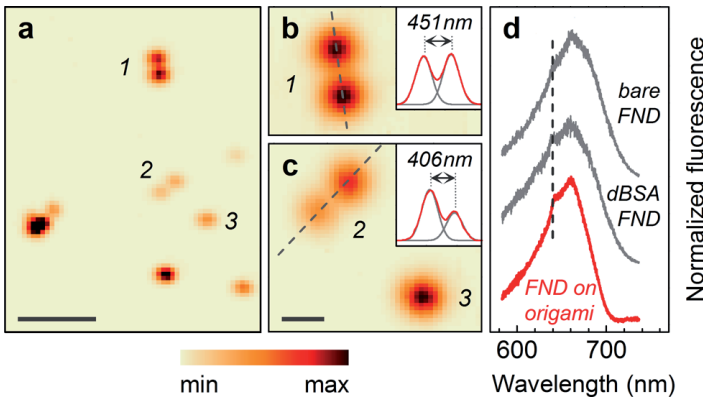

Figure 2.9: Optical analysis of DNA origami-assembled fluorescent NDs. a, color-coded confocal fluorescence map of ND dimers on 6 helix bundle. The dimer assemblies appear as pairs or individual fluorescence hotspots in the confocal map. Scale bar is 2 µm. b&c, zoom-in on ND dimers with corresponding line scans fitted with two gaussians. Scale bar is 400 nm. d, fluorescence spectrum of a bare ND, dBSA-PEG3000-biotin-modified ND (gray traces) and self-assembled ND on DNA origami (red trace). The spectra are offset for clarity to highlight the characteristics of negatively charged N-V center fluorescence, which was unaffected by our procedures. Reprinted with permission from American Chemical Society.

2.2 Quantum dots

Colloidal quantum dots with tunable sizes, composition and core/shell design are another promising candidates to investigate the energy transfer among the self-assembled quantum emitters. In this section, three surface functionalization methods for QDs and QDs self-assembly on DNA origami templates are demonstrated.

2.2.1 Introduction

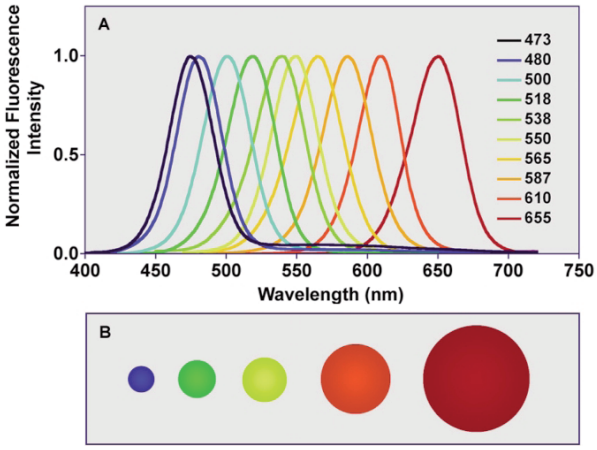

Figure 2.10: Size-tunable fluorescence spectra of CdSe quantum dots (A), and illustration of the relative particle sizes (B). From left to right, the particle diameters are 2.1 nm, 2.5 nm, 2.9 nm, 4.7 nm, and 7.5 nm. Reproduced from Ref. [135] with permission from the Royal Society of Chemistry.

Colloidal quantum dots (QDs) have a three-dimensional confinement for charge carriers (electrons and holes). In semiconductor material quantum dots, the absorption of a photon leads to an excitation of an electron into the conduction band, leaving a hole behind in the valence band. The recombination energy of the electron and the hole is emitted in the form of a photon. The relationship between the band gap and the particle size can be given by the Effective mass approximation (also known as Brus equation).[136]

$$E_{qd} = E_{bulk} + \frac{\hbar^2 \pi^2}{2R^2} \left\{ \frac{1}{m_e} + \frac{1}{m_h} \right\} - \frac{1.8e^2}{4\pi\xi_0 R} + smallerterm \tag{2.1}$$

Here, E is the band gap of the quantum dot, E_g is the band gap of the bulk material, m_e and m_h are the effective masses for the electrons and holes in that quantum dot, $\hbar$ is the Planck's constant, ξ_0 is the permitivity of the free space, and R is the quantum dot radius. According to the Brus equation (Equation 2.1), when size is reduced, band gap of the quantum dots increases. In addition, the composition and shape of the quantum dots will also dictate the energy state. In other words, the energy values of these states which

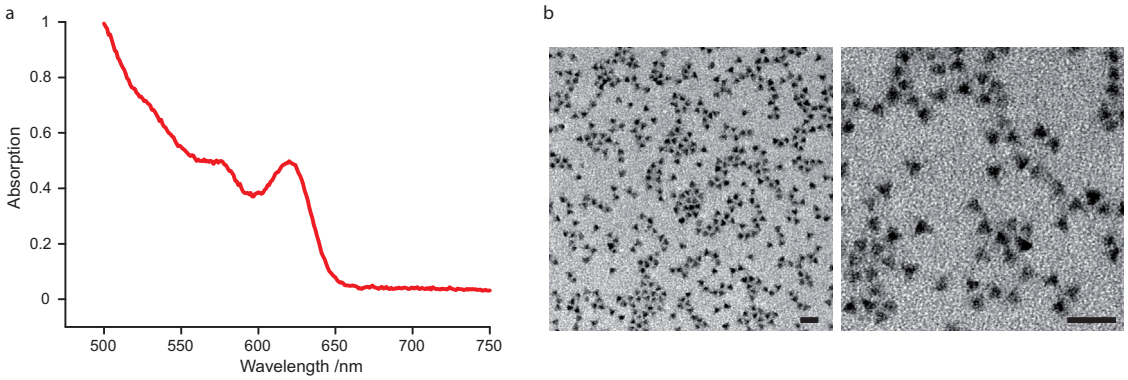

Figure 2.11: The typical absorption and TEM images (in hexane) of core/shell quantum dots CdSe/CdS/ZnS. Materials were obtained from Efrat Lifshitz group at Israel Institute of Technology. Scale bars are 20 nm.

are dependent on the radius, shape, and composition imparts quantum dots with highly tunable electronic and optical properties (Figure 2.10).

Top-down method like molecular beam epitaxy[137] can produce quantum dots with a wide range of shapes and sizes directly incorporated into optoelectronic devices. Wet-chemistry synthesis provides exceptional control over size, shape, core/shell design, and monodispersity. So far, solvothermal methods synthesized colloidal quantum dots with narrow size distribution (example can be found in Figure 2.11) have shown versatile applications in nano-optics, self-assembly, and biomolecular conjugation for cellular imaging and labeling.[138]

In contrast to single QD alone, when QDs are placed in precisely defined geometrical arrangements they are expected to exhibit advanced electronic and photonic properties.[139] This is because the physical properties, of geometrically arranged quantum dots networks, are determined by both their inner electronic states and the energetic communication to neighboring particles. The neighboring particles can be other types of quantum dots or metallic nanoparticles. The desired collective effects of assembled QD-networks often do not emerge in random QD clusters, but require that particles can be placed with specific order. A range of applications can be envisioned for such systems. First, if dimers of QDs can be precisely positioned it would allow for studying of distance dependent energy transfer, which only happens if they are less than 5 nm apart.[140] Second, self-assembled quantum dots in regular one- or two-dimensional patterns would be powerful tools to study energy cascades between QDs and harvesting of light. In particular, sequentially aligned quantum dots with different band gap may broad absorption of the Sun's spectrum, leading to higher solar power conversion efficiencies in solar cells.[141] Third, due to the coherent interaction of QDs and light, if QDs are arranged in a compact group they will emit light with a greater intensity.[142] Fourth, Large-scale patterning of QDs with precise inner distance can be used for data storage, processing, and communication of quantum information.[143]

While the benefits of precise patterning of QDs are well understood, the challenge is to

develop practical approaches that enables placement of particles with nanometer precision and control over the order in which they appear. Using solvent evaporation methods, close-packed QDs lattices can be constructed as if the sticking coefficient and solvent evaporation speed are low, QDs have time to find their equilibrium position and form highly-ordered QDs lattices.[144] The driving forces for this assembly process include geometrical packing and a variety of other factors such as van der Waals attractions, ligand-ligand interactions, capillary forces, electrostatic interactions, and kinetic factors. Thereby nanoparticle size, shape, surface chemistry (ligands, ligands length, solubility) and QDs dispersing medium have crucial influence in the geometries and quality of QDs lattices.[145] However, with solvent evaporation methods, it is challenging to prepare hetero-structures of more than two components. Furthermore, generation of finite-size assembly containing discrete numbers of components, with control particle-particle distance, lattice geometry and boundary shape is not currently possible.

DNA nanotechnology provides a bottom-up approach to arrange QDs at site-specific positions. As mentioned above, usually colloidal QDs are synthesized in non-polar organic solvents and stabilized with hydrophobic ligands which render the nanoparticle hydrophobic surfaces. To assemble QDs with aqueous soluble DNA origami, their hydrophobic surface ligands have to be exchanged. In the following sections, the conjugation methods of QDs-DNA for the addressable assembly will be introduced.

2.2.2 Direct conjugation of target molecules to QDs surface

The straight forward way of QDs surface modification is to directly conjugate functional group labeled DNA molecules to the present ligands on the QDs surface.

As mentioned above, most of the QDs are synthesized in non-aqueous solution organometallic precursors. The capping ligands (like oleic acid (OA), octadecylamine (ODA), trioctylphosphine (TOP), or trioctylphosphine oxide (TOPO), Figure 2.12 a) are the key parameter (concentration, chain length) to control the nucleation, rate of growth, particle morphology and size distribution. Moreover, the ligands electronic structure and the interaction to QDs surface also contributes to the overall optical profiles of the the QDs. The functional residues which interact with QDs surface atoms usually are the phosphine oxide moiety, primary amines, carboxylic acid (acted like bidentate ligands), or thiol groups. For example, the TOPO binds to the surface cadmium sites through the lone pairs of electrons on the phosphine oxide moiety, forming dative bonds. In particular, thiol groups have slightly higher binding energy (Table 2.1 [146]) to the Zn or Cd (the common materials for QDs) compared to amine or carboxylic acids and can be used as phase transfer reagents from non-polar to polar solution. However, the key limitation is the instability of monodentate thiol (for example 3-mercaptopropionic acid (MPA)), where thiol ligands constantly bind and unbind to QDs. Also, some thiolated molecules increase emission quenching after phase transfer.[36][147]

If synthesizing in aqueous solution, according to the “like dissolves like”(in Latin Similia similibus solventur), the hydrophilic ligands may include several oxygen, thiol, or amine groups (or containing some of these). Some of these groups render the ligands wa-

Table 2.1: Bond energy of metal-oxygen and metal-thiol of cadmium and zinc and the comparison to gold.[146]

Metal-oxygen bond	Bond energy (ΔH, kJ/mol)	Metal-thiol bond	Bond energy (ΔH, kJ/mol)
Au-O	221.8	Au-S	418
Cd-O	235.6	Cd-S	208.4
Zn-O	159	Zn-S	205

ter soluble, some act as ligands caping the QDs. The multiple functions of ligands may distract their functions and inhibit the nucleation/growth and shape/size control. Besides, oxygen molecules and protons (pH) in water are the additional factors to take into account. All in all, reliable and robust quantum dots surface modification without disturbing the nanoparticle optical property is important to achieve the site-specific assembly.

Figure 2.12 shows two kinds of chemistry of direct linking DNA to the hydrophilic ligands of QDs. Figure 2.12 b step 1 shows the ligands exchange and phase transfer using GSH (glutathione) and labeled the QDs with amine groups. To conjugate DNA, we can use a amine-to-sulfhydryl heterocrosslinker of EMCS (N-ξ-malemidocaproyl-oxysuccinimide ester, step 2), where the NHS-ester group can conjugate to amino groups on QDs and the maleimide reactive group can react with thiolated DNA oligos (step 3).[148] Figure 2.12 c shows another direct conjugation using EDC/NHS coupling. Same to the GSH methods, QDs are transfered to aqueous phase using MPA (3-mercaptopropionic acid, Figure 2.12 c step 1), the thiol groups head inside to the QDs surface and carboxylic groups make the QDs water soluble. DNA then can be conjugated to QDs *via* standard EDC/NHS coupling (Figure 2.12 c step 2).

Figure 2.13 shows a typical agarose gel loaded with amino-DNA conjugated MPA-QDs *via* EDC/NHS coupling. Control lane (the first one from left, ctrl) with MPA stabilized QDs already showed a smeared band. The second to fourth bands are amino-DNA conjugated MPA-QDs but with different amount of EDC (1 mM, 5 mM, and 10 mM). The higher amount of EDC, the more amino-DNA attach to QDs. As smeared band of MPA-QDs indicated that the stabilizer MPA molecules have already disassociated from the QDs.

MPA capped QDs (CdSe/CdS/ZnS) after ligands exchange stored at 4 °C started to aggregate in around a week. Reddish cloudy clustering appeared at the ep tube bottom. After shaking, the clusters can be re-suspended. Fig:32QDdirectEM shows re-suspended MPA-QDs. It shows clustered QDs but in an odd chain-shape (Figure 2.14).

GSH can bring the QDs to aqueous solution. Heterocrosslinker EMCS solved in acetonitrile were added to GSH-QDs aqueous solution to react with amino residues. After Amicon (ultra centrifugal filters from Millipore) purification, tris(2-carboxyethyl)phosphine hydrochloride (TCEP) treated thiolated DNA strands then can attach to the free maleimide group. DNA modified QDs were obtained after another Amicon purification to exclude free thiolated DNA strands.[148] Using classic Rothemund one-layer sheet origami (R-origami, size 70 $\times$ 90 nm), staple strands at different positions are elongated as docking strands.

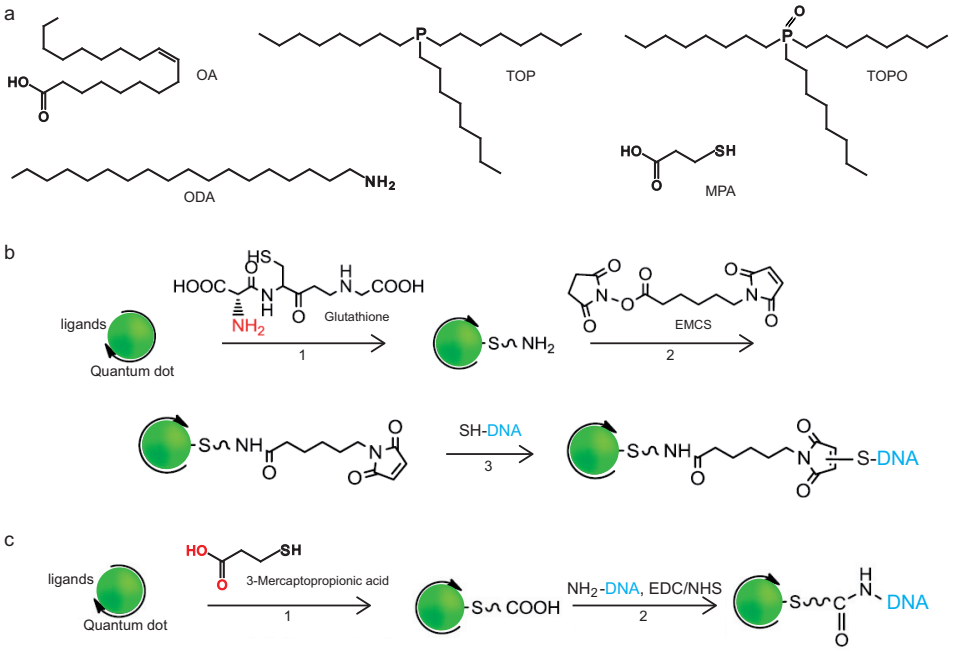

Figure 2.12: a, molecular structures of the common ligands for QDs. Hydrophobic ligands: oleic acid (OA), octadecylamine (ODA), trioctylphosphine (TOP), trioctylphosphine oxide (TOPO) and hydrophilic ligand: 3-mercaptopropionic acid (MPA). b & c, schematic illustration of ligands exchange for phase transfer and the QDs-DNA direct conjugation *via* heterocrosslinker (b) or EDC/NHS coupling (c).

These docking strands have the complementary sequences to thioaled DNA which were attached to QDs. After incubation of ten times more DNA-QDs with R-origami bearing docking strands, QDs-origami assemblies were purified *via* 0.7 % agarose gel electrophoresis (11 mmol L^{-1} Mg^{2+}, 1× TAE buffer).

Figure 2.15 shows the representative TEM images of QDs dimer assemblies on R-origami. Different separation can be well-controlled. Almost no QDs non-specifically attached to the R-origami ends. However, unbound QDs are also visible on TEM grids. Some of them form small groups of aggregates. In addition, the assembly yield on R-origami is low. There are two assembly sites on R-origami, however, few origamis bears two quantum dots, though for close dimer (6 nm separation), the steric effect lower the assembly yield.

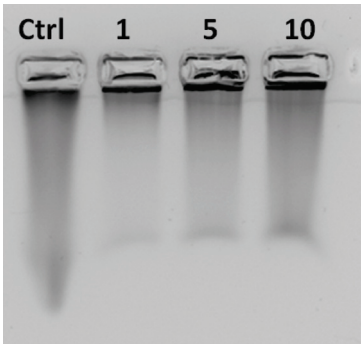

Figure 2.13: Agarose gel electrophoresis of amino-DNA conjugated MPA-QDs *via* EDC/NHS coupling. Lane control indicates the MPA modified QDs. Numbers 1, 5, 10 indicates different EDC concentration of 1 mM, 5 mM, and 10 mM respectively. 2 % agarose gel electrophoresis (11 mmol L^{-1} Mg^{2+}, 1× TAE buffer).

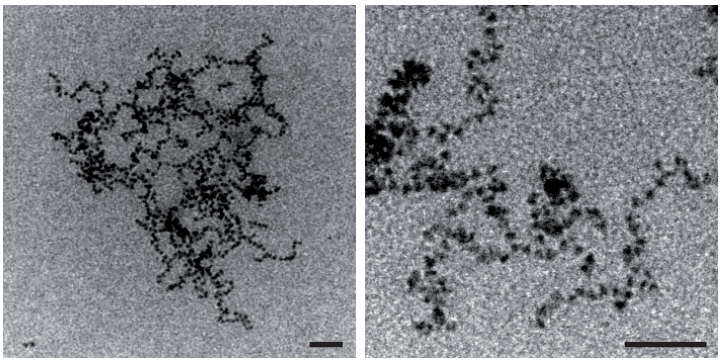

Figure 2.14: TEM images of re-suspended MPA-QDs. Scale bars are 50 nm.

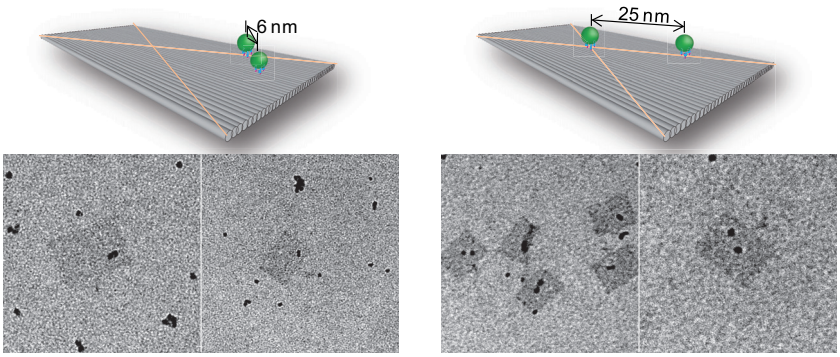

Figure 2.15: TEM images of DNA-QDs (via GSH/EMCS) self-assembled on Rothemund one-layer sheet origami (R-origami). QDs dimer assemblies with different separation can be well-controlled using R-origami.

2.2.3 Amphiphilic polymer

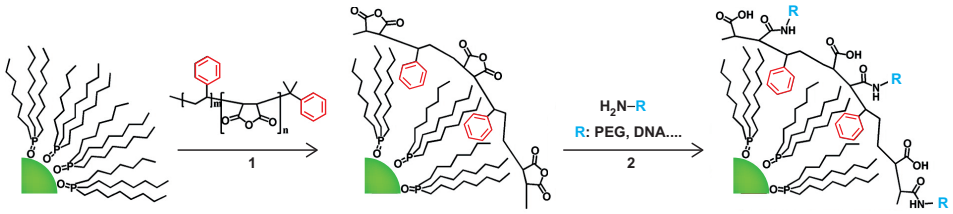

Figure 2.16: Schematic illustration of QDs coating with amphiphilic polymer. Reprinted with permission from American Chemical Society.[149]

Ligands exchanges replaced the primary hydrophobic ligands and transfer the QDs to aqueous phase, however, it also inevitably alters the chemical and physical states of the quantum dot surface atoms and in most cases diminishes the quantum efficiency of the quantum dots. Also, thiolated molecules (mercaptocarbonic acids) undergo constantly binding and unbinding events and over time come off from the quantum dot surface leading to precipitation out of water. Therefore it is beneficial to have a non-covalent bonding to achieve effective QDs surface modification.

Figure 2.16 shows a strategy to functionalise QDs using hydrophobic interactions. Functional groups are introduced *via* amphiphilic polymer. Their hydrophobic side chains (here the benzene ring highlighted in red) intercalate with the alkyl group (of OA, ODA, TOP, or TOPO) on QDs surface and ensure the water solubility of QDs with hydrophilic residues (here through the hydrolysis of maleic anhydride). Secondary residues (R highlighted in blue) like DNA, PEG can be furthered attached to the carboxylic groups.[149][150][151]

The advantages of using amphiphilic polymers coating are: 1) no replacement of primary ligands and no no direct interaction with the quantum dot surface atoms therefore the original optical properties are mostly protected; 2) large number of hydrophobic side chains strengthen the hydrophobic interaction and form more steady structures; 3) additional ligands can be attached to the hydrophilic residues.

Here I adopted the method of *ref.* [151] to coat QDs. In short, dodecylamine were grafted to poly(maleic anhydride) to form amphiphilic polymer through spontaneous amide linkage. The prepared amphiphilic polymer were added to oleic acid coated QDs in hexane. The mixture were then dried under slow evaporation (Eppendorf concentrator) and then 100 mmol L^{-1} NaOH aqueous solution were added to bring the QDs to water phase. Without cross-linking the polymer shell which was wrapped around the nanoparticles using bis(6- aminohexyl)amine, I then attached amino-DNA to polymer coated QDs using EDC/NHS coupling. As shown in Figure 2.17 uranyl acetate negatively stained TEM images, polymer encapsulated QDs generally adds a large volume to the QDs, resulting in a final size that may be bulkier than desired. The surface polymer shell was too thick to put two QDs close enough, which is necessary in energy transfer process. Both empty vesicles and vesicles that capsulating more than one QDs exist.

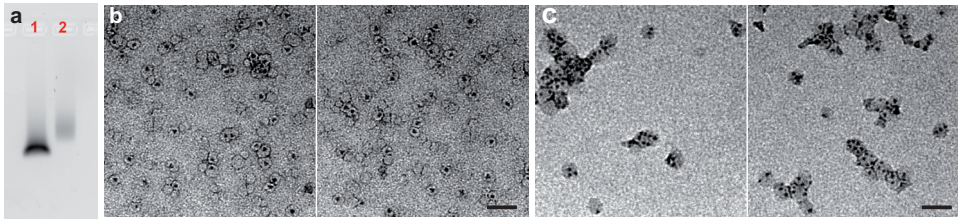

Figure 2.17: Gel and TEM images of QDs coated with amphiphilic polymer. a, agarose gel electrophoresis shows the different mobility of amphiphilic polymer QDs before and after DNA conjugation. Higher band in lane 2 contains sample DNA conjugated QDs, which has a slower migration speed. b, uranyl acetate negatively stained polymer coated QDs. Empty amphiphilic polymer vesicles exist. c, uranyl acetate negatively stained polymer coated QDs conjugated with DNA. Sample were extracted from lane 2. Some vesicles merged together and have more than one quantum dot. Scale bars are 50 nm.

2.2.4 Extra thin shell growth with PTO-oligos

To position QDs on DNA nanotructures, an ideal scenario is that there is a chemistry allowing DNA strands directly attaching to QDs like thiolated DNA strands to gold nanoparticles. As proposed in many reports[152][153], multidentate ligands permit strong and stable interactions with QDs. If multiple ligands that are preferential to QDs can be integrated in DNA strands, stable DNA-QDs conjugates can be achieved. PTO(PhosphoroThioate Oligonucleotides)-DNA is an example of DNA strands with multiple functional groups of thiol. In this section, the QDs *in situ* conjugation using PTO-DNA is introduced.

The method was first introduced from the QDs synthesis using DNA as ligands. Levina *et al.* synthesized infrared-emitting PbS nanocrystal on DNA templates. DNA phosphate backbone, purine, and pyrimidine bases are the possible interaction sites for PbS growth. The synthesized PbS has quantum yield up to 11.5 %.[154] Tikhomirov *et al.* synthesized CdTe using PTO-DNA as ligands and MPA as a co-ligands to passivate sites left open by the DNA. The PTO-DNA ligands were specially designed to contain three segments, the QDs-binding domain featuring phosphorothioate linkages within the backbone, the spacer of ten adenine bases, and the DNA-binding domain for complementary assembly.[155] Deng et al. developed this method to synthesize different PTO-DNA modified core/shell QDs and realized the QDs positioning on DNA origami template.[146] According to the latter two papers, PTO sections are the functional part which were "inserted within a CdS shell during its formation".

Modifying the methods of QDs synthesizing from metal ion precursor, I attached PTO-DNA to customized ZnS shelled QDs. Figure 2.18 shows the work flow. With MPA modified CdSe/CdS/ZnS QDs, a growing materials containing MPA, Zn^{2+}, PTO-DNA (9 phosphorothioated g-9T), NaOH were added and the mixture were incubated at 90 °C for half hour. DNA modified QDs were purified using Amicon purification with four times washing. Different from Deng's paper to grow a new shell, here I suppose the ZnS shell can grow thicker with PTO section oligonucleotides incorporated. This method seems to

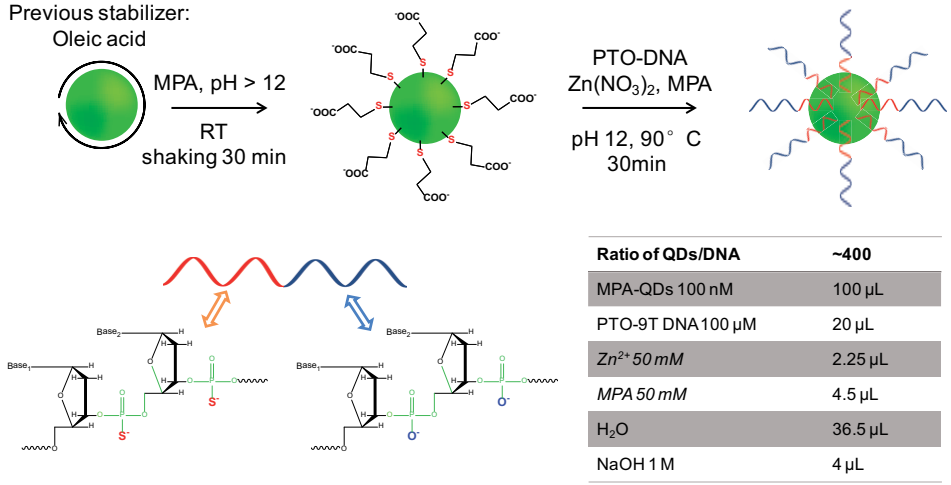

Ratio of QDs/DNA	~400
MPA-QDs 100 nM	100 µL
PTO-9T DNA 100 µM	20 µL
Zn^{2+} 50 mM	2.25 µL
MPA 50 mM	4.5 µL
H_2O	36.5 µL
NaOH 1 M	4 µL

Figure 2.18: PTO-oligos modified QDs with extra thin shell growth. Using MPA stabilized ZnS shelled QDs as precursor, PTO-DNA can attach to QDs during the extra thin shell growth in a hot solution containing zinc ions, stabilizers of 3-mercaptopropionic acid, and PTO-DNA. PTO is the abbreviation of PhosphoroThioate Oligonucleotides. In PTO oligos, a non-bridging oxygen is replaced by a sulfur atom. PTO-DNA strands that are used here contains two parts: PTO segment containing thiol are supposed to attach to QDs and native DNA segment serves as handles for hybridization.

be applicable to either ZnS shelled QDs like lab synthesized CdSe/CdS/ZnS and commercialized one of CdSeS/ZnS. Figure 2.19 shows TEM images of mono-dispersed PTO-DNA modified commercial QDs with different emissions (540 nm, 575 nm, and 630 nm). We also investigated the influence of different incubation time to size changes(Figure 2.19 c), as longer incubation with allow a thicker shell to grow. However, with our TEM resolution, we didn't find significant size changes over 15 mins to 1 hour incubation. Although lower temperature like 50 °C also worked, we simply followed the protocol of *ref.* [146] and used 90 °C for all samples.

It was then possible to assemble PTO-DNA modified QDs on different DNA nanotructures. Typically, ten times more (per binding sites) Amicon purified PTO-DNA modified QDs were mixed with target origami structures in a buffer containing 5-10 mM Mg^{2+} and 1× TAE buffer. After incubation for over night (>10 hours), QDs-origami assemblies were separated from extra QDs and aggregates using 0.7 % agarose gel electrophoresis. The gel band corresponding to the target assemblies were extracted and solution containing the assemblies were squeezed out. As shown in TEM images of Figure 2.20, QDs-origami assemblies with different separations, 50 nm, 25 nm, and 12 nm, as well as the left-handed chiral arrangement were achieved. For QDs dimers with center-to-center distance of 50 nm, statistics showed that around 55 % desired assemblies after purification (Table 2.2). But the shortest distance of 12 nm, only about 10-20 %. Different batch of QDs and modification may give different yield, however, site-specific assembly of QDs on DNA origami

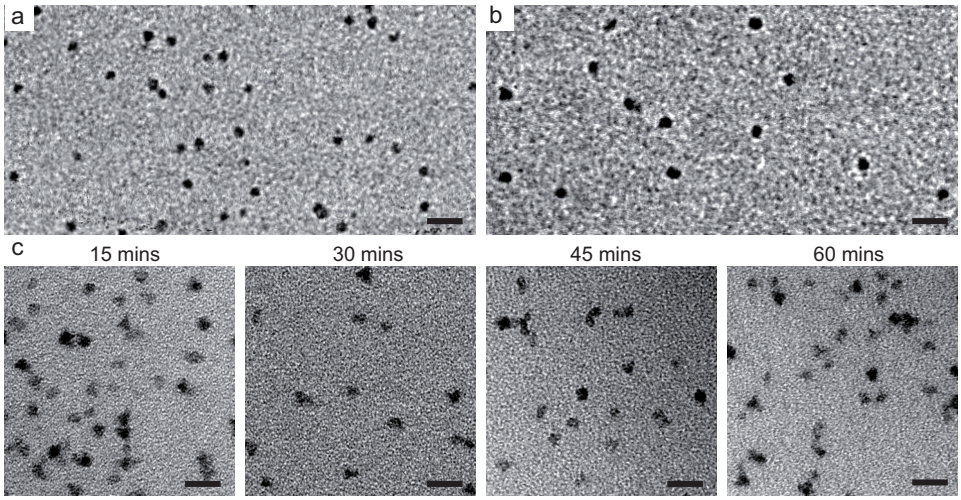

Figure 2.19: TEM images of PTO-DNA modified CdSeS/ZnS quantum dots with emission at 540 nm (a), 575 nm (b), and 630 (nm). Panel c also showed TEM images of QDs incubated with different time. Despite of size distribution, the difference of newly-grown shell thickness is barely distinguishable. Scale bars are 20 nm.

Table 2.2: Statistics of QDs dimer assemblies on one-layer sheet origami with center-to-center distance of 50 nm.

QDs numbers per origami	Numbers	Percentage (%)
Zero dot	7	2.9
One dot	41	17.3
Two dots at right position	131	55.3
Else (clusters, more dots)	58	24.5
Total count	237	100

are feasible. Note that comparing to plasmonic gold or sliver nanoparticles, QDs are comprised of materials with low electron density and it is hard to distinguish the single QD especially after uranyl acetate staining. Also, QDs with similar emitting wavelength but from different sources could have different material composition and core/shell design and show different contrast. In Figure 2.20, dimer assembly used QDs of CdSe/CdS/ZnS (emitting at 640 nm) and stained with 1 % uranyl acetate in order to see the one-layer sheet origami. The chiral assembly used commercial QDs CdSeS/ZnS (emitting at 630 nm) and TEM images were taken without staining as negatively stained TEM images showed only origami and QDs are barely visible.

To investigate the optical properties of QDs after modification and assembly, the blinking behaviors was investigated using fluorescence microscope. QDs sample were spread on glass slides surface and were observed using fluorescence microscope at ambient conditions. Figure 2.21 showed the fluorescence intensity time traces of ten selected blinking spots. In a time range of about 2 mins, multiple bight (ON) and dark (OFF) states are visible,

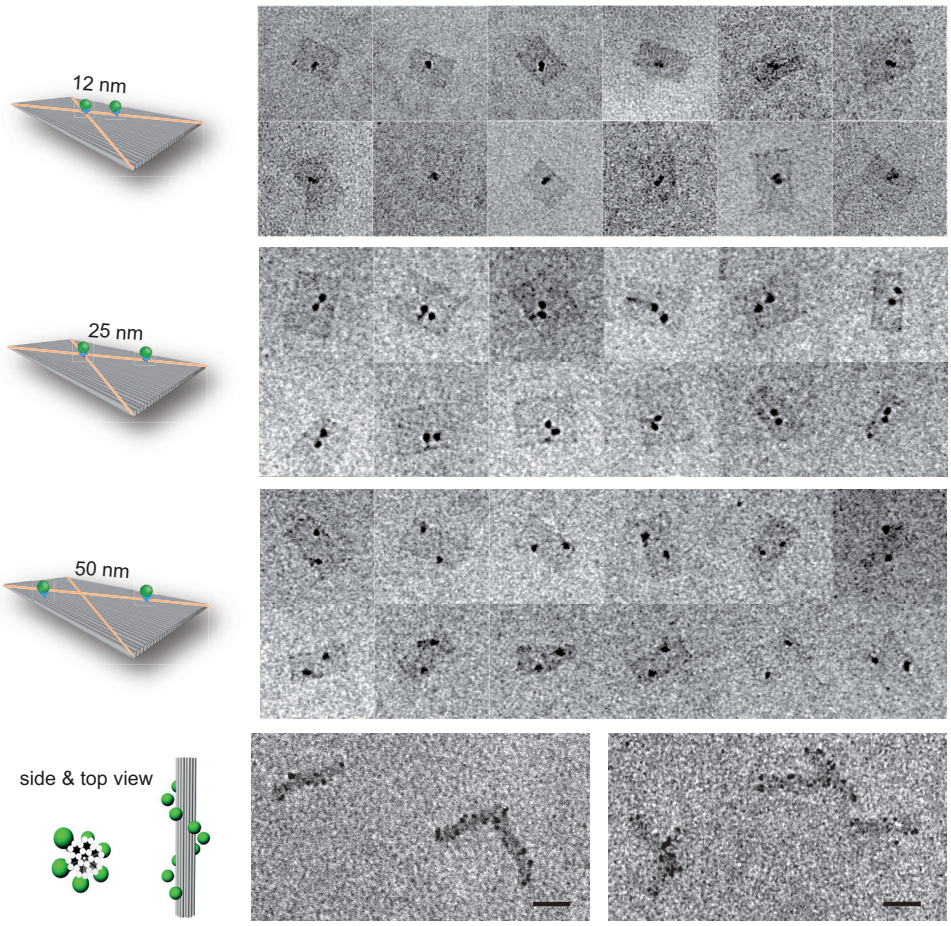

Figure 2.20: TEM images of PTO-DNA modified QDs assembled on different origami, the dimer assembly with different separation and chiral assembly. Scar bars are 50 nm.

which indicates the optically active quantum dots. For different quantum dots, it does have different time periods for ON or OFF states, which depends on the different quantum dots quality.

When QDs were assembled on DNA origami, blinking behaviors of single QDs are not resolved due to the collective effect of QDs groupings, as the origami size (70×90 nm) is below the diffraction limit. In addition, the low assembly yield of dimer assemblies, clusters and non-specifically attached extra QDs to origami ends increased the difficulties to distinguish the expected signal. Comparing to single QDs, however, I did observed different phenomena for QDs-origami assemblies. First, the bleaching speed was accelerated after the working procedure of QDs modification, assembly and purification. For QDs dimer assemblies, fluorescent intensity of bright states are expected show two levels, given the possibility of both QDs are ON, or one is ON, or both are OFF. However, the survived QDs barely shows a regular ON or OFF blinking states, without mentioning the different fluorescent intensity. Second, with QDs dimers assembled with different separation, intensity

time traces show no significant differences. This can be explained that the measured sample didn't reach the QDs efficient coupling distances which usually less than 5 nm.[140] On the other hand, methods have been established to quantify the quantum dots quality after each step, in particular the influence from the surface atomic distortion after modification and oxidization in aqueous solution. In our case, the low assembly yield is a big challenge. For current surface modification, the buffer solution for origami containing 10 mM Mg^{2+} is the other factor cause clusters and non-specific attachment. Future efforts should still focus on the surface chemistry of QDs, the site specific assembly using templates besides DNA origami. Instead of cadmium, zinc, another kinds of quantum dots bearing similar optical properties but with easier surface chemistry should be also considered.

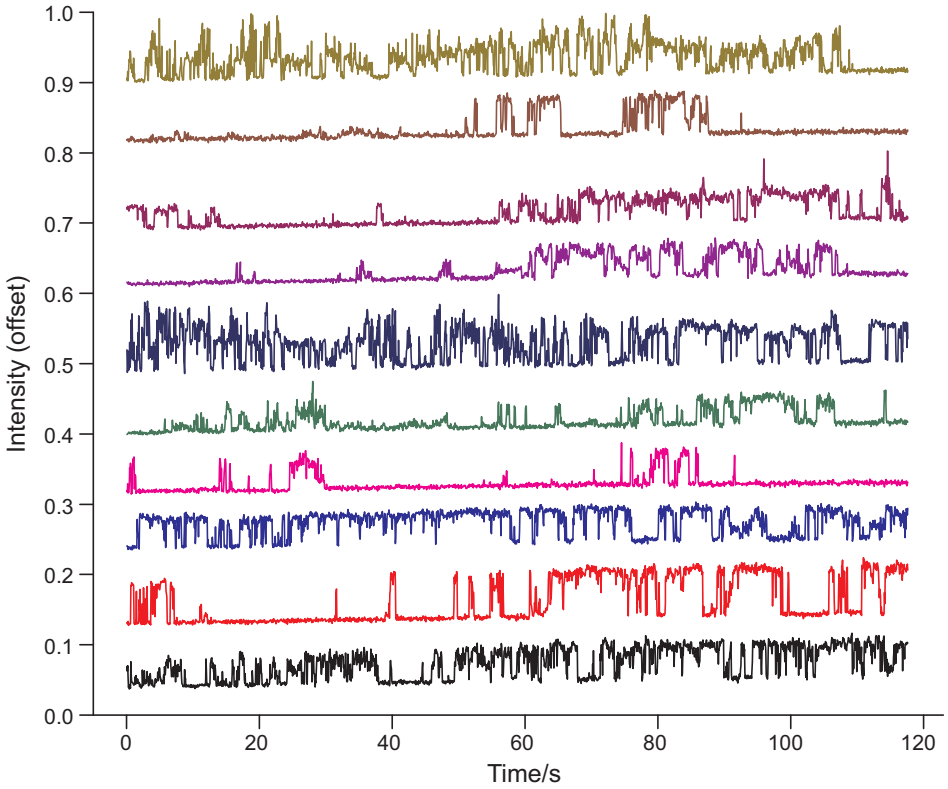

Figure 2.21: Fluorescence intensity time trace of PTO-DNA modified commercial QDs with emission at 575 nm.

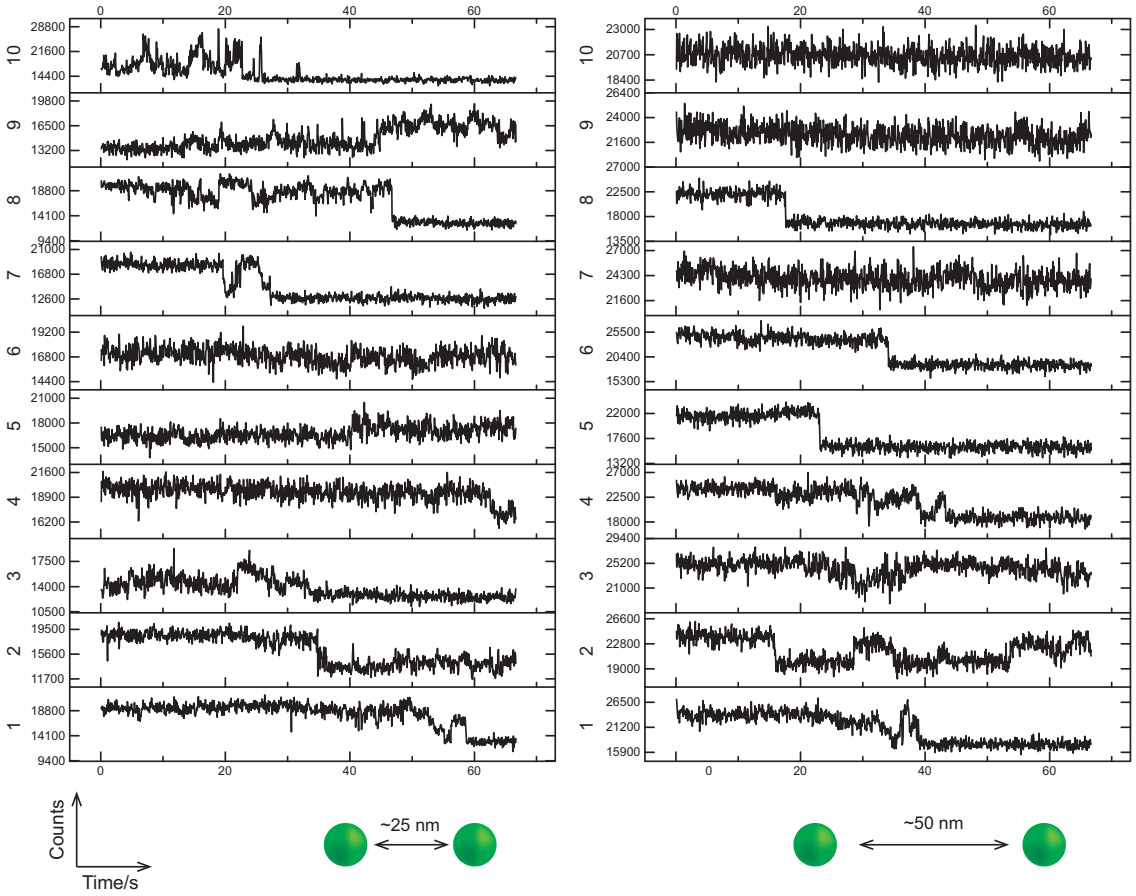

Figure 2.22: Fluorescence intensity time trace of PTO-DNA modified QDs assembled on one-layer sheet origami with two separations, 25 and 50 nm.

2.2.5 Nucleotide dependent DNA-quantum dots interaction

DNA contains four kinds of bases, adenine (A), guanine (G), cytosine (C), and thymine (T). Adenine and guanine are also known as purine bases and cytosine and thymine as pyrimidine bases. Each of them bears different molecular details and form specific base pairs, A to T and G to C. The programmable assembly of DNA mostly rests on such interactions. In addition, some enzymes could only recognize specific sequences. Moreover, people have found more DNA bases dependent interactions in nanotechnological field. The aromatic nucleobases of single stranded DNA are believed to stack with six-member carbon ring of single walled carbon nanotubes and nucleobase binding strength was revealed in an order of G > C > A > T.[156] When functionalizing thiolated DNA strands to gold nanoparticles, adenine bases have the highest non-specific interactions to nanoparticles' surface, therefore it is better to avoid poly adenine sequences for modification. In another way, poly adenine sequences can serve as an effective anchor for preferential binding for gold nanoparticles.[157] If using single stranded DNA of repeating bases (30 base long) as ligands for gold nanoparticles synthesis, interestingly that A's produced rough, round gold particles; T's, stars; C's, round, flat discs; G's, hexagons.[158] People also showed that among the four nucleotide triphosphates (NTP), only GTP served as a competent ligand for nucleation, growth, and capping of soluble PbS nanocrystals.[159] In the paper mentioned above about CdTe synthesis using PTO-DNA[155], the authors also found that quantum efficiency of CdTe quantum dots capped with PTO G-residue pentamers yield the highest luminescence efficiency.

While performing control experiments, we found that the conjugation of DNA to ZnS shelled QDs is not dependent on phosphorothioate (PTO) segment, but different bases. Note that all oligos that used here contains two sections: the functional section of bases repeating strands, with or without PTO modification, and the handle section of 12T. As shown in the agarose gel image of Figure 2.23 b, when incubating different kinds of DNA strands with commercial QDs (emitting at 540 nm), QDs with PTO modified poly-T or poly-C didn't give a single condensed band. However, single stranded native DNA of poly-G or poly-G functionalised QDs showed a single band. Therefore we think that the DNA-QDs conjugation are feasible in water solutions by mixing MPA-QDs with native single stranded DNA containing a G- or A-rich section, no PTO segment required (Figure 2.23).

We then designed different experiments to gain more insights of base-dependent QDs modification. In a typical experiment, a mixture of 100 µL water, 0.5 µL × 10 µmol L^{-1} QDs (CdSeS/ZnS) from stocking solution, and 20 µL × 100 µmol L^{-1} poly-G(or A)-12T DNA (400 times more) were incubated at 90 °C for certain time. If for additional assembly, extra DNA were removed using 4 times Amicon purification. Figure 2.23 c shows agarose gel of QDs modified with different length of repeating A or G. For both A or G base, pentamers are the critical length. As one or three A or G modified QDs gives smeared QDs bands. It seems 9G has a better affinity to QDs than 9A. The incubation time can be as short as 10 mins if incubating them at 90 °C. Also, TEM shows a good uniformity of QDs after modification (Figure 2.24).

In collaboration with M. Pilo-Pais and F. Nicoli, the newest finding is that poly-G or

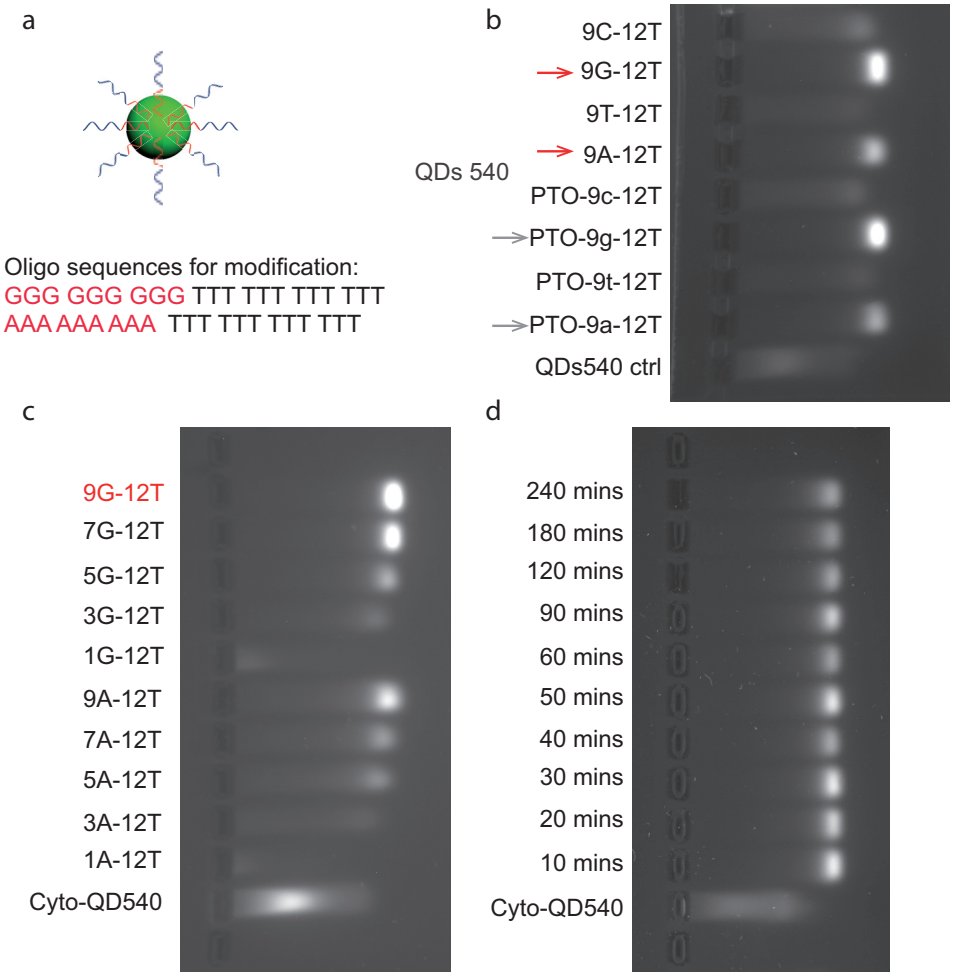

Figure 2.23: Nucleotide dependent DNA-quantum dots interaction. a, schematic figure of DNA modified QDs, a functional section containing G- or A-rich will attach to QDs, the rest serves as handles. b, an agarose gel shows PTO modified DNA doesn't always give a properly functionalised QDs. G- or A-rich segments are the functional parts that interact with QDs. c, the influence of different G- or A- repeating length on QDs modification. Pentamers are the critical length and it seems G works better than A. d, the influence of incubating time for QDs modification.

A/QDs modification can be finished at room temperature as short as 15 mins. We think gentle conditions like room temperature with short time can preserve the primary ligands without altering the optical properties. However, we still need to figure out the specificity of DNA funcionlised QDs to bind at the right complementary docking strands.

Although here we tried QDs with ZnS shell, coordination chemistry shows native DNA containing poly-G/A might be able functionalise QDs with shell containing cadmium, lead, and copper.[160] In the case of Cd^{2+} and Zn^{2+}, the guanine N7 position is the strongest intrinsic binding site. Charged phosphate units assist to stabilize the chelates.

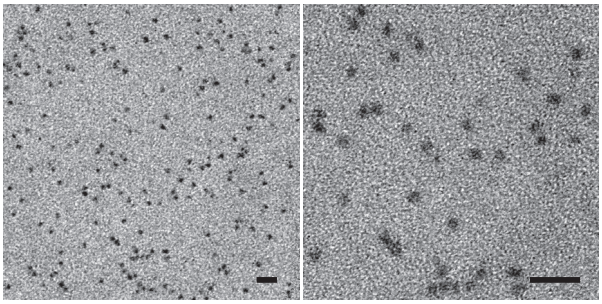

Figure 2.24: TEM images of QDs modified with 9G12T after Amicon purification. Scale bars are 20 nm.

2.2.6 Summary

Due to their standard wet-chemistry synthesis, tunable optical properties, relatively stable fluorescence (compare to fluorescent dyes), and commercial availability, colloidal quantum dots in general have broader applications. Here, I showed different surface modifications for ZnS shelled QDs towards DNA-based QDs assembly, as well as QDs assembly in different configurations such as dimer and chiral assembly. To understand the further details, QDs-origami assembly with further precise control are demanded. Before a reliable DNA-QDs conjugation method developed, both polymer-coating or neutravidin modified QDs are good compromise.

2.3 Gold Nanoparticles

In subsection 1.3.1 and subsection 1.3.2, plasmonic properties and applications of colloidal gold nanoparticles and their assemblies have been described. In this section, we aim to build a gold nanoparticles dimer assembly to investigate the hotspot enhancement and plasmon-exciton interaction.

2.3.1 Introduction

The incident light with a specific frequency induces a collective oscillation of surface electrons of the plasmonic nanoparticles (e.g. gold or silver nanoparticles). This electron oscillation around the particle surface causes a charge separation, which results in a dipole oscillation along the direction of the electric field of the light. The maximum frequency of the amplitude of the oscillation reached is called surface plasmon resonance (SPR). SPR creates a local electric field enhancement with strengths (modest enhancement, of ten fold to maximum 100) that is higher than that of the incident field. Both the SPR frequency and local plasmonic enhancement are tunable by varying the parameters of metal composition, size, shape, spacing to the neighboring nanoparticles, and surrounding medium.[161]

Take spherical gold nanoparticle as example, when $2R \ll \lambda$ (R is the radius of the particles and λ is the wavelength of the light in the media), extinction coefficient is mainly determined by the metal dielectric functions, which is correlated to the atomic orbital structures. When the nanoparticle size is greater than 20 nm, the particle radius R begins to play a role. Together with the retardation effects of the electromagnetic field across the particle, SPR shifts to red and peak broadening occurs. When the shape is no longer a sphere, additional SPR appear, such as a longitudinal lower energy plasmon resonance and transverse higher energy mode for the case of nanorods.[162]

For less trivial structures such as nanoshell, Prodan *et al.*[163] developed a plasmon hybridization model to explain their plasmon resonances. The model can be understood as the hybridization of plasmon modes, analogues to the hybridization of atomic orbital in molecules. Figure 2.25 shows the energy-level diagram that describes the hybridized plasmon resonance in metallic nanoshells by the plasmon interaction of sphere surface ω_{sp} and inner cavity ω_c. The two dipolar modes of nanoshell structure emerge due to the hybridization of dipolar modes of spherical particles and a cavity, which results in the splitting and shifting of these plasmon resonances to higher energy assymmetrically coupled anti-bonding mode (ω_+) and lower energy symmetrically coupled bonding mode (ω_-).The plasmon hybridization model is universal and able to predict plasmon interaction of nanoparticle-nanoparticle and nanoparticle-guest molecule couplings.

When two spherical nanoparticles are placed in close proximity to each other, their plasmons can couple through near-field interactions. One unique feature of coupled nanoparticles is the further enhanced electromagnetic (EM) field at the junction of two nanoparticles (hot spot), when the incident light is polarized along the nanoantenna main axis and the wavelength is matching the localized SPR. The multifeatured palsmon response of dimers,

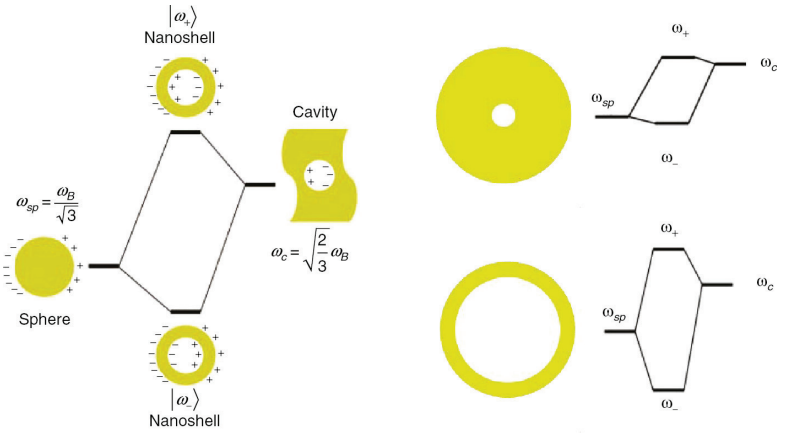

Figure 2.25: Plasmon hybridization in metal nanoshells resulting from the interaction between the sphere and cavity plasmons. Hybridization for thick and thin metallic shells reveals that the hybridization is much more significant for the thin metallic shell. Reprinted with permission from the American Association for the Advancement of Science.[163]

homo- or hetero-dimers [164], can be understood as that their surface plasmon modes hybridize and lead to bonding (red-shifted) and anti-bonding (blue-shifted) plasmon mode.

The electronic resonance occurred in the host spot act like a antenna, able to amplify the radiation from small molecules placed in. When foreign molecules are placed at hot spot region, three types interactions can happen: refractive index-independent plasmon resonance, palsmonic-molecular resonance coupling, and plasmon influenced fluorescence process.[165] In the first case, the electronic absorption energies of foreign moleucles are far away from plasmon resonance. Their adsorption increases the refractive index or the dielectric constant of the nanoenvironment surrounding nanoparticles. In the second case, the molecules exhibit strong absorption at the plasmon resonance which leads to a strong coupling and the hybridization of the plasmonic and molecular resonances. *Ref.* [28] gives an ideal example of such phenomenon with an example of plasmon and exciton interaction. In the third case, plasmon can cause quenching by enhancing non-radiative decay, or fluorescent enhancement if fluorescent molecules are at a certain spacing to plasmon source and enhancement of excitation and radiative decay can overcome the non-radiative decay rate.

In order to understand the interaction of hot spot and guest molecules, in this section, two kinds of gold nanoparticles dimers assembly with DNA are introduced. In the first example, we aimed to build a hybrid nanopore system with both ionic and optical signals and are able to realize optical signal detection using Raman enhancement of Rhodamine. In the second example, we established a robust method to place a single colloidal quantum dot or gold nanoparticles at the hot spot center of 40 nm gold nanoparticles dimers.

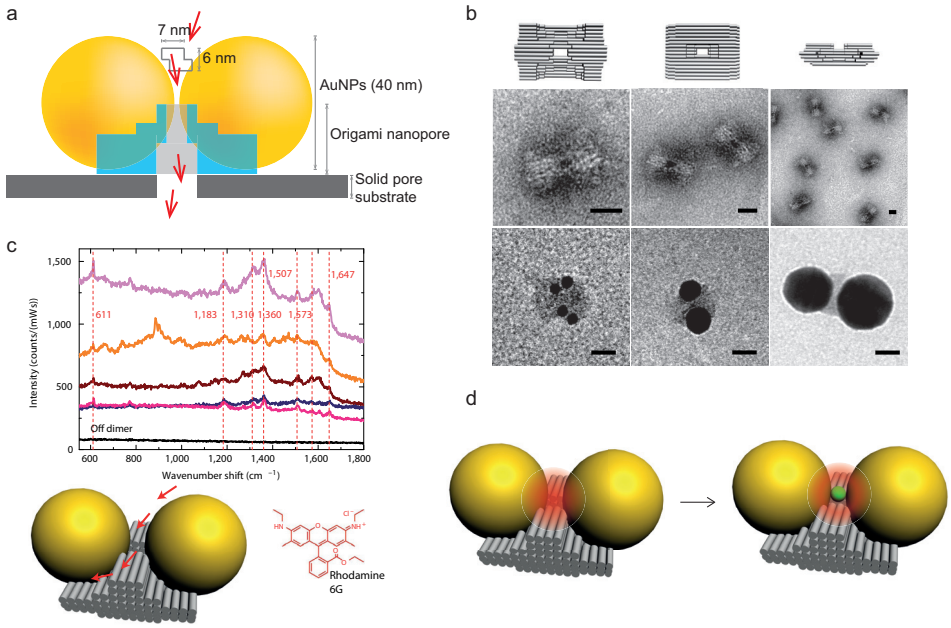

Figure 2.26: Scheme of gold nanoparticles dimer on DNA origami nanopore structure. a, scheme of hybrid nanopore which can give ionic current and optical signals. b, TEM images of origami nanopore and gold nanoparticles attachment at the hollow parts. Scale bars are 20 nm. c, Raman signal enhancement in the hot spot of gold nanoparticles dimers assembled on nanopore structure. d. the potential application for assembling gold nanoparticle-quantum dot-gold nanoparticle to study the exciton and plasmon interactions.

2.3.2 Gold nanoparticles dimer assembly on nanopore structure

Channels that have a dimension at nanoscale offers opportunities to investigate fundamental phenomenons upon the the molecular translocation. With small voltage bias imposed across the nanopore, when target molecules enter the channel, ionic current decreases due to the blocking of target molecules. When molecules leave, the channel is reopen and ionic current goes back to open state. Monitoring the ionic current modulation induced by analytes translocation allows to explore the molecular behaviors inside the channel, such as its physical conformational changes, interaction with the nanopore, and particle-particle interactions.[166] Consequently it enables several applications in molecular sensing[167], DNA sequencing[168], force analysis[169], molecules separation and determinations. So far, however, nano channel based sensing or detection has only one signal of ionic current changes.

Hence we proposed a hybrid nanopore system with DNA origami based nanopore structures with designable size and functionality. The main goal of the nanopore design is to create a new kind of synthetic hybrid nanopore with both, ionic current as well as optical signal upon target molecule translocation. To achieve this goal, we designed and folded the origami nanopore assembled with two 40 nm gold nanoparticles which serve as an antenna.

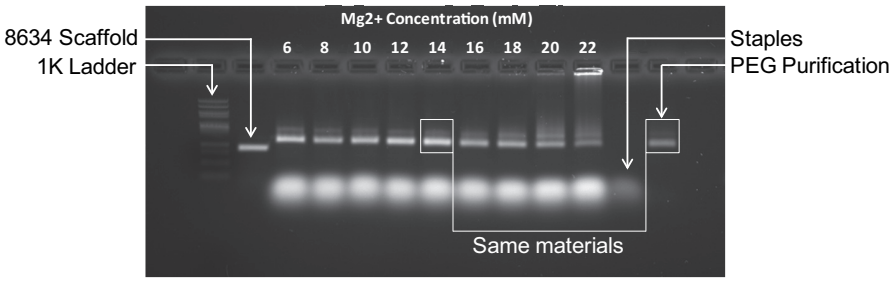

Figure 2.27: Magnesium screening of origami nanopore structure. The fastest bands indicates the excessive staples in the folding solution. From the magnesium screening, 14 mmol L^{-1} magnesium chloride concentration gives the best folding. Besides the main band, a slower band appears which might be the dimers aggregations. Higher magnesium concentration cause more clusters and smearing. One time PEG precipitation purified origami structure were also loaded and they have similar speed as the others.

The nanoparticles close proximity creates an enhanced field (hotspot) at the gate of the pore (Figure 2.26 a). When target molecule transports through the nanopore, it will pass by the hot spot region and give a responsive optical signal. At the same time, it will also cause an ionic current decrease due to the transient blocking. These two simultaneous signal output may significantly enhance the differentiation and sensitivity of target molecular detection. The other design novelty of the origami structures is that it has two hollow sides where nanoparticles can embed in. This will in our expectation to reduce nanoparticles wobbling and achieve a better control over nanoparticles gap.

Figure 2.26 b shows the TEM images of purified origami nanopore structures and the assembly with gold nanoparticles. Negatively stained images clearly show the pore position and hollow parts at both sides. As the structure was designed to assemble two 40 nm gold nanoparticles, when using small gold nanoparticles, they could assemble at the designed positions but multiparticles can attach. Magnesium screening gel (Figure 2.27) shows the origami nanopore folding with good yield. High concentrated origami structures can be obtained using PEG precipitation. PEG precipitation removes most of the free staples and barely causes clusters.

In collaboration with Ulrich Keyser's group, preliminary results show that the dimers assembly leads to a strong plasmonic coupling in a controllable gap of about 3-5 nm. Surface enhanced Raman scattering was employed to demonstrate the local field enhancement of guest molecules Rhodamine 6G (Figure 2.26 c). As gold nanoparticles that fully covered with handles oligonucleotides may show background signal of DNA bases, sequence dependent Raman measurement was also described in *ref.* [170].

Although the nanopore was originally designed to measure single molecule translocations, it can be used in any experiment that requires plasmonic enhancement. As shown in the schematic illustration of Figure 2.26 d, one single quantum dot can be positioned at the center of hot spot region and achieve heterostructure assembly of gold nanoparticle-quantum dot-gold nanoparticle. Such trimer assembly will offer a platform to study the

plasmon-exciton interaction, plasmon induced enhancement or quenching phenomenons. However, as mentioned in section 2.2, the non-specific binding of quantum dots is a big barrier for such controlled trimer assemblies. Instead of assembly at the designed hot spot position, quantum dots tend to bind at the scaffold loop region (both ends of the origami structure) and the gold nanoparticles positions.

2.3.3 Gold nanoparticles & quantum dots heterostructures

Experimental realization of quantum-dots and gold nanoparticles hybrid structure and the optical measurement can reveal more detail of plasmon-exciton interaction, thereby to better understand the energy transfer mechanism.[26][27][28] In collaboration with M. Pilo-Pais and F. Nicoli, we established a robust method to construct gold nanoparticle-quantum dot-gold nanoparticle trimer structure.

In detail, we functionalized 40 nm gold nanoparticles with 5' prime thiolated oligonucleotides, as well as the quantum dots with complementary sequences but with functional poly-G segment at 3' prime (subsection 2.2.5). When titrating 5 nm quantum dots into 40 nm gold nanoparticle in a buffer containing $5\,\mathrm{mmol\,L^{-1}}$ magnesium chloride and 1× TAE buffer, due to the steric effect of big gold nanoparticles, only linear assemblies of quantum dot/gold nanoparticle (...Au-QD-Au-QD-Au...) alternate structures can form. An ideal scenario will be the concentration of quantum dots in solution is half of the gold nanoparticles and mostly they will form gold nanoparticle-quantum dot-gold nanoparticle trimer assembly. However, the exact concentration of quantum dots and gold nanoparticles are not perfectly accurate. Therefor the assembly results in a distribution of monomers (gold nanoparticles), dimers, trimers, and higher oder assemblies. Fortunately, these assemblies containing 40 nm gold nanoparticles can be separated by agarose gel electrophoresis. The gel band contains corresponding assembly can be exacted and liquid containing target assembly can be squeezed out.

Figure 2.28 shows the scheme of gold nanoparticle-quantum dot-gold nanoparticle (Au-QD-Au) trimer assembly. Due the steric effect of big (40 nm) gold nanoparticles, when titrating 5 nm quantum dots in, only linear assembly (...Au-QD-Au-QD-Au...) can form. Figure 2.28 c shows the agarose gel image of samples with different Au/QD ratio. Isolated red colored bands indicating assemblies containing different numbers gold nanoparticles. The lowest bands are free gold nanoparticles as they has same mobility with gold nanoparticles control. The first band above labeled with D is the desired gold nanoparticles dimer assembly bridged with one quantum dot. The bands labeled T and Q are gold nanoparticles trimer and tetramer assembly bridged with quantum dots, respectively. TEM images (Figure 2.28 b&c) clearly show the assembly as described. In particular the trimer assembly has a very high yield. Due to the material low contrast, quantum dots are not always visible. When apply same assembly strategy to gold nanoparticle 40 nm-5 nm-40 nm assembly, 5 nm gold nanoparticles are clearly visible under TEM and link two big nanoparticles together. Longer linear assembly can also form and be separated as shown in Figure 2.28 f.

Before the systematic studying of Au-QD-Au structure, we first measured the scattering

spectra of the Au-Au-Au(40 nm-5 nm-40 nm) trimer assembly. In comparison to the spectra range of 570 ± 3 *nm* of gold nanoparticles dimer with 5 nm gap([171]), the trimer assembly have red shifts (Figure 2.29). In addition, the maximum resonances are in a range from 550 nm to 620 nm, which indicates that during sample preparation, the two big gold antennas may have different separation due to the capillary and drying effect.

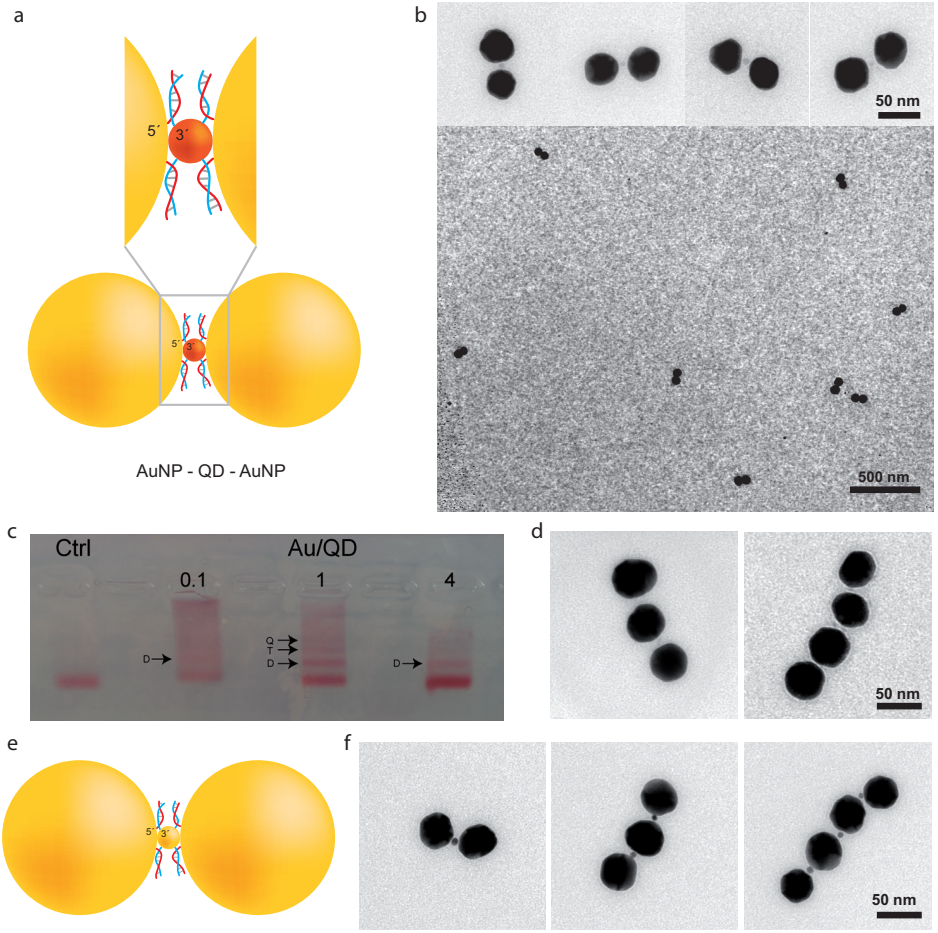

Figure 2.28: Scheme of (gold nanoparticle-quantum dot-gold nanoparticle)Au-QD-Au assembly without origami. a, the DNA strands hybridization detain of quantum dot and gold nanoparticles. Quantum dots and gold nanoparticles are fully covered with DNA strands. Due the steric effect of big (40 nm) gold nanoparticles, when titrating 5 nm quantum dots in, only linear assembly (...Au-QD-Au-QD-Au...) can form. b, TEM images of Au-QD-Au trimer assembly. Quantum dot has low contrast comparing to gold nanoparticles and are barely visible. c, agarose gel electrophoresis shows isolated red colored bands (indicating the gold nanoparticles) when using different Au/QD ratio. D: dimer; T: trimer; Q: tetramer. d, TEM images of Au/QD trimer and tetramer assembly. e & f, same strategy can be applied to gold nanoparticle 40 nm-5 nm-40 nm assembly. 5 nm gold nanoparticles are clearly visibly under TEM and supported our assembly using quantum dots.

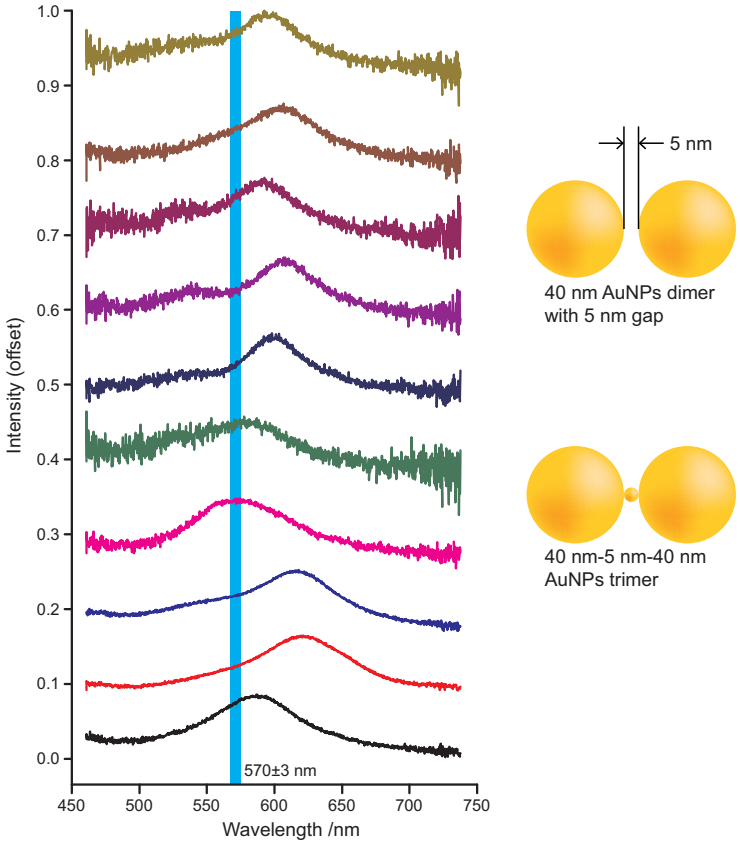

Figure 2.29: Dark field scattering spectra of gold nanoparticles (AuNPs) trimer assembly of 40 nm-5 nm-40 nm. Scattering spectra range AuNPs dimer with 5 nm gap was highlighted in blue at $570 \pm 3\ nm$([171]). In comparison to AuNPs dimers, the scattering peak of the trimers have red shift.

2.3.4 Summary

Due to the robustness of gold-thiol bonding, the gold nanoparticles functionalization is not always a problem. Protocols can be easily found and to be carried out with patience.[107] Here in this section, we're able to observed the surface enhanced Raman signal by assembling gold nanoparticles on the DNA origami nanopore structures. The design novelty of using two hollow sides allows two 40 nm gold nanoparticles embed in the structures with fixed separation. For the Au/QD heterostructures, we established a robust methods to assembly Au-QD-Au trimer without using DNA origami. Using same strategy, 40 nm - 5 nm - 40 nm Au-Au-Au trimer was also assembled. Scattering spectra measurement under dark field microscope show that the maximum resonances of different samples are in a big range, which imply the trimer structures can have different configurations when deposited on surface. With further improved assembly yield, investigating these structures with single molecular measurement can allow us to study the expected energy transfer and fluorescence enhancement events.

2.4 Challenges & Outlook

Self-assembled optically-active nanocomponents in a periodic way can exhibit collective optical responses. The spatial arrangement of nanoparticles with careful control offers a robust platform to study distance, orientation, and materials dependent energy transfer and coupling phenomena. In particular, DNA structures templated assembly in principle can achieve such assemblies high precision. In this chapter, aiming to reveal fundamental processes associated with energy and information transfer between individually addressable but photon-coupled nanoparticles, nanoparticles assemblies of homodimers, heterodimers, and heterotrimers are built. I demonstrated the newly-developed and the optimized existing surface functionalization methods for nanodiamonds, quantum dots, and gold nanoparticles. The functionalized nanoparticles then allow to assemble at site specific positions on the DNA structures with high accuracy. From optical measurements, we observed the preserved optical properties of nanodiamonds (NV color center) and quantum dots, as well as the surface enhanced Raman signal of Rhodamine 6G placed at the hot spot of gold nanoparticles dimers.

Though challenges remain to realize the designed functions, it is a big leap from the colloidal nanoparticles synthesis to site-specific assembly. With improved assembly quality, future it would be possible to realize the observation and interpretation of expected photonic and energy transfer events by single-molecule-sensitive optical measurements.

Chapter 3

DNA origami crystalline assembly

One initial motivation for the creation of DNA nanotechnology is to build a three dimensional framework for co-crystallization of guest nanocomponents. The evolution of this field has permitted the free design of DNA nanostructures as well as the templated assembly for external molecules. In this section, two DNA origami-based nanostructures are demonstrated aiming for three-dimensional DNA origami polymerization and incorporation of guest components.

3.1 Introduction

As described in subsection 1.3.2, bottom-up self-assembly has the potential to position various nanocomponents with an accuracy that top-down approaches can not achieve. Spatially arranged components with designed configurations and geometries allow to build advanced three dimensional materials to study the fundamental questions in light-matter interactions, energy harvesting, and the reaction pathways along the cascades.

To achieve such precision, the building blocks and their interactions have to be carefully engineered. Synthetic colloidal nanoparticles are one kind of widely-used building blocks due to their ease of synthesis of different sizes and shape, as well as the well-established surface modification methods. Spherical gold, silver or semiconductor nanoparticles can be densely packed *via* surface ligands based interactions such as electrostatic interactions[172], protein-protein interactions[173], and DNA base pairings[44][43]. Such packing methods have to be individually designed for different nanoparticle sizes and compositions due to the different surface chemistries.

To arrange arbitrary nanoparticles regardless of their sizes and compositions, the other approach is to assemble nanoparticles on pre-assembled templates. Programmable DNA assembly has developed designing methods such as DNA tiles[78], DNA origami[79], v-helix[174], and single stranded DNA tiles[82][175]. These methods provide the possibility to fold diverse building blocks with efficient size and shape control. The folded DNA structures then comprise the powerful toolbox for templated assembly. Moreover, the polymerization of monomeric structures can assemble micrometer-sized DNA structures

while the precision for addressable assembly is preserved.

In principle, any DNA conjugatable guest molecules can be placed on DNA structures in designed positions. DNA structures templated-assembly offers an ideal platform to study the distance-, orientation- dependent electronic, optical and enzymatic properties. Typically, selected oligonucleotides at desired positions are identified and modified either with functional residues (such as biotin or thiol), or with an extended sequences which serve as docking strands for the hybridization with DNA oligonucleotides on guest nanoobjects. So far, examples for templated-assembly on DNA nanostructures include nanotube cross-junction on flat DNA origami[176], chirally arranged gold nanoparticles on 24HB origami[32], and enzyme pairs of glucose oxidase/horseradish peroxidase on flat DNA structure[177].

However, current DNA templated-assembly is limited to two dimensions and small sizes. [77][86][93][94][100] Building blocks used in former attempts were not able to form 3D objects due to the geometrical design constraints. Branched DNA-tiles can be assembled into polyhedra by adding unpaired DNA spacers to increase the flexibility.[178] The flexible tile based monomer design lacks rigidity and sufficient control over directionality for large assembly. Single stranded DNA tiles can potentially grow into three dimensional objects.[175] However, it is difficult to arrange guest components in three dimensions because each single strand serves as an assembly unit, which cannot carry large guest molecules.

The first example of three dimensional DNA crystal used a building block of triangular shaped DNA duplex. Three 19 bases pairs long DNA duplex are interconnected through Holliday junctions to form a over-under, over-under, over-under structure. Rhombohedral shaped DNA crystals can be obtained by slowly annealing a 80 µL sitting drop in a thermally controlled incubator. After about 7 days incubation, 90 % volume of the drop diminished and DNA crystals formed at the end of cooling step. X-ray scattering shows that the three dimensional DNA crystal has a resolution down to 4 Å.[99] Small molecules such as Cy3 (molecular weight 767) or Cy5 (molecular weight 792) can be incorporated inside the crystal cavity with 103 nm^3 size.[179] Recently, Hao Yan group showed a different DNA-helix based monomer design for DNA crystallization.[180] Hendrik Dietz group systematically investigated the crystallization robustness of the triangle design even in a random pool of foreign 179 different DNA oligonucleotides.[181]

To spatially arrange large components, such as gold nanoparticles, a three dimensional DNA lattice with large unit cell is demanded. In addition, it should have high structural rigidity and can polymerize in three dimensions.

As mentioned in section 1.3.3, the computer assisted DNA origami technique has several advantages compared to the other DNA assembling techniques. An ideal DNA origami design for three dimensional assembly should bear the features of: (i) high structural rigidity, (ii) long edges to provide a large unit cell volume to host guest particles, and (iii) polymerizibility along for three axes in space.

In this chapter, two DNA origami designs are presented to exploit DNA structure three dimensional polymerization, with rationally designed building blocks and monomer-monomer interactions. Because of the large unit cells of these origami designs, guest components such as spherical nanoparticles of up to 20 nm diameter can be co-crystallized

into the origami lattices. In principle, external components can be organized at selected positions regardless of their sizes, compositions, and numbers. With this, we aim to scale up origami-based assembly to manufacture three dimensional photonic nanocrystals and study the emerging optical properties.

3.2 Cubic lattice

3.2.1 Structure design

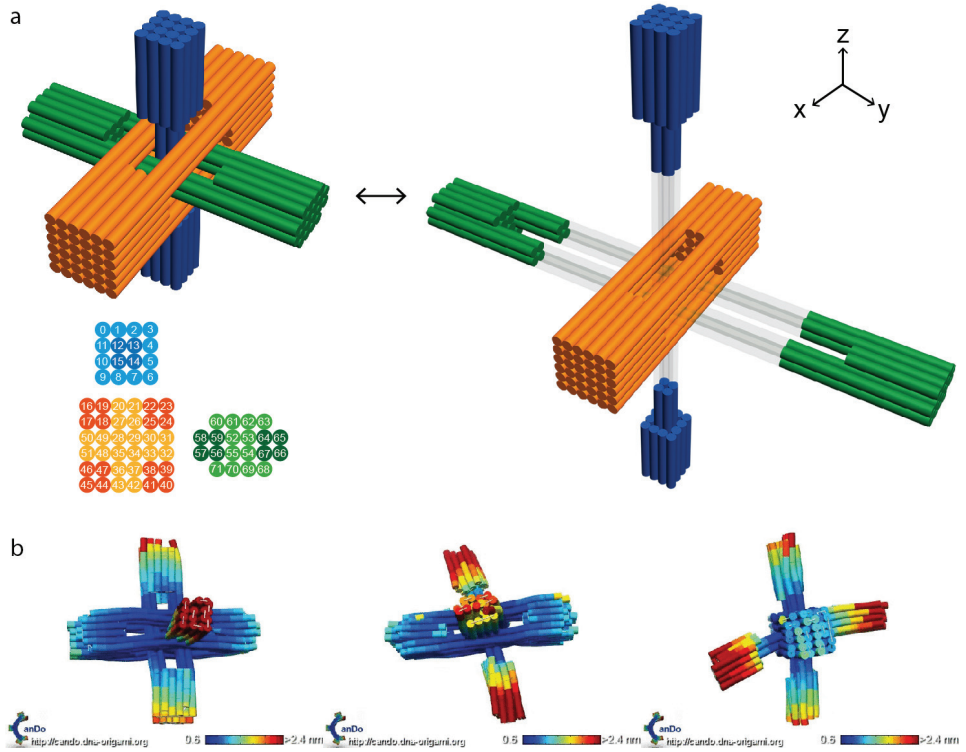

Figure 3.1: Schematic illustration of cubic structure design. a, three dimensional model of cubic design including three interlocked subunits. Orange subunit serves as body to maintain the structure and the blue and green subunits are connected by using only staples. b, CanDo simulation of the corresponding design using caDNAno.

Cubic lattice is a straight forward crystal geometry that can be designed with DNA origami. As shown in Figure 3.1, our origami structure consists of three subunits, highlighted in orange, blue and green which points to X, Y, and Z direction, respectively. The orange subunit for the X direction is designed to maintain the whole structure. The green and blue subunits are interlocked through the orange subunit. The three subunits are designed to be perpendicular to each other to fulfill the requirement of cubic lattice.

In detail, the cubic design comprises 71 duplexes that are packed in a square lattice (Figure 3.1 a cross section image), of which 16 duplexes in blue for the Z direction, 36 duplexes in orange for the X direction, and 20 duplexes in green for the Y direction. Duplexes in dark blue, dark orange, and dark green serve as the main body. All three bundles have their own shape complementary blunt ends for stacking introduced polymerization, blue stacks to blue, orange stacks to orange, and green stacks to green. Because the green subunit (Y) and blue subunit (Z) have thick ends but have the main body intercalated

through the orange subunit (X), over all the design can be considered as a self constrained structure.

To fold the structures properly, scaffold path of both of the green and blue subunits is re-routed. The two ends of the green subunit or the blue subunits are connected with only staples. Notably, the cubic structure is designed to be folded with one 8634 bases scaffold, not three separated ones. Using a one-pot reaction with one scaffold can avoid hierarchical assembly caused material loss after multi-step purifications. The caDNAno file was also analyzed with the online origami simulation tool CanDo. The simulation results fit well with the design of three intercalated subunits which are perpendicular to each other (Figure 3.1 b).

3.2.2 Folding and assembly

A 500 µL folding mix containing 10 nM of scaffold strand (8634 base-long scaffold), 100 nM of staple oligonucleotide (without endcap oligonucleotides for polymerization), 14 mmol L^{-1} $MgCl_2$ and 1×TE buffer (pH 8.2) was prepared and subsequently folded using the following temperature profile. The folding program is about 27 h: 15 min at 65 °C, cooling to 58 °C with a cooling rate of −1 °C per 5 min, 58 °C to 35 °C with rate of −1 °C per 1 h, and from 35 °C to 4 °C with rate of −1 °C per 5 min. The folded cubic structures were then purified by agarose gel electrophoresis.

For polymerization, 10 times endcap oligonucleotides were mixed with purified cubic structural monomers. The mixed sample were then incubated in 25 mmol L^{-1} Mg^{2+}[86], 1 × TAE buffer, at 35 °C for 50 hours. As different subunits (blue, green, or orange) shares different segments of the 8634 scaffold and have different sets of staples strands, as well as the polymerization oligonucleotides. When applying different set of polymerization oligonucleotides to the folded monomer origami, it can result in polymerization into certain directions.

Figure 3.2 shows the TEM characterization of single cubic monomer, one- and two-dimensional polymerizations. As TEM images give only one projection of the sample, the six branches in three dimensions are not fully visible. To confirm the successful folding, one dimensional assembly were carried out by adding different set of polymerization oligonucleotides. As shown in Figure 3.2 b-d, one dimensional polymerization can be realized in different directions. As the bundles at the X and Y directions are thicker and more rigid than in the Z direction, the polymerization in these directions are more rigid. The flexible assembly in the Z direction is most likely because 1), the main body at Z direction has only four helixes which is not rigid enough, 2) there is no scaffold spacer from the X subunit to Z, which might have too much tension to straighten the bundles in the Z direction.

Two dimensional polymerization can be carried out by adding the corresponding sets of polymerization oligonucleotides. Figure 3.2 e shows two dimensional polymerization in the X and Y directions. Cubic structures can be arranged in periodic patterns. However, the periodicity appears to be broken after about ten monomers due to the distortion, mismatched, and error assembly.

In the cubic origami lattice system, the interactions of stacking forces come from the

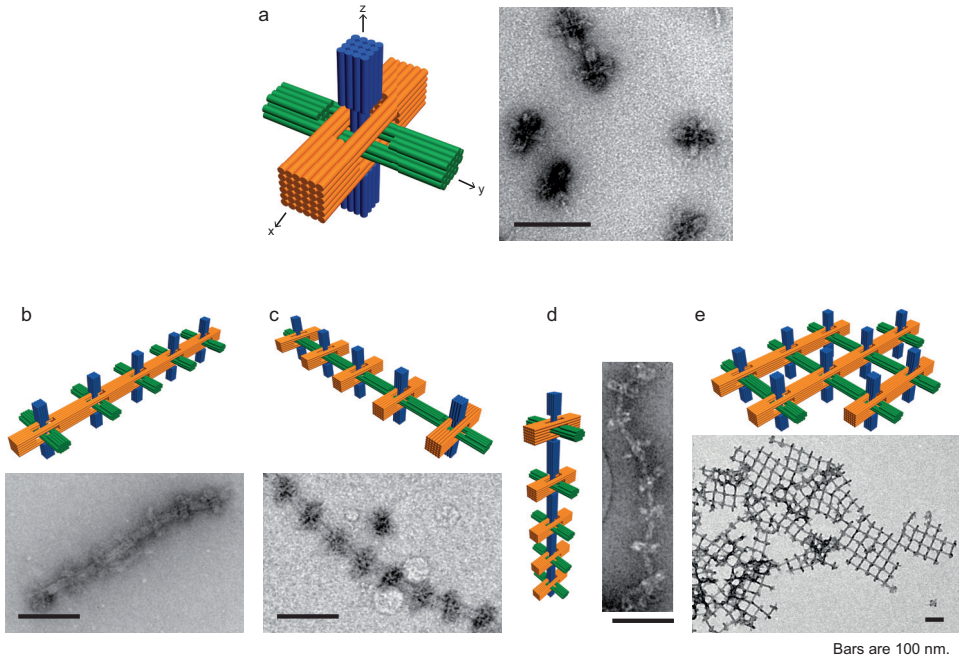

Figure 3.2: TEM images of cubic structures. a, gel purified monomers. b-d, one dimensional polymerization to X, Y and Z directions if different sets of end cap oligonucleotides were added. e, two dimensional polymerization using end cap oligonucleotides at X and Y directions.

shape complementary blunt ends, which are created through the hybridization of polymerization oligonucleotides to the corresponding scaffold loop at the ends. To optimize the conditions for large scale polymerization, constant temperature in a range from 33 °C to 40 °C incubation has been applied. Figure 3.3 shows the TEM images of two dimensional polymerization at different temperatures. The origami assemblies tend to form clusters at lower temperature and regular pattern at higher temperatures. Higher temperature inhibits the binding of the polymerization oligonucleotides to the scaffold loop and decrease the possibilities to form shape complementary blunt ends. A proper high temperature therefore can generate a weak force between the monomers. The generated weak interactions during the polymerization permits the constant binding-unbinding of monomers to self-adjust their orientations in order to construct highly-ordered assemblies. However, when the temperature is over high, it leads to even weaker interaction and prevent the polymerizations. On the other hand, when a lower temperature that is favourable for blunt ends forming, the introduced strong stacking forces prevent the crystal self-adjustment. From the TEM imaging of two dimensional polymerization, an optimized temperature of 37 °C is determined. Due to the bundle flexibility in Z direction, polymerization at three dimensions was only found to be a giant cluster. Partially this is due to the limitation of TEM imaging which relied on the collection of transmission electrons and requires a flattened, dry and thin sample. It will be difficult to reconstruct the three dimensional

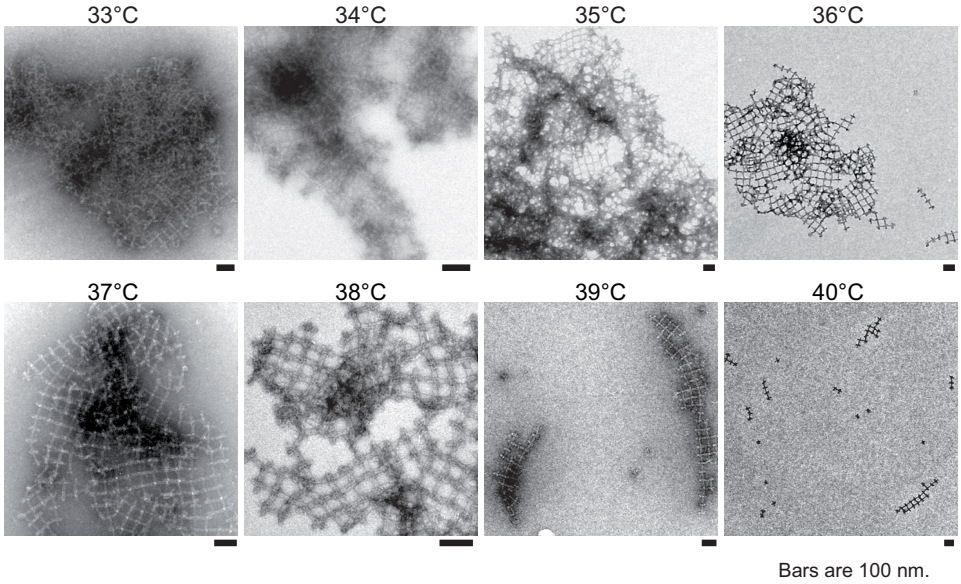

Figure 3.3: Temperature dependent polymerization. Lower temperature leads to more clusters, and higher temperature decrease the stacking strength and inhibit polymerization. An optimized polymerization temperature is about 37 °C in 25 mmol L^{-1} Mg^{2+}, 1 × TAE buffer for 50 hours.

shape from collapsed origami lattices.

3.2.3 Summary

Cubic lattice is the most common geometry in crystallography. In this section, a cubic origami design and its polymerization are presented. Polymerization at one, two dimensions to periodic arrays are realized in a short range after incubation at certain temperature. The low quality of elementary units is most likely the main barrier to achieve large scale assembly. The non-spacer connection between each subunits may cause more tension at the interconnections sites. Such tension will also prevent the engagement of staple strands to corresponding scaffold loop and lead to a low monomer folding yield.

In addition, the size of origami structure is confined by the length of DNA scaffold. In the cubic design, 8634 bases long scaffold is used. Still there are not enough scaffold to build a thick and rigid Z direction bundles. A flexible Z direction bundle maybe the main bottleneck to assemble a stable three dimensional structure. Different bundles numbers can also cause different stacking strength at three directions. In particular when using incubation at a constant temperature, it can have different effect on blunt ends forming. Future design should take account of these factors. For example, a symmetric origami design with equally distributed three bundles can generate similar stacking strength at three directions.

3.3 Rhombohedral lattice

3.3.1 Structure design

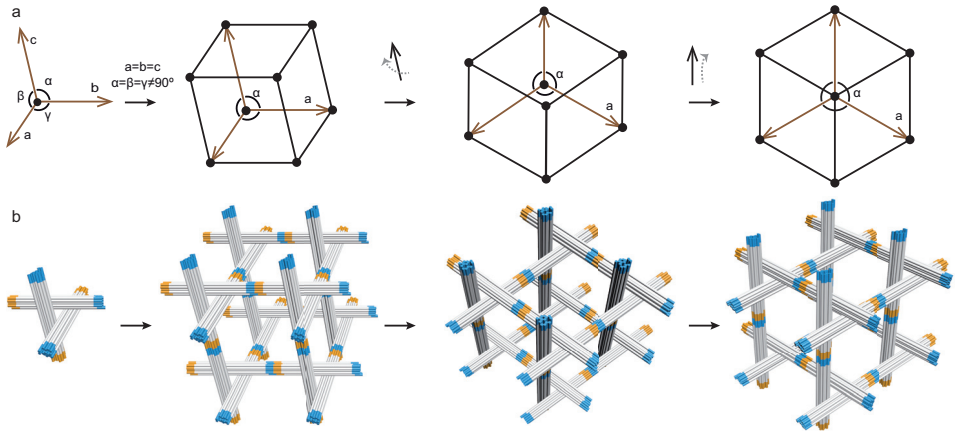

Figure 3.4: Schematic illustration of rhombohedral lattices. a, rhombohedron can be a special case of cubic lattice but with same value of axial distances and angles. After two times rotation, three fold symmetry are visible. b, the corresponding layout of the origami design. From left to right, triangular origami of three same edges; eight triangular monomer stacked from orange ends to blue ends form a single unit cell; after two times rotation, it shows same pattern as shown in panel a.

As mentioned in the summary of subsection 3.2.3, we aim for a structure that can be polymerized in three directions with bundles sharing a similar stacking strength in three directions. Inspired by Chengde Mao & Ned Seeman's crystal design[99], a triangular origami-based monomer is presented. Figure 3.4 a shows the general idea of a rhombohedral lattices design (from left to right). Starting from a single unit, vectors parameters of rhombohedral lattices meet the conditions of axial distances $a = b = c$, while axial angles $\alpha = \beta = \gamma \neq 90°$. Started from a front view of a rhombohedron, which can be considered as a stretched cube with six identical faces. Brown lines are the edges at the behind. After stepwise rotation, a top view projection shows the three fold symmetry of the rhombohedral lattice. Figure 3.4 b shows the corresponding layout of rhombohedral lattices built from DNA origami structure. An ideal monomer design contains three parts of equal length and bundle numbers. The connection points between each bundles should also be symmetric to meet the requirement of $\alpha = \beta = \gamma$. Monomers then can be stacked together to form a rhombohedral unit cell.

Figure 3.5 shows the design details of the triangle DNA origami structure. Each edge is a 14-helix bundle (14HB) with helices packed on a honeycomb lattice. The design was completed on the software of caDNAno. Initially, three 14-helix bundles (14HB) were designed by selecting scaffold path in honeycomb-type lattice (14HB cross-section). These three 14HB have the same length and shared the same blunt-ends shape. Secondly, 14HB were

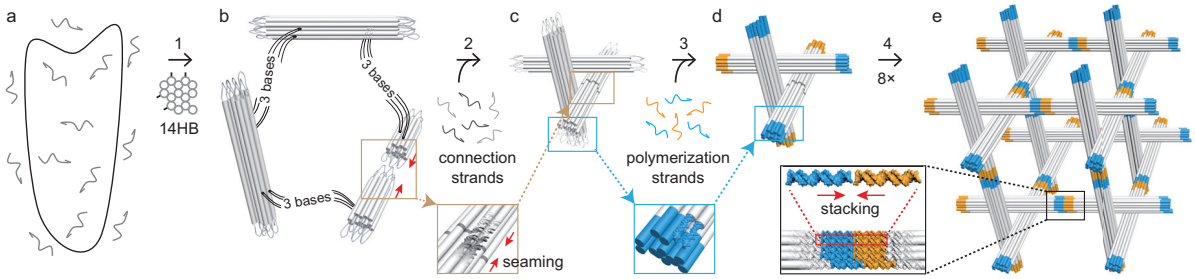

Figure 3.5: Structural details of the triangular DNA origami structure and the sequential workflow to form the triangular DNA origami monomer and the DNA origami lattices. a, The mixed sample of one 8634 nucleotides long DNA scaffold with the core staple strands (without connection oligonucleotides and polymerization oligonucleotides). Step 1: the mixed scaffold and staple strands of core oligonucleotides were annealed from 65 °C. Cross section image shows the honeycomb design of the 14 helix bundles and the scaffold interconnection positions. b, The interconnection between each 14 helix bundles with 3 nucleotide long scaffold spacers. Step 2: during folding, connection oligonucleotides are added to link the unjoined two parts of one 14 helix bundle. The folded triangular DNA origami monomer can be purified from agarose gel electrophoresis or PEG precipitation. c, The successfully folded triangular DNA origami monomer (without polymerization oligonucleotides). Step 3, polymerization oligonucleotides are added to purified origami monomer for creating blunt ends. d, The triangular DNA origami with blunt ends created. Step 4, triangular DNA origami monomers with shape complementary blunt ends will polymerize to three dimensional lattices *via* stacking. Due to three equally designed 14 helix bundles, the triangular DNA origami bears three fold symmetry which allows any of the blue ends to interact with any of the orange ones. e, The unit cell consisting of eight triangular DNA origami monomers.

interconnected at selected positions by using force crossovers of three bases scaffold spacers. Then we re-routed the scaffold path to apply a circular virus-based single stranded DNA. The carefully selected spacer positions and the short brevity of the scaffold loop resulted in a self-restricting over-under, over-under, over-under origami triangle structure. Thirdly, staples were generated accordingly and were broken manually into shorter segments of 18 to 50 bases. Oligonucleotides were sorted into different groups, core oligonucleotides, connecting oligonucleotides, end cap oligonucleotides (for polymerization). Polymerization was achieved by using stacking interaction of shape complementary blunt-ends. Blunt-ended helices highlighted in blue can stack to any ends in orange, hence the origami monomer has a three-fold rotational symmetry (C3 symmetry) as designed. Such symmetry will increase the chance of correct polymerization by tolerating three-fold orientations for the collision of free monomers, therefore giving a larger lattice with fewer errors. From our design, the interplanar spacing is about 199 bp, which equals to the length of each 14HB. The interaxial angles were assumed to be about 120 degrees. This would correspond to an inside cavity size of about 50 nm × 50 nm × 60 nm per unit cell.

3.3.2 Single object folding

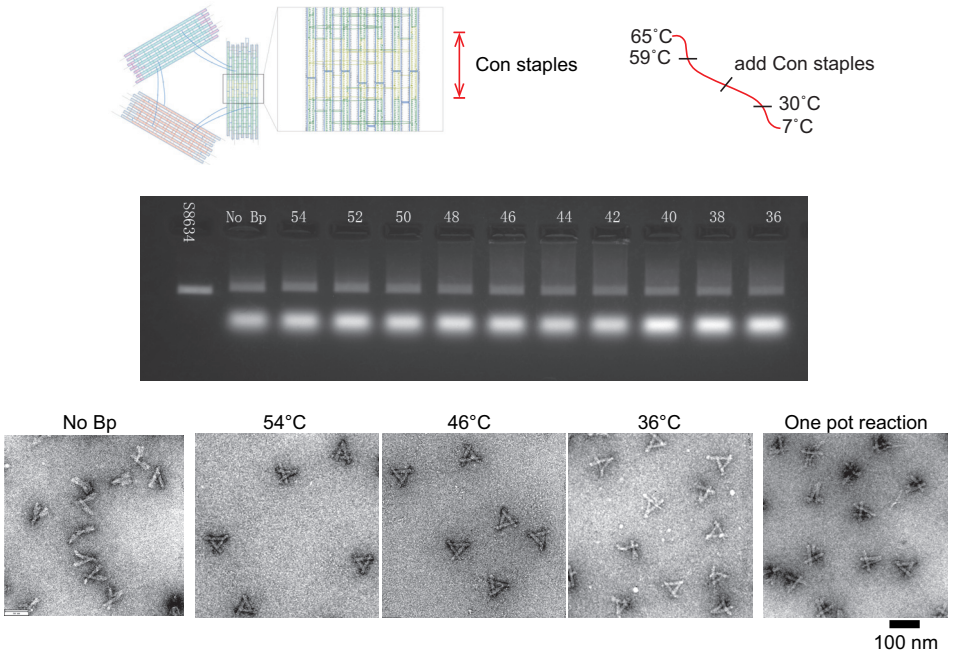

Figure 3.6: Folding conditions optimization. The one pot reaction resulted in a mixture of rightly folded triangular origami and A-shaped origami, while without connection oligonucleotides, an open structure was formed. An increased folding yield was achieved by adding connection oligonucleotides during the folding. However, no proper temperature was found to achieve 100% monomeric folding.

We found that a one-pot folding reaction (scaffold mixed with all the staples) resulted in a low yield of properly folded triangular structures. This is most likely due to the fact that it is difficult to bypass the kinetic trap during the folding of the topological triangle structures. In order to solve this problem, the scaffold path was re-routed and the triangular structure was folded with certain connection oligonucleotides injected during folding.(Figure 3.5).

In detail, we re-arranged the scaffold path and made one of the 14 helix bundles being connected by only staples (connections oligonucleotides). In a typical folding, scaffold with all rest oligonucleotides except polymerization-oligonucleotides and connecting-oligonucleotides annealed from 65 °C. Connection oligonucleotides were added at a certain temperature during the folding (Figure 3.5, annealing program is as described in subsection 3.2.2). The folded origami structures were purified with agarose gel electrophoresis.

As shown in Figure 3.6, one pot reaction yielded a mixture of rightly folded ones and the irregular A shaped structures. When no connection oligonucleotides were added, an open triangular structure was formed. To optimize the folding process even more, different addition temperature for connection oligonucleotides were investigated. The TEM images

shows that addition temperature of 54 °C improved the folding yield of the triangular origami in comparison to one-pot reaction. We also found the addition temperatures can be in a big range, from 54 °C to 44 °C but with folding yield of about 60%. However, as TEM only gives the projection of the structures, the over-under design style can not be solved with TEM. Choosing 54 °C for connection oligonucleotides, the folded triangular DNA origami structures were purified from from excessive staples and clusters *via* agarose gel.

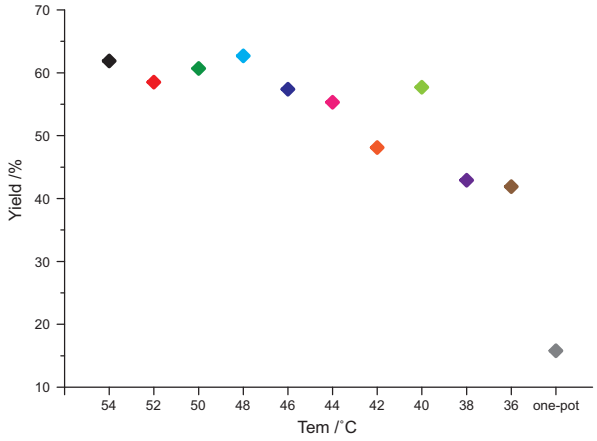

Figure 3.7: Statistics of correctly folded triangular DNA origami structures folding with connection oligonucleotides added at different temperatures. One-pot reaction with all staples folded together give a lowest assembly yield of 15.6%. With connection oligonucleotides injected at different temperature from 36 to 54 °C, the folding yield of triangular DNA origami structures can be improved to about 60%.

3.3.3 3D origami crystalline assembly

To enable 3D polymerization, the purified origami monomers and the polymerization-oligonucleotides were incubated at constant temperature for 3 - 4 days. Hybridization of polymerization-oligonucleotides to free scaffold loops at each 14HB ends creates the shape complementarity blunt ends, where blue ends stack to orange ends (Figure 3.4 b). Successful crystallization requires apposite weak interactions between monomers to obtain correct transient binding and dissociation rates for both nucleation and growth. In our system, these stacking forces furthermore are highly dependent on the salt concentration and the temperature. Thus the stacking strength can be regulated indirectly by tuning one or both of these parameters.

As mentioned above, a great advantage of the triangular design with C3 symmetry is that the polymerization conditions have the same effects in all three directions. Under same buffer conditions (11 mmol L^{-1} Mg^{2+} and 0.5× TAE, pH 8.2 buffer), lower temperature favors the blunt end formation with increased stacking interaction which will inhibit the

dissociation of incorrect binding, while higher temperatures result in a much more fragile interaction which prevents the growth.

Through fine tuning, it was found that the critical temperature for polymerization is about 47 °C. The polymerized origami structures were then characterized by both TEM and SEM (Figure 3.8). For this, polymerized origami crystals were directly deposited on TEM grids and stained with diluted uranyl acetate. TEM images showed a regular, hexagonal pattern. We infer that due to the obtuse interaxial angle, polymerized origami structures are easier to expand on 2D to form applanate structures. When dried and collapsed on substrates, they tend to exhibit hexagonal lattices from a top view perspective. As a comparison, Figure 3.11 gives a 3D model of the structures of different viewpoints. While regular bright spots in TEM images indicated the ordered assembly of origami lattices in 3D, SEM revealed the surface morphology. Samples on TEM grids were sputtered with gold/platinum for SEM analysis. Figure 3.8 d shows similar hexagonal patterns that are consistent with TEM observations. Zoomed-in images show the over-under, over-under, over-under design of single tensegrity triangle origami with at least three layers visible. From low magnification TEM and SEM micrographs, crystallinity can be seen more clearly (Figure 3.12-Figure 3.13). There are distinct boundaries between hexagonal patterns and domains of hexagonal pattern with several micrometer scales were observed.

To get more insights about the 3D structures as well as to demonstrate the possibility to host guest molecules, gold nanoparticles (AuNPs) were attached at the center of triangular DNA origami. Purification and conjugation of AuNPs to origami monomer followed the published procedures.[107] The polymerization-conditions were as for the non-modified structures. TEM analysis once again revealed a hexagonal pattern, in this case containing the AuNPs as desired in groupings at three hexagonal vertices (Figure 3.8 f). The numbers of nanoparticles indicated the number of origami layers in the lattice. Note that only crystal growth of only a few layers showed a perfect hexagonal patterning and thicker assembly tended to show a different layout. Figure 3.8 g shows the gold nanoparticles in a tilted origami lattices hence exhibiting nanoparticles rows.

Small-angle X-ray scattering (SAXS) data collected from the resultant AuNP-origami assemblies showed several peaks at ordered positions with different intensities indicating a 3D periodic nanoparticles arrangement. In collaboration with Stefan Fischer and Kilian Frank, data fitting suggested a rhombohedral lattice, where $a = b = c = 665\,\text{Å}$ and $\alpha = \beta = \gamma = 110.8°$[45], which is in a good agreement with our design and is comparable to the reported DNA duplex crystal[99]. Some of the scattering peaks were also visible for the pure DNA lattice. However, they are less pronounced as DNA soft materials scatters less than metal materials.

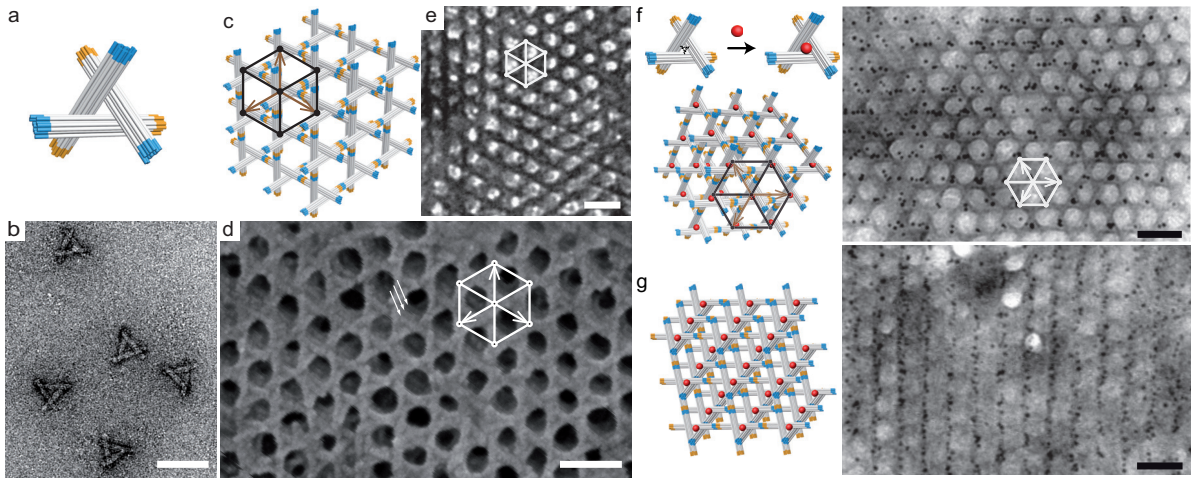

Figure 3.8: Transmission electron microscopy and scanning electron microscope images of single and polymerized triangle DNA origami structures. a & b, TEM images of agarose gel purified tensegrity triangle DNA origami monomers without polymerization oligonucleotides. c & e, TEM image of polymerized origami crystalline. The regular hexagonal lattices indicated the periodic assembly. c & d, SEM images of polymerized origami crystalline. Hexagonal pattern is consistent with TEM images. White color arrows pointed out different layers of the assembly and here at least three layers are visible. f & g, TEM images of DNA origami lattices incorporated with gold nanopartilces. Depends on how the lattices dried on surface, they can exhibit gold nanoparticles groups in the hexagonal pattern, or tilted gold nanoparticles lines.

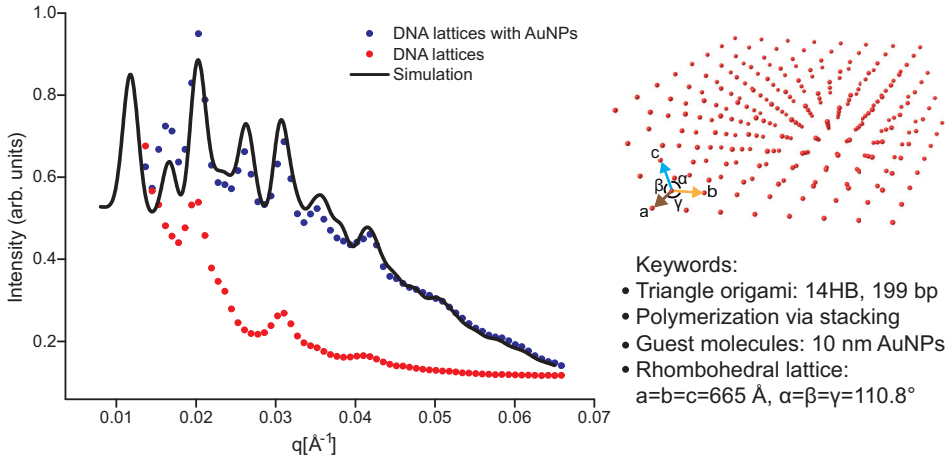

Figure 3.9: Small angle X-ray scattering data of gold nanoparticles lattices (black dots) and DNA origami lattices (red dots). Data fitting of the SAXS data of gold nanoparticles lattice suggested the rhombohedral lattices with lattice constants of $a = b = c = 665\,\text{Å}$ and $\alpha = \beta = \gamma = 110.8°$.

3.3.4 Summary

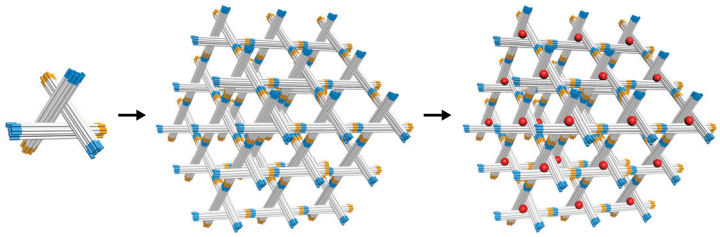

Figure 3.10: Table of contents of triangular origami assembly and gold nanoparticles incorporation.

The research area of DNA nanotechnology is triggered by the idea of programming branched DNA junctions as scaffold to orient guest molecules. The simple rule of complementary DNA hybridization provides access to the manipulation of nanocomponents with efficient control. Inspired by Chengde Mao & Ned Seeman's triangle motif, here the triangular DNA origami structures can polymerize into 3D micrometer-sized periodic lattices. It also shows a prototypical example to scale up DNA origami-based self-assembly. Characterization confirmed the assembly of DNA origami lattices and the origami lattice hosting guest nanoparticles. Instead of using nanoparticles as building blocks for crystalline assembly[43][44], our DNA origami frameworks can simultaneously host different sizes and types of guest molecules for co-crystallization. Moreover, fully programmable DNA origami structures provide various elementary units with controlled size, shape and interactions for arbitrary lattice geometries. It can also build a robust platform to study the crucial aspects during crystallization such as controlled nucleation and growth, coordinated assembly, as well as the applications in photonic crystal and 3D metamaterials[182].

To demonstrate the universality for co-crystallization of multiple nanocomponents, further experiments aim to host different sizes and shapes of gold nanoparticles (Figure 3.15), as well as different numbers of gold nanoparticles. In order to obtain origami crystal with high quality, homogeneities of single structures have to be improved and the polymerization conditions need to be optimized to achieve the growth of DNA origami single crystal.

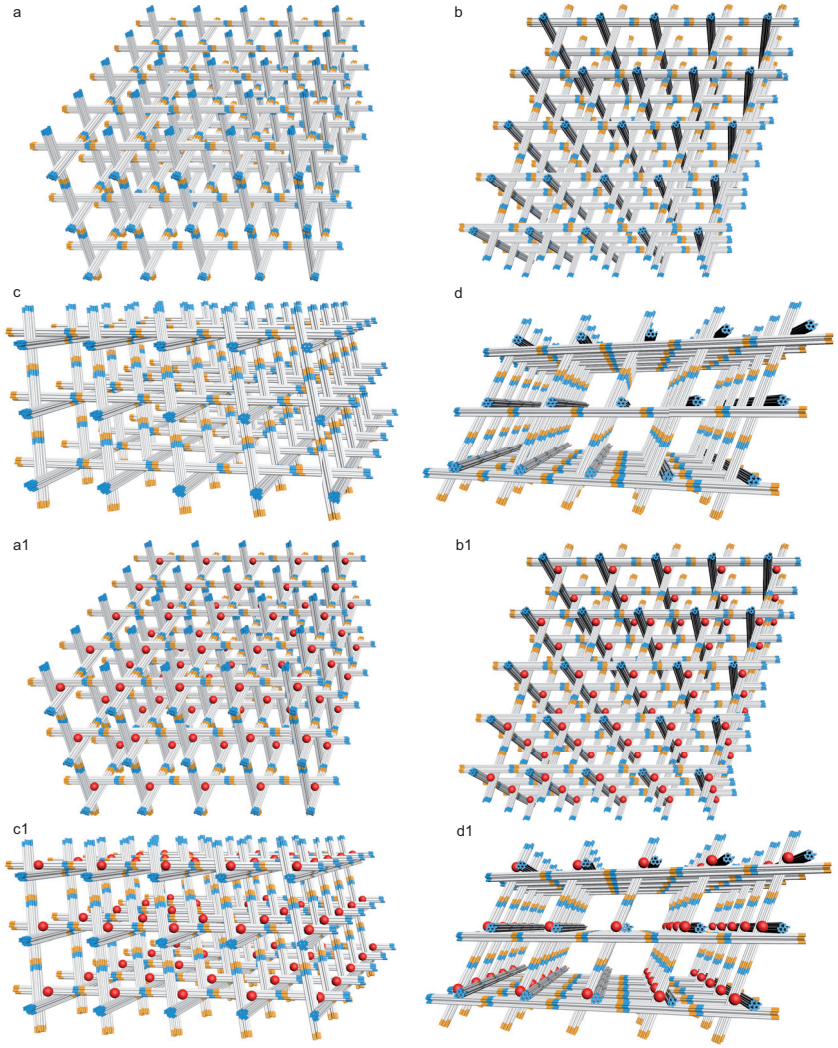

Figure 3.11: 3D model of origami lattices with and without gold nanoparticles incorporated from different viewpoints.

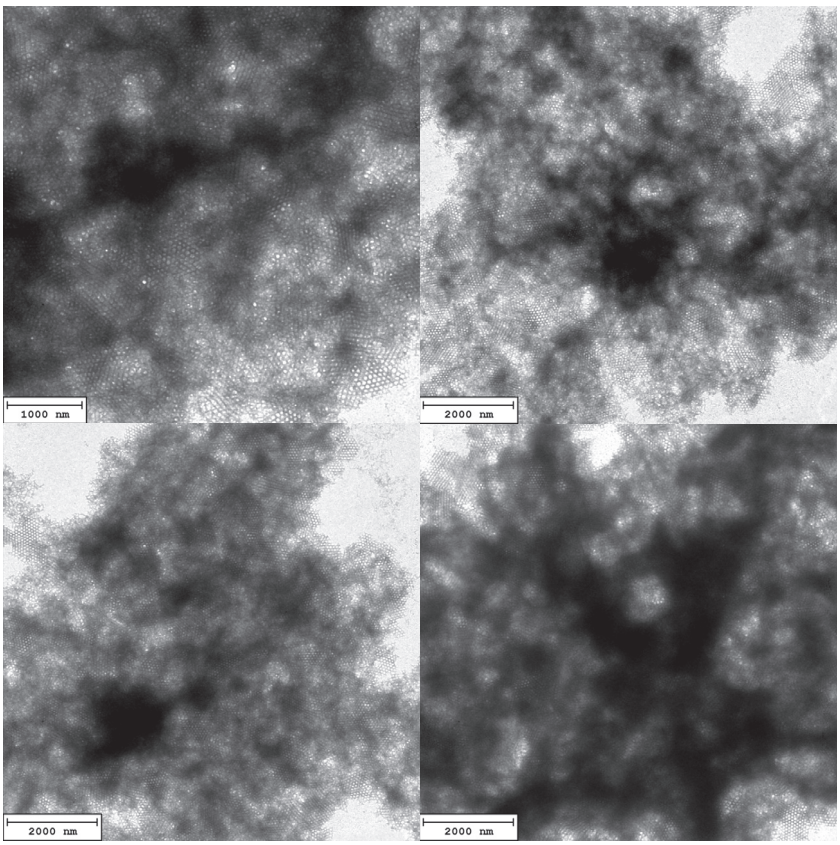

Figure 3.12: TEM images of zoomed-out view of DNA origami lattices.

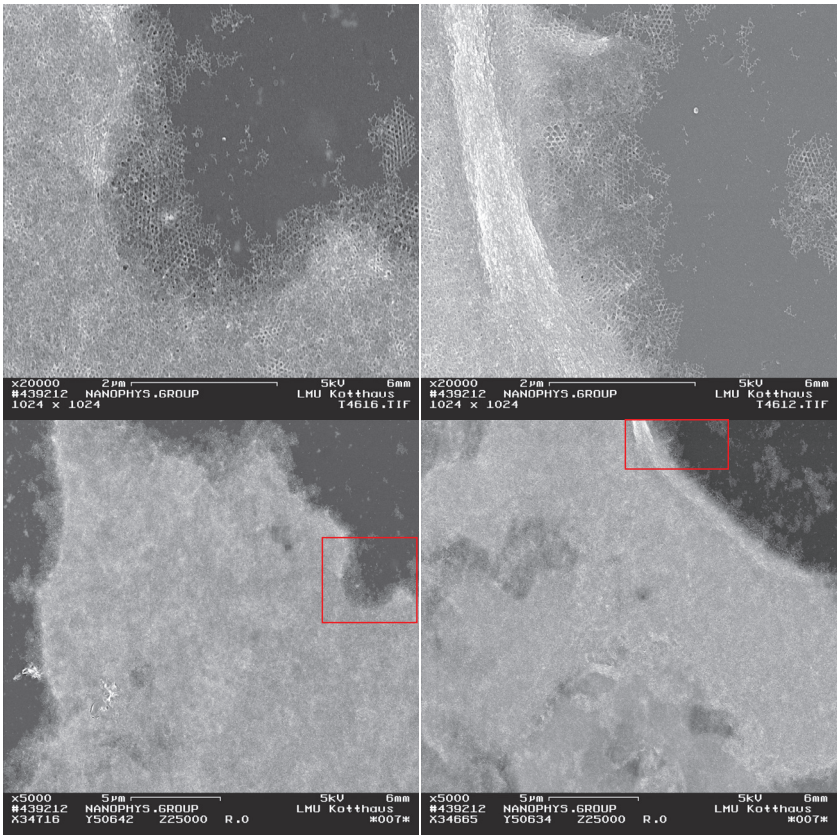

Figure 3.13: SEM images of zoomed-out view of DNA origami lattices. Images above are the zoomed in view of area highlighted in red square.

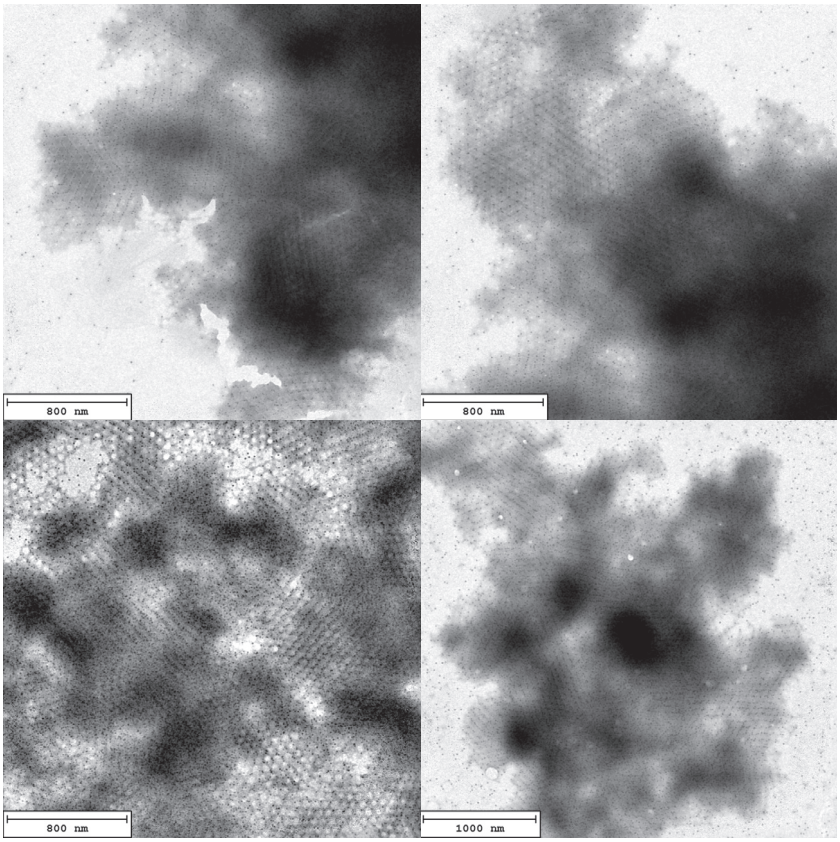

Figure 3.14: TEM images of zoomed-out view of DNA origami lattices with 10 nm gold nanoparticles.

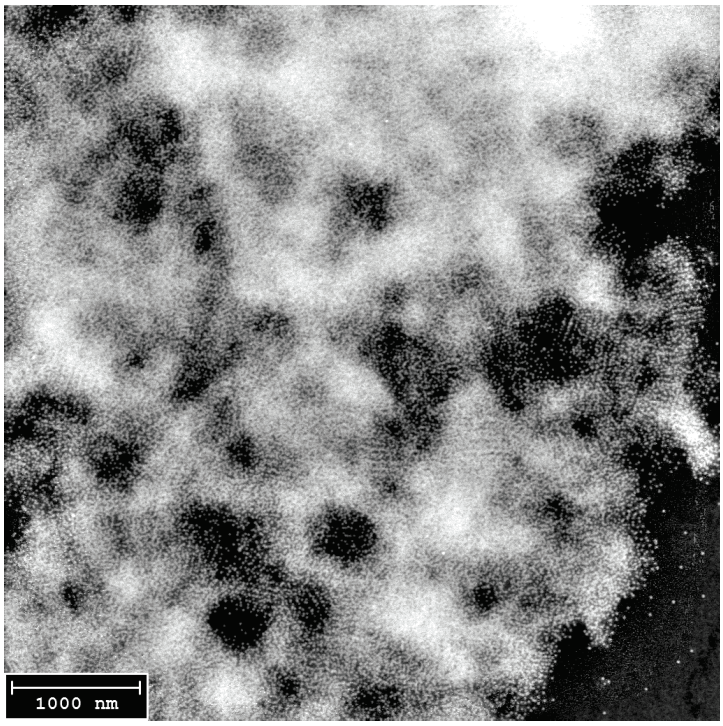

Figure 3.15: TEM images of zoomed-out view of DNA origami lattices with 20 nm gold nanoparticles without staining (contrast inverted).

3.4 Challenges & Outlook

Structural DNA nanotechnology permits the designing, folding, and purification of DNA based nanostructures in a range of several ten to hundred nanometers. Templated-assembly on DNA structures allows the precise positioning of guest nanocomponents into different assemblies. Moreover, polymerization of monomeric DNA nanostructures creates periodic arrays in two or three dimensions, with the capability of templated-assembly being preserved.

This chapter focuses on DNA origami based nanostructure design, polymerization, and the incorporation of nanoparticles. The cubic lattice represents a common and simple crystal geometry. Towards this kind of crystal geometry, a DNA origami structure that in principle can polymerize to cubic lattices is designed. However, due to the low folding yield of the monomer and the uneven stacking strength at three directions, periodic assembly is achieved only in a short range.

The second design is inspired by Chengde Mao & Ned Seeman's DNA duplex based triangular motif. In their design, three 19 bp duplex are interconnected using three Holliday junctions. The over-under style enables the polymerization in three dimensions. Using DNA-origami technique, a big version of such triangular structure is designed. The three edges of 14HB are connected by three bases scaffold spacers. The origami monomer could be folded from one-pot reaction, which avoided the time-consuming hierarchical assembly. Incubation at constant temperature for a certain time, the triangular structures polymerize into three dimensional origami lattice of tens of micrometers size. The large unit cell also allows to host large guest components. Both 10 nm and 20 nm gold nanoparticles can be co-crystallized into the origami lattices. Characterization of EM and small angle X-ray diffraction confirmed the formation of origami lattices and the successful incorporation of gold nanoparticles.

Catalyzed by the idea to orient guest molecules on DNA frameworks from Ned Seeman, DNA nanotechnology has grown rapidly in the last three decades. The polymerization of triangular DNA origami nanostructures to three dimensions presented here expands the dimensionality and scale of DNA-based self-assembly. Moreover, the design principle exploits the possibility to create three dimensional lattices based on programmable DNA-based building blocks of controlled size, shape, and interactions. This will enable the creation of a robust crystallization system with defined unit cell and cavity sizes. We envision that with guest molecules spatially arranged in a three dimensional matrix, light-matter interaction and reaction pathways among the guest molecules can be carefully engineered with desired configurations. The insights obtained from such complex systems will help to construct three dimensional structures for various purposes and applications.

Chapter 4

Conclusion

This thesis demonstrates DNA enabled self-assembly, using the example of arranging optically-active nanocomponents on individual DNA structures as well as on three dimensional origami lattices.

To place nanocomponents on DNA templates, the key is to find a linker to attach them to DNA. These linkers can be complementary DNA oligonucleotides, neutravidin, or other dual linkers which have dual binding sites to nanoparticles and docking strands on structures. Modified nanoparticles of interests should also be dispersible in ionic strength without aggregation. Because a certain amount of Mg^{2+} concentration (for example $11\,\mathrm{mmol\,L^{-1}}$) in buffer is often required for stabilizing DNA nanostructures. Here, I introduced the surface coating modification methods for nanodiamonds (with enclosed nitrogen-vacancy centers) using denatured denatured bovine serum albumin (BSA) that is functionalised with PEG3000-biotin. The stabilizing forces include charge-charge and hydrophobic interaction between negatively charged nanodiamonds surface and positively charged BSA backbones. Site specific assembly on DNA structures is realized with the help of neutravidins. For colloidal quantum dots, we find that the important residues for QDs modification are not only thiol atoms from PTO (PhosphoroThioate Oligonucleotides)-DNA but also the adenine (A) or guanine (G) bases. When PTO modified cytosine (C) and thymine (T) are used to modify QDs, it does not give a condensed single QDs band on agarose gel. This finding simplifies the QDs surface modification and allows to establish a robust method to assemble gold-QD-gold hybrid trimers.

To spatially arrange nanocomponents in three dimensional matrices, two kinds of DNA origami structures are designed. Periodic assembly with DNA origami building blocks are demonstrated. In particular, the triangular origami structure with three-fold symmetry can polymerize into three dimensional frameworks. Their large cavity size allows to incorporate guest nanocomponents for co-crystallization. Using gold nanoparticles, the nanoparticles co-crystallization is confirmed by electron microscope and small-angle X-ray scattering. Although with only poly-crystalline assembly is achieved, this structure may inspire other types of monomer design towards large periodic DNA structures.

Structural DNA nanotechnology has shown the power to fabricate DNA nanostructures with rationally designed geometry, size, and topology for templated-assembly for

guest components. With the efforts from all scientists in the field, further improvement can be realized in DNA nanostructural quality, dynamic assembly, scaled-up assembly, as well as the expanded applications in templated-assembly.[183] The design principles and characterization techniques in DNA nanotechnology can be also used in other research fields with self-assembling materials such as peptide nucleic acid (PNA)[184] or locked nucleic acid (LNA)[185], as well as rationally designed protein motifs.[186][187]

Appendix: scaffold/staples layout of DNA origami structures design

1. Nanopore structure origami design
2. Cubic structure origami design
3. Triangular structure origami design

All DNA origami structures are designed with the help of caDNAno (http://cadnano.org).

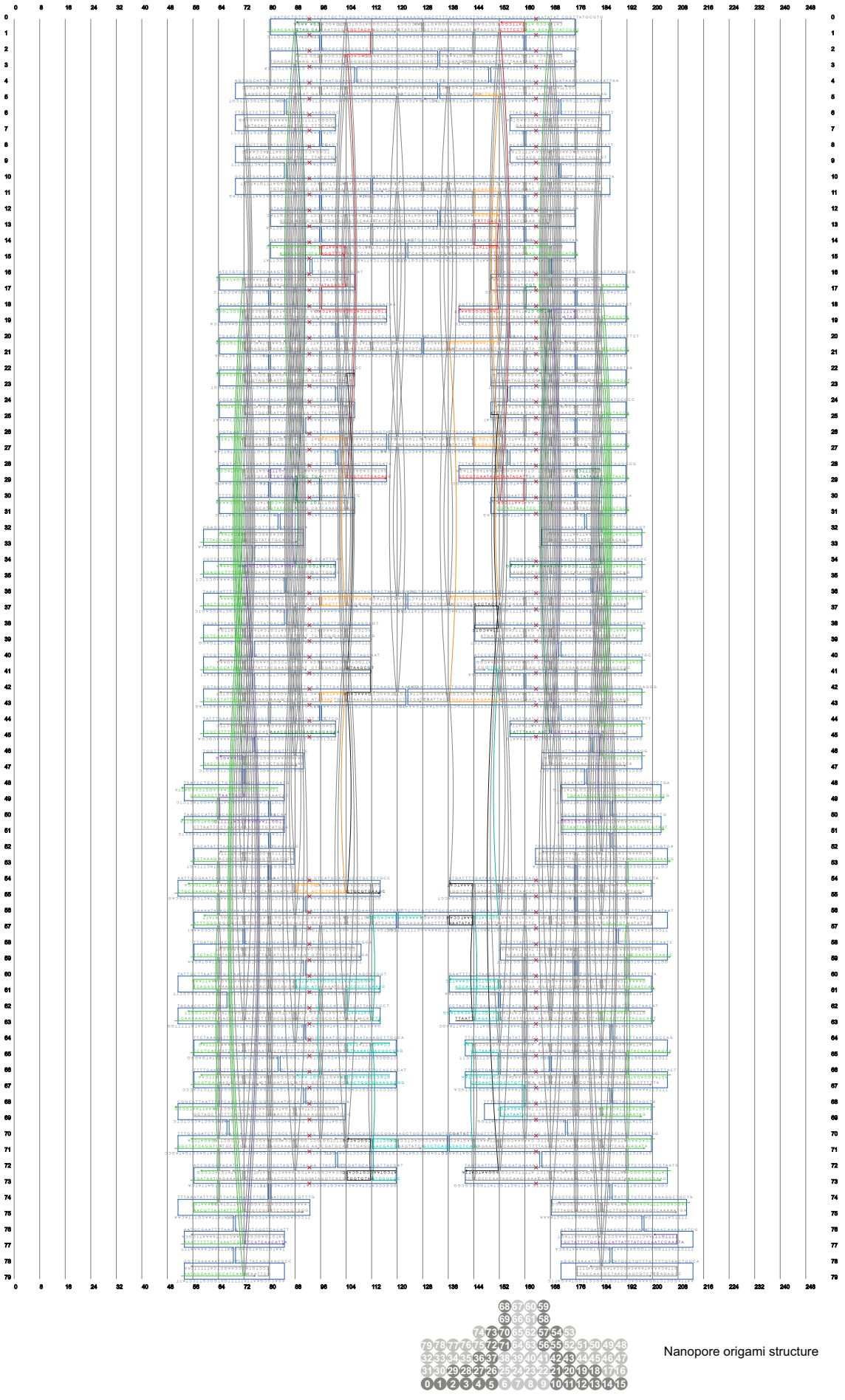

Nanopore origami structure

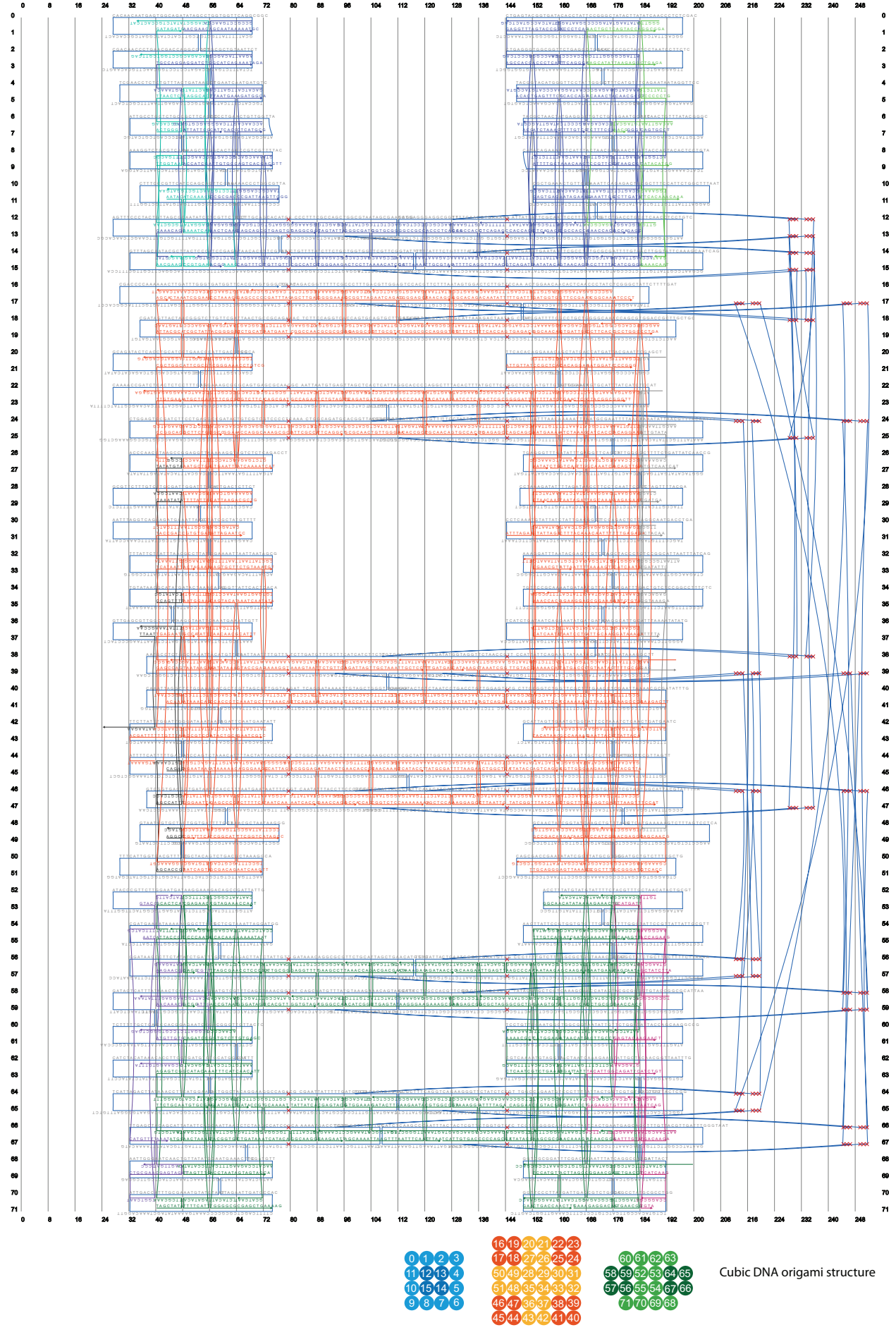

Cubic DNA origami structure

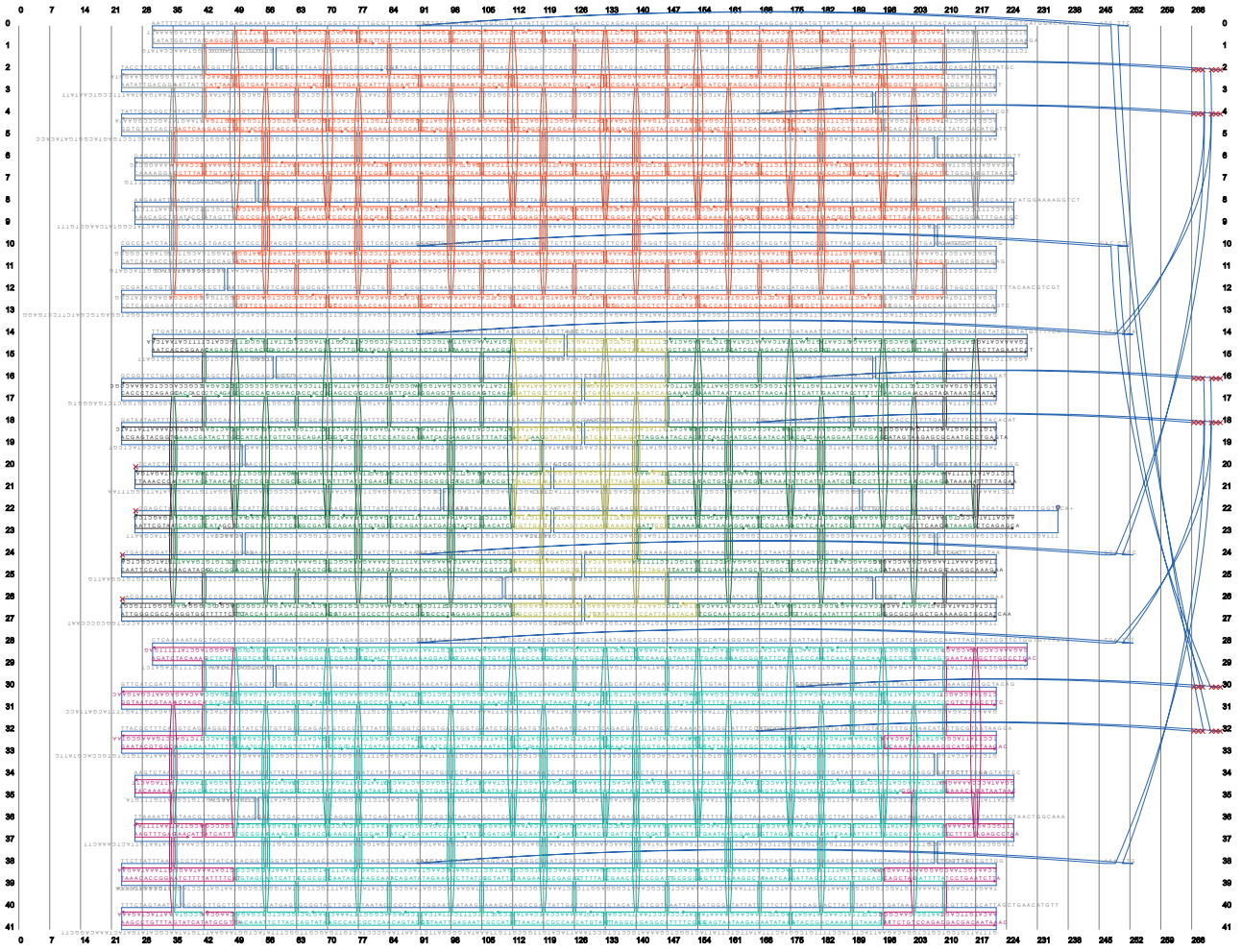

Triangular DNA origami structure

Bibliography

[1] Cao, G. & Wang, Y. *Nanostructures and Nanomaterials: Synthesis, Properties, and Applications*. World Scientific series in nanoscience and nanotechnology (World Scientific, 2011). (page 1)

[2] Feynman, R. P. There's plenty of room at the bottom. *Engineering and Science* **23**, 22–36 (1960). (page 1)

[3] Freestone, I., Meeks, N., Sax, M. & Higgitt, C. The lycurgus cup — a roman nanotechnology. *Gold Bulletin* **40**, 270–277 (2007). (page 1)

[4] Koch, C. Synthesis of nanostructured materials by mechanical milling: problems and opportunities. *Nanostructured Materials* **9**, 13–22 (1997). (page 3)

[5] Eigler, D. M. & Schweizer, E. K. Positioning single atoms with a scanning tunnelling microscope. *Nature* **344**, 524–526 (1990). (page 3)

[6] Liu, N., Tang, M. L., Hentschel, M., Giessen, H. & Alivisatos, A. P. Nanoantenna-enhanced gas sensing in a single tailored nanofocus. *Nature Materials* **10**, 631–636 (2011). (page 4)

[7] Yu, N. & Capasso, F. Flat optics with designer metasurfaces. *Nature Materials* **13**, 139–150 (2014). (page 4)

[8] Liu, N. & Giessen, H. Coupling effects in optical metamaterials. *Angewandte Chemie International Edition* **49**, 9838–9852 (2010). (page 4)

[9] Luk'yanchuk, B. *et al.* The fano resonance in plasmonic nanostructures and metamaterials. *Nature Materials* **9**, 707–715 (2010). (page 4)

[10] Wang, W. *et al.* Use of the interparticle i-motif for the controlled assembly of gold nanoparticles. *Langmuir* **23**, 11956–11959 (2007). (page 5, 6)

[11] Slot, J. W. & Geuze, H. J. A new method of preparing gold probes for multiple-labeling cytochemistry. *European Journal of Cell Biology* **38**, 87–93 (1985). (page 6)

[12] Jana, N. R., Gearheart, L. & Murphy, C. J. Wet chemical synthesis of high aspect ratio cylindrical gold nanorods. *The Journal of Physical Chemistry B* **105**, 4065–4067 (2001). (page 6)

[13] Nikoobakht, B. & El-Sayed, M. A. Preparation and growth mechanism of gold nanorods (nrs) using seed-mediated growth method. *Chemistry of Materials* **15**, 1957–1962 (2003). (page 6)

[14] Millstone, J. E., Hurst, S. J., Métraux, G. S., Cutler, J. I. & Mirkin, C. A. Colloidal gold and silver triangular nanoprisms. *Small* **5**, 646–664 (2009). (page 6)

[15] Sun, Y. & Xia, Y. Shape-controlled synthesis of gold and silver nanoparticles. *Science* **298**, 2176–2179 (2002). (page 6)

[16] Murray, C., Norris, D. J. & Bawendi, M. G. Synthesis and characterization of nearly monodisperse cde (e= sulfur, selenium, tellurium) semiconductor nanocrystallites. *Journal of the American Chemical Society* **115**, 8706–8715 (1993). (page 6)

[17] Peng, X. *et al.* Shape control of cdse nanocrystals. *Nature* **404**, 59–61 (2000). (page 6)

[18] Manna, L., Scher, E. C. & Alivisatos, A. P. Synthesis of soluble and processable rod-, arrow-, teardrop-, and tetrapod-shaped cdse nanocrystals. *Journal of the American Chemical Society* **122**, 12700–12706 (2000). (page 6)

[19] Mie, G. Articles on the optical characteristics of turbid tubes, especially colloidal metal solutions. *Annalen der Physik* **25**, 377–445 (1908). (page 6)

[20] Lee, K.-S. & El-Sayed, M. A. Dependence of the enhanced optical scattering efficiency relative to that of absorption for gold metal nanorods on aspect ratio, size, end-cap shape, and medium refractive index. *The Journal of Physical Chemistry B* **109**, 20331–20338 (2005). (page 6)

[21] Jain, P. K., Lee, K. S., El-Sayed, I. H. & El-Sayed, M. A. Calculated absorption and scattering properties of gold nanoparticles of different size, shape, and composition: applications in biological imaging and biomedicine. *The Journal of Physical Chemistry B* **110**, 7238–7248 (2006). (page 6)

[22] De Abajo, F. G. Optical excitations in electron microscopy. *Reviews of Modern Physics* **82**, 209 (2010). (page 7)

[23] Govorov, A. O. *et al.* Gold nanoparticle ensembles as heaters and actuators: melting and collective plasmon resonances. *Nanoscale Research Letters* **1**, 84–90 (2006). (page 7)

[24] Govorov, A. O. & Richardson, H. H. Generating heat with metal nanoparticles. *Nano Today* **2**, 30–38 (2007). (page 7)

[25] Mirkin, C. A., Letsinger, R. L., Mucic, R. C., Storhoff, J. J. *et al.* A dna-based method for rationally assembling nanoparticles into macroscopic materials. *Nature* **382**, 607–609 (1996). (page 7, 8)

[26] Govorov, A. O. *et al.* Exciton-plasmon interaction and hybrid excitons in semiconductor-metal nanoparticle assemblies. *Nano Letters* **6**, 984–994 (2006). (page 7, 57)

[27] Zhang, W., Govorov, A. O. & Bryant, G. W. Semiconductor-metal nanoparticle molecules: Hybrid excitons and the nonlinear fano effect. *Physical Review Letters* **97**, 146804 (2006). (page 7, 57)

[28] Roller, E.-M., Argyropoulos, C., Högele, A., Liedl, T. & Pilo-Pais, M. Plasmon–exciton coupling using dna templates. *Nano Letters* **16**, 5962–5966 (2016). (page 7,

54, 57)

[29] Kühn, S., Håkanson, U., Rogobete, L. & Sandoghdar, V. Enhancement of single-molecule fluorescence using a gold nanoparticle as an optical nanoantenna. *Physical Review Letters* **97**, 017402 (2006). (page 7)

[30] Fan, Z. & Govorov, A. O. Plasmonic circular dichroism of chiral metal nanoparticle assemblies. *Nano Letters* **10**, 2580–2587 (2010). (page 7)

[31] Fan, Z. & Govorov, A. O. Helical metal nanoparticle assemblies with defects: plasmonic chirality and circular dichroism. *The Journal of Physical Chemistry C* **115**, 13254–13261 (2011). (page 7)

[32] Kuzyk, A. *et al.* Dna-based self-assembly of chiral plasmonic nanostructures with tailored optical response. *Nature* **483**, 311–314 (2012). (page 7, 18, 19, 25, 64)

[33] Grzelczak, M., Vermant, J., Furst, E. M. & Liz-Marzán, L. M. Directed self-assembly of nanoparticles. *ACS Nano* **4**, 3591–3605 (2010). (page 7, 8)

[34] Whitesides, G. M. & Grzybowski, B. Self-assembly at all scales. *Science* **295**, 2418–2421 (2002). (page 8)

[35] Sperling, R. A. & Parak, W. Surface modification, functionalization and bioconjugation of colloidal inorganic nanoparticles. *Philosophical Transactions of the Royal Society of London A: Mathematical, Physical and Engineering Sciences* **368**, 1333–1383 (2010). (page 8)

[36] Boles, M. A., Ling, D., Hyeon, T. & Talapin, D. V. The surface science of nanocrystals. *Nature Materials* **15**, 141–153 (2016). (page 8, 39)

[37] Nie, Z., Petukhova, A. & Kumacheva, E. Properties and emerging applications of self-assembled structures made from inorganic nanoparticles. *Nature Nanotechnology* **5**, 15–25 (2010). (page 8)

[38] Whitesides, G. M. & Boncheva, M. Beyond molecules: Self-assembly of mesoscopic and macroscopic components. *Proceedings of the National Academy of Sciences* **99**, 4769–4774 (2002). (page 8, 9)

[39] Nickel, B. & Liedl, T. Dna-linked superlattices get into shape. *Nature Materials* **14**, 746–749 (2015). (page 8)

[40] Rogers, W. B., Shih, W. M. & Manoharan, V. N. Using dna to program the self-assembly of colloidal nanoparticles and microparticles. *Nature Reviews Materials* **1**, 16008 (2016). (page 8)

[41] Boles, M. A., Engel, M. & Talapin, D. V. Self-assembly of colloidal nanocrystals: From intricate structures to functional materials. *Chemical Reviews* **116**, 11220–11289 (2016). (page 8)

[42] Alivisatos, A. P. *et al.* Organization of'nanocrystal molecules' using dna. *Nature* **382**, 609–611 (1996). (page 8)

[43] Park, S. Y. *et al.* Dna-programmable nanoparticle crystallization. *Nature* **451**, 553–556 (2008). (page 9, 11, 63, 77)

[44] Nykypanchuk, D., Maye, M. M., van der Lelie, D. & Gang, O. Dna-guided crystallization of colloidal nanoparticles. *Nature* **451**, 549–552 (2008). (page 9, 63, 77)

[45] Yager, K. G., Zhang, Y., Lu, F. & Gang, O. Periodic lattices of arbitrary nano-objects: modeling and applications for self-assembled systems. *Journal of Applied Crystallography* **47**, 118–129 (2014). (page 10, 75)

[46] Fischer, S. *et al.* Shape and interhelical spacing of dna origami nanostructures studied by small-angle x-ray scattering. *Nano Letters* **16**, 4282–4287 (2016). (page 10)

[47] Macfarlane, R. J. *et al.* Nanoparticle superlattice engineering with dna. *Science* **334**, 204–208 (2011). (page 10, 12)

[48] Jones, M. R. *et al.* Dna-nanoparticle superlattices formed from anisotropic building blocks. *Nature Materials* **9**, 913–917 (2010). (page 10)

[49] Auyeung, E. *et al.* Synthetically programmable nanoparticle superlattices using a hollow three-dimensional spacer approach. *Nature Nanotechnology* **7**, 24–28 (2012). (page 10)

[50] Zhang, C. *et al.* A general approach to dna-programmable atom equivalents. *Nature Materials* **12**, 741–746 (2013). (page 10)

[51] Auyeung, E. *et al.* Dna-mediated nanoparticle crystallization into wulff polyhedra. *Nature* **505**, 73–77 (2014). (page 10)

[52] Tian, Y. *et al.* Prescribed nanoparticle cluster architectures and low-dimensional arrays built using octahedral dna origami frames. *Nature Nanotechnology* **10**, 637–644 (2015). (page 10)

[53] Liu, W., Halverson, J., Tian, Y., Tkachenko, A. V. & Gang, O. Self-organized architectures from assorted dna-framed nanoparticles. *Nature Chemistry* **8**, 867–873 (2016). (page 10)

[54] Liu, W. *et al.* Diamond family of nanoparticle superlattices. *Science* **351**, 582–586 (2016). (page 10)

[55] Tian, Y. *et al.* Lattice engineering through nanoparticle-dna frameworks. *Nature Materials* **15**, 654–661 (2016). (page 10, 13)

[56] Jones, M. R., Seeman, N. C. & Mirkin, C. A. Programmable materials and the nature of the dna bond. *Science* **347**, 1260901 (2015). (page 10)

[57] Boal, A. K. *et al.* Self-assembly of nanoparticles into structured spherical and network aggregates. *Nature* **404**, 746–748 (2000). (page 10)

[58] Nie, Z. *et al.* Self-assembly of metal–polymer analogues of amphiphilic triblock copolymers. *Nature Materials* **6**, 609–614 (2007). (page 10)

[59] Liu, K. *et al.* Step-growth polymerization of inorganic nanoparticles. *Science* **329**, 197–200 (2010). (page 10)

[60] Tinoco, I., Sauer, K. & Wang, J. *Physical Chemistry: Principles and Applications in Biological Sciences* (Prentice-Hall, 1978). (page 14)

[61] Elkin, L. O. Rosalind franklin and the double helix. *Physics Today* **56**, 42–48 (2003).

(page 14)

[62] Franklin, R. E. & Gosling, R. G. Molecular configuration in sodium thymonucleate. *Nature* **171**, 740–741 (1953). (page 14)

[63] Wilkins, M. H. F., Stokes, A. R. & Wilson, H. R. Molecular structure of nucleic acids: molecular structure of deoxypentose nucleic acids. *Nature* **171**, 738–740 (1953). (page 14)

[64] Watson, J. D., Crick, F. H. *et al.* Molecular structure of nucleic acids. *Nature* **171**, 737–738 (1953). (page 14)

[65] Ho, P. S. & Carter, M. Dna structure: Alphabet soup for the cellular soul. In Seligmann, H. (ed.) *DNA Replication-Current Advances* (InTech, 2011). (page 14)

[66] Seeman, N. Nanotechnology and the double helix. *Scientific American* **290**, 64–75 (2004). (page 15)

[67] Seeman, N. C. Nucleic acid junctions and lattices. *Journal of Theoretical Biology* **99**, 237–247 (1982). (page 15)

[68] Seeman, N. C. Dna in a material world. *Nature* **421**, 427–431 (2003). (page 15)

[69] Ma, R.-I., Kallenbach, N. R., Sheardy, R. D., Petrillo, M. L. & Seeman, N. C. Three-arm nucleic acid junctions are flexible. *Nucleic Acids Research* **14**, 9745–9753 (1986). (page 15)

[70] Wang, Y., Mueller, J. E., Kemper, B. & Seeman, N. C. Assembly and characterization of five-arm and six-arm dna branched junctions. *Biochemistry* **30**, 5667–5674 (1991). (page 15)

[71] Fu, T. J. & Seeman, N. C. Dna double-crossover molecules. *Biochemistry* **32**, 3211–3220 (1993). (page 15)

[72] Chen, J. & Seeman, N. C. Synthesis from dna of a molecule with the connectivity of a cube. *Nature* **350**, 631–633 (1991). (page 15)

[73] Seeman, N. C. Dna engineering and its application to nanotechnology. *Trends in Biotechnology* **17**, 437–443 (1999). (page 15)

[74] Seeman, N. C. Biochemistry and structural dna nanotechnology: an evolving symbiotic relationship. *Biochemistry* **42**, 7259–7269 (2003). (page 15)

[75] Seeman, N. C. At the crossroads of chemistry, biology, and materials: structural dna nanotechnology. *Chemistry & Biology* **10**, 1151–1159 (2003). (page 15)

[76] Seeman, N. C. An overview of structural dna nanotechnology. *Molecular Biotechnology* **37**, 246–257 (2007). (page 15)

[77] Winfree, E., Liu, F., Wenzler, L. A. & Seeman, N. C. Design and self-assembly of two-dimensional dna crystals. *Nature* **394**, 539–544 (1998). (page 15, 16, 64)

[78] He, Y., Chen, Y., Liu, H., Ribbe, A. E. & Mao, C. Self-assembly of hexagonal dna two-dimensional (2d) arrays. *Journal of the American Chemical Society* **127**, 12202–12203 (2005). (page 15, 63)

[79] Rothemund, P. W. Folding dna to create nanoscale shapes and patterns. *Nature*

440, 297–302 (2006). (page 15, 16, 63)

[80] Douglas, S. M. *et al.* Self-assembly of dna into nanoscale three-dimensional shapes. *Nature* **459**, 414–418 (2009). (page 15, 16)

[81] Dietz, H., Douglas, S. M. & Shih, W. M. Folding dna into twisted and curved nanoscale shapes. *Science* **325**, 725–730 (2009). (page 15)

[82] Wei, B., Dai, M. & Yin, P. Complex shapes self-assembled from single-stranded dna tiles. *Nature* **485**, 623–626 (2012). (page 15, 16, 63)

[83] Sanderson, K. Bioengineering: What to make with dna origami. *Nature* **464**, 158 (2010). (page 16)

[84] Wagenbauer, K. F., Wachauf, C. H. & Dietz, H. Quantifying quality in dna self-assembly. *Nature Communications* **5** (2014). (page 16)

[85] Shih, W. M., Quispe, J. D. & Joyce, G. F. A 1.7-kilobase single-stranded dna that folds into a nanoscale octahedron. *Nature* **427**, 618–621 (2004). (page 16)

[86] Gerling, T., Wagenbauer, K. F., Neuner, A. M. & Dietz, H. Dynamic dna devices and assemblies formed by shape-complementary, non–base pairing 3d components. *Science* **347**, 1446–1452 (2015). (page 16, 17, 19, 64, 67)

[87] Kauert, D. J., Kurth, T., Liedl, T. & Seidel, R. Direct mechanical measurements reveal the material properties of three-dimensional dna origami. *Nano Letters* **11**, 5558–5563 (2011). (page 17, 33)

[88] Pfitzner, E. *et al.* Rigid dna beams for high-resolution single-molecule mechanics. *Angewandte Chemie International Edition* **52**, 7766–7771 (2013). (page 17)

[89] Douglas, S. M. *et al.* Rapid prototyping of 3d dna-origami shapes with cadnano. *Nucleic Acids Research* gkp436 (2009). (page 17)

[90] Castro, C. E. *et al.* A primer to scaffolded dna origami. *Nature Methods* **8**, 221–229 (2011). (page 17)

[91] Martin, T. G. & Dietz, H. Magnesium-free self-assembly of multi-layer dna objects. *Nature Communications* **3**, 1103 (2012). (page 17)

[92] Stahl, E., Martin, T. G., Praetorius, F. & Dietz, H. Facile and scalable preparation of pure and dense dna origami solutions. *Angewandte Chemie International Edition* **126**, 12949–12954 (2014). (page 17)

[93] Liu, W., Zhong, H., Wang, R. & Seeman, N. C. Crystalline two-dimensional dna-origami arrays. *Angewandte Chemie International Edition* **123**, 278–281 (2011). (page 17, 19, 64)

[94] Aghebat Rafat, A., Pirzer, T., Scheible, M. B., Kostina, A. & Simmel, F. C. Surface-assisted large-scale ordering of dna origami tiles. *Angewandte Chemie International Edition* **53**, 7665–7668 (2014). (page 17, 64)

[95] Ke, Y., Bellot, G., Voigt, N. V., Fradkov, E. & Shih, W. M. Two design strategies for enhancement of multilayer–dna-origami folding: underwinding for specific intercalator rescue and staple-break positioning. *Chemical Science* **3**, 2587–2597 (2012). (page 18)

[96] Zheng, J. *et al.* Two-dimensional nanoparticle arrays show the organizational power of robust dna motifs. *Nano Letters* **6**, 1502–1504 (2006). (page 18, 19)

[97] Sharma, J. *et al.* Control of self-assembly of dna tubules through integration of gold nanoparticles. *Science* **323**, 112–116 (2009). (page 18, 19)

[98] Ke, Y. *et al.* Dna brick crystals with prescribed depths. *Nature Chemistry* **6**, 994–1002 (2014). (page 18, 19)

[99] Zheng, J. *et al.* From molecular to macroscopic via the rational design of a self-assembled 3d dna crystal. *Nature* **461**, 74–77 (2009). (page 19, 64, 71, 75)

[100] Wang, P. *et al.* Programming self-assembly of dna origami honeycomb two-dimensional lattices and plasmonic metamaterials. *Journal of the American Chemical Society* **138**, 7733–7740 (2016). (page 19, 64)

[101] Jungmann, R. *et al.* Single-molecule kinetics and super-resolution microscopy by fluorescence imaging of transient binding on dna origami. *Nano Letters* **10**, 4756–4761 (2010). (page 18)

[102] Bell, N. A. *et al.* Dna origami nanopores. *Nano Letters* **12**, 512–517 (2011). (page 18)

[103] Wei, R., Martin, T. G., Rant, U. & Dietz, H. Dna origami gatekeepers for solid-state nanopores. *Angewandte Chemie International Edition* **124**, 4948–4951 (2012). (page 18)

[104] Langecker, M. *et al.* Synthetic lipid membrane channels formed by designed dna nanostructures. *Science* **338**, 932–936 (2012). (page 18)

[105] Nickels, P. C. *et al.* Molecular force spectroscopy with a dna origami–based nanoscopic force clamp. *Science* **354**, 305–307 (2016). (page 18)

[106] Douglas, S. M., Bachelet, I. & Church, G. M. A logic-gated nanorobot for targeted transport of molecular payloads. *Science* **335**, 831–834 (2012). (page 18)

[107] Schreiber, R. *et al.* Hierarchical assembly of metal nanoparticles, quantum dots and organic dyes using dna origami scaffolds. *Nature Nanotechnology* **9**, 74–78 (2014). (page 19, 25, 61, 75)

[108] Woo, S. & Rothemund, P. W. Programmable molecular recognition based on the geometry of dna nanostructures. *Nature Chemistry* **3**, 620–627 (2011). (page 19)

[109] Jungmann, R. *et al.* Dna origami-based nanoribbons: assembly, length distribution, and twist. *Nanotechnology* **22**, 275301 (2011). (page 19)

[110] Moloney, M. P., Govan, J., Loudon, A., Mukhina, M. & Gun'ko, Y. K. Preparation of chiral quantum dots. *Nature Protocols* **10**, 558–573 (2015). (page 21)

[111] Gopinath, A., Miyazono, E., Faraon, A. & Rothemund, P. W. Engineering and mapping nanocavity emission via precision placement of dna origami. *Nature* **535**, 401–405 (2016). (page 22)

[112] Jin, Z. *et al.* Metallized dna nanolithography for encoding and transferring spatial information for graphene patterning. *Nature Communications* **4**, 1663 (2013). (page 22)

[113] Chang, D. E., Sørensen, A. S., Demler, E. A. & Lukin, M. D. A single-photon transistor using nanoscale surface plasmons. *Nature Physics* **3**, 807–812 (2007). (page 25)

[114] Awschalom, D. D., Epstein, R. & Hanson, R. The diamond age diamond age of spintronics. *Scientific American* **297**, 84–91 (2007). (page 26)

[115] Balasubramanian, G. *et al.* Nanoscale imaging magnetometry with diamond spins under ambient conditions. *Nature* **455**, 648–651 (2008). (page 26)

[116] Schietinger, S., Barth, M., Aichele, T. & Benson, O. Plasmon-enhanced single photon emission from a nanoassembled metal- diamond hybrid structure at room temperature. *Nano Letters* **9**, 1694–1698 (2009). (page 26)

[117] Dolde, F. *et al.* Room-temperature entanglement between single defect spins in diamond. *Nature Physics* **9**, 139–143 (2013). (page 26, 27)

[118] Krueger, A. The structure and reactivity of nanoscale diamond. *Journal of Materials Chemistry* **18**, 1485–1492 (2008). (page 26)

[119] Zaitsev, A. Vibronic spectra of impurity-related optical centers in diamond. *Physical Review B* **61**, 12909 (2000). (page 26)

[120] Aharonovich, I., Greentree, A. D. & Prawer, S. Diamond photonics. *Nature Photonics* **5**, 397–405 (2011). (page 27)

[121] Baidakova, M. *et al.* New prospects and frontiers of nanodiamond clusters. *Journal of Physics D: Applied Physics* **40**, 6300–6311 (2007). (page 27)

[122] Ōsawa, E. Monodisperse single nanodiamond particulates. *Pure and Applied Chemistry* **80**, 1365–1379 (2008). (page 27)

[123] Ho, D. Beyond the sparkle: the impact of nanodiamonds as biolabeling and therapeutic agents. *ACS Nano* **3**, 3825–3829 (2009). (page 27)

[124] Mochalin, V. N., Shenderova, O., Ho, D. & Gogotsi, Y. The properties and applications of nanodiamonds. *Nature Nanotechnology* **7**, 11–23 (2012). (page 27, 28)

[125] Wenmackers, S. *et al.* Diamond-based dna sensors: surface functionalization and read-out strategies. *Physica Status Solidi (a)* **206**, 391–408 (2009). (page 27)

[126] Takahashi, K., Tanga, M., Takai, O. & Okamura, H. Dna preservation using diamond chips. *Diamond and Related Materials* **12**, 572–576 (2003). (page 27)

[127] Yang, W. *et al.* Dna-modified nanocrystalline diamond thin-films as stable, biologically active substrates. *Nature Materials* **1**, 253–257 (2002). (page 27)

[128] Knickerbocker, T. *et al.* Dna-modified diamond surfaces. *Langmuir* **19**, 1938–1942 (2003). (page 27)

[129] Ushizawa, K. *et al.* Covalent immobilization of dna on diamond and its verification by diffuse reflectance infrared spectroscopy. *Chemical Physics Letters* **351**, 105–108 (2002). (page 28)

[130] Huang, L.-C. L. & Chang, H.-C. Adsorption and immobilization of cytochrome c on nanodiamonds. *Langmuir* **20**, 5879–5884 (2004). (page 28)

[131] Kong, X., Huang, L. L., Liau, S.-C. V., Han, C.-C. & Chang, H.-C. Polylysine-coated diamond nanocrystals for maldi-tof mass analysis of dna oligonucleotides. *Analytical Chemistry* **77**, 4273–4277 (2005). (page 28)

[132] Krüger, A., Liang, Y., Jarre, G. & Stegk, J. Surface functionalisation of detonation diamond suitable for biological applications. *Journal of Materials Chemistry* **16**, 2322–2328 (2006). (page 28)

[133] Khachatryan, A. K. *et al.* Graphite-to-diamond transformation induced by ultrasound cavitation. *Diamond and Related Materials* **17**, 931–936 (2008). (page 30)

[134] Zhang, T. *et al.* Dna-based self-assembly of fluorescent nanodiamonds. *Journal of the American Chemical Society* **137**, 9776–9779 (2015). (page 35)

[135] Smith, A. M. & Nie, S. Chemical analysis and cellular imaging with quantum dots. *Analyst* **129**, 672–677 (2004). (page 37)

[136] Brus, L. Electronic wave functions in semiconductor clusters: experiment and theory. *The Journal of Physical Chemistry* **90**, 2555–2560 (1986). (page 37)

[137] Marzin, J.-Y., Gérard, J.-M., Izraël, A., Barrier, D. & Bastard, G. Photoluminescence of single inas quantum dots obtained by self-organized growth on gaas. *Physical Review Letters* **73**, 716 (1994). (page 38)

[138] Smith, A. M. & Nie, S. Semiconductor nanocrystals: structure, properties, and band gap engineering. *Accounts of Chemical Research* **43**, 190–200 (2009). (page 38)

[139] Govorov, A. Spin and energy transfer in nanocrystals without tunneling. *Physical Review B* **68**, 075315 (2003). (page 38)

[140] Kagan, C., Murray, C., Nirmal, M. & Bawendi, M. Electronic energy transfer in cdse quantum dot solids. *Physical Review Letters* **76**, 1517 (1996). (page 38, 48)

[141] Lan, X., Masala, S., Sargent, E. H. *et al.* Charge-extraction strategies for colloidal quantum dot photovoltaics. *Nature Materials* **13**, 233–240 (2014). (page 38)

[142] Gross, M. & Haroche, S. Superradiance: An essay on the theory of collective spontaneous emission. *Physics Reports* **93**, 301–396 (1982). (page 38)

[143] O'Brien, J. L. Optical quantum computing. *Science* **318**, 1567–1570 (2007). (page 38)

[144] Kagan, C. R. & Murray, C. B. Charge transport in strongly coupled quantum dot solids. *Nature Nanotechnology* **10**, 1013–1026 (2015). (page 39)

[145] Murray, C. B., Kagan, C. & Bawendi, M. Synthesis and characterization of monodisperse nanocrystals and close-packed nanocrystal assemblies. *Annual Review of Materials Science* **30**, 545–610 (2000). (page 39)

[146] Deng, Z., Samanta, A., Nangreave, J., Yan, H. & Liu, Y. Robust dna-functionalized core/shell quantum dots with fluorescent emission spanning from uv–vis to near-ir and compatible with dna-directed self-assembly. *Journal of the American Chemical Society* **134**, 17424–17427 (2012). (page 39, 40, 44, 45)

[147] Green, M. The nature of quantum dot capping ligands. *Journal of Materials Chemistry* **20**, 5797–5809 (2010). (page 39)

[148] Freeman, R., Liu, X. & Willner, I. Chemiluminescent and chemiluminescence resonance energy transfer (cret) detection of dna, metal ions, and aptamer–substrate complexes using hemin/g-quadruplexes and cdse/zns quantum dots. *Journal of the American Chemical Society* **133**, 11597–11604 (2011). (page 40)

[149] Lees, E. E., Nguyen, T.-L., Clayton, A. H. & Mulvaney, P. The preparation of colloidally stable, water-soluble, biocompatible, semiconductor nanocrystals with a small hydrodynamic diameter. *ACS Nano* **3**, 1121–1128 (2009). (page 43)

[150] Pellegrino, T. *et al.* Hydrophobic nanocrystals coated with an amphiphilic polymer shell: a general route to water soluble nanocrystals. *Nano Letters* **4**, 703–707 (2004). (page 43)

[151] Lin, C.-A. J. *et al.* Design of an amphiphilic polymer for nanoparticle coating and functionalization. *Small* **4**, 334–341 (2008). (page 43)

[152] Uyeda, H. T., Medintz, I. L., Jaiswal, J. K., Simon, S. M. & Mattoussi, H. Synthesis of compact multidentate ligands to prepare stable hydrophilic quantum dot fluorophores. *Journal of the American Chemical Society* **127**, 3870–3878 (2005). (page 44)

[153] Medintz, I. L., Uyeda, H. T., Goldman, E. R. & Mattoussi, H. Quantum dot bioconjugates for imaging, labelling and sensing. *Nature Materials* **4**, 435–446 (2005). (page 44)

[154] Levina, L. *et al.* Efficient infrared-emitting pbs quantum dots grown on dna and stable in aqueous solution and blood plasma. *Advanced Materials* **17**, 1854–1857 (2005). (page 44)

[155] Tikhomirov, G. *et al.* Dna-based programming of quantum dot valency, self-assembly and luminescence. *Nature Nanotechnology* **6**, 485–490 (2011). (page 44, 50)

[156] Albertorio, F., Hughes, M. E., Golovchenko, J. A. & Branton, D. Base dependent dna–carbon nanotube interactions: activation enthalpies and assembly–disassembly control. *Nanotechnology* **20**, 395101 (2009). (page 50)

[157] Pei, H. *et al.* Designed diblock oligonucleotide for the synthesis of spatially isolated and highly hybridizable functionalization of dna–gold nanoparticle nanoconjugates. *Journal of the American Chemical Society* **134**, 11876–11879 (2012). (page 50)

[158] Wang, Z., Tang, L., Tan, L. H., Li, J. & Lu, Y. Discovery of the dna genetic code for abiological gold nanoparticle morphologies. *Angewandte Chemie International Edition* **51**, 9078–9082 (2012). (page 50)

[159] Hinds, S. *et al.* Nucleotide-directed growth of semiconductor nanocrystals. *Journal of the American Chemical Society* **128**, 64–65 (2006). (page 50)

[160] Sigel, R. K. & Sigel, H. A stability concept for metal ion coordination to single-stranded nucleic acids and affinities of individual sites. *Accounts of Chemical Research* **43**, 974–984 (2010). (page 52)

[161] Jain, P. K. & El-Sayed, M. A. Plasmonic coupling in noble metal nanostructures. *Chemical Physics Letters* **487**, 153–164 (2010). (page 53)

[162] Ghosh, S. K. & Pal, T. Interparticle coupling effect on the surface plasmon resonance of gold nanoparticles: from theory to applications. *Chemical Reviews* **107**, 4797–4862 (2007). (page 53)

[163] Prodan, E., Radloff, C., Halas, N. J. & Nordlander, P. A hybridization model for the plasmon response of complex nanostructures. *Science* **302**, 419–422 (2003). (page 53, 54)

[164] Sheikholeslami, S., Jun, Y.-w., Jain, P. K. & Alivisatos, A. P. Coupling of optical resonances in a compositionally asymmetric plasmonic nanoparticle dimer. *Nano Letters* **10**, 2655–2660 (2010). (page 54)

[165] Chen, H. *et al.* Plasmon–molecule interactions. *Nano Today* **5**, 494–505 (2010). (page 54)

[166] Misiunas, K., Pagliara, S., Lauga, E., Lister, J. R. & Keyser, U. F. Nondecaying hydrodynamic interactions along narrow channels. *Physical Review Letters* **115**, 038301 (2015). (page 55)

[167] Bell, N. A. & Keyser, U. F. Digitally encoded dna nanostructures for multiplexed, single-molecule protein sensing with nanopores. *Nature Nanotechnology* **11**, 645–651 (2016). (page 55)

[168] Branton, D. *et al.* The potential and challenges of nanopore sequencing. *Nature Biotechnology* **26**, 1146–1153 (2008). (page 55)

[169] Keyser, U. F. *et al.* Direct force measurements on dna in a solid-state nanopore. *Nature Physics* **2**, 473–477 (2006). (page 55)

[170] Thacker, V. V. *et al.* Dna origami based assembly of gold nanoparticle dimers for surface-enhanced raman scattering. *Nature Communications* **5**, 3448 (2014). (page 56)

[171] Kühler, P. *et al.* Plasmonic dna-origami nanoantennas for surface-enhanced raman spectroscopy. *Nano Letters* **14**, 2914–2919 (2014). (page 58, 60)

[172] Kalsin, A. M. *et al.* Electrostatic self-assembly of binary nanoparticle crystals with a diamond-like lattice. *Science* **312**, 420–424 (2006). (page 63)

[173] Kostiainen, M. A. *et al.* Electrostatic assembly of binary nanoparticle superlattices using protein cages. *Nature Nanotechnology* **8**, 52–56 (2013). (page 63)

[174] Benson, E. *et al.* Dna rendering of polyhedral meshes at the nanoscale. *Nature* **523**, 441–444 (2015). (page 63)

[175] Ke, Y., Ong, L. L., Shih, W. M. & Yin, P. Three-dimensional structures self-assembled from dna bricks. *science* **338**, 1177–1183 (2012). (page 63, 64)

[176] Maune, H. T. *et al.* Self-assembly of carbon nanotubes into two-dimensional geometries using dna origami templates. *Nature Nanotechnology* **5**, 61–66 (2010). (page 64)

[177] Fu, Y. *et al.* Single-step rapid assembly of dna origami nanostructures for addressable nanoscale bioreactors. *Journal of the American Chemical Society* **135**, 696–702 (2012). (page 64)

[178] He, Y. *et al.* Hierarchical self-assembly of dna into symmetric supramolecular polyhedra. *Nature* **452**, 198–201 (2008). (page 64)

[179] Wang, T. *et al.* A dna crystal designed to contain two molecules per asymmetric unit. *Journal of the American Chemical Society* **132**, 15471–15473 (2010). (page 64)

[180] Simmons, C. R. *et al.* Construction and structure determination of a three-dimensional dna crystal. *Journal of the American Chemical Society* **138**, 10047–10054 (2016). (page 64)

[181] Stahl, E., Praetorius, F., de Oliveira Mann, C. C., Hopfner, K.-P. & Dietz, H. Impact of heterogeneity and lattice bond strength on dna triangle crystal growth. *ACS Nano* **10**, 9156–9164 (2016). (page 64)

[182] Liu, N. *et al.* Three-dimensional photonic metamaterials at optical frequencies. *Nature Materials* **7**, 31–37 (2008). (page 77)

[183] Tørring, T., Voigt, N. V., Nangreave, J., Yan, H. & Gothelf, K. V. Dna origami: a quantum leap for self-assembly of complex structures. *Chemical Society Reviews* **40**, 5636–5646 (2011). (page 86)

[184] Nielsen, P. E., Egholm, M., Berg, R. H. & Buchardt, O. Sequence-selective recognition of dna by strand displacement with a thymine-substituted polyamide. *Science* **254**, 1497–1500 (1991). (page 86)

[185] Koshkin, A. A. *et al.* Lna (locked nucleic acids): Synthesis of the adenine, cytosine, guanine, 5-methylcytosine, thymine and uracil bicyclonucleoside monomers, oligomerisation, and unprecedented nucleic acid recognition. *Tetrahedron* **54**, 3607–3630 (1998). (page 86)

[186] Kuhlman, B. *et al.* Design of a novel globular protein fold with atomic-level accuracy. *Science* **302**, 1364–1368 (2003). (page 86)

[187] Das, R. & Baker, D. Macromolecular modeling with rosetta. *Annual Review of Biochemistry* **77**, 363–382 (2008). (page 86)

Acknowledgement

The most important thanks go to Tim Liedl, for taking me as PhD student, for creating a great lab atmosphere for us, for giving me chances to visit other labs and join academic conferences, for your mentoring, encouragement, and insightful advices, and for the freedom you gave me to pursue my own ideas. Thank you, Tim!

Thanks to all the Liedl group members. I will just list all your names: Alex Maier, Alina Fedorchuk, Amelie Heuer-Jungemann, C**a**roline Hartl, Christoph Schneider, Daniel Schiffels, David Smith, Eva-Maria Roller, Francesca Nicoli, Iain MacPherson, Kevin Martens, Linh Nguyen, Luisa Kneer, Luzia Kilwing, Marina Polo, Mauricio Pilo-Pais, Philipp Nickels, Robert Schreiber, Samet Kocabey, Stephanie Simmel, Susanne Kempter, Thomas Zettl, Timon Funck, Verena Schüller, Wooli Bae, and Yongzheng Xing. I just realized that I have stayed so long in the group and have overlap with so far all the Liedlers. It was my great fortune to join you. I want to say our lab is the best. I love you all and sure will miss you all!

Thanks to all collaborators, Tanja Weil group, Ulrich Keyser group, and Fedor Jelezko group. Special thanks to my second supervisor Alexander Högele, and to Andre Neumann and Jessica Lindlau. Special thanks to Bert Nickel, Stefan Fischer, and Kilian Frank. Thanks for all your great support to successfully complete our projects together!

Thanks to Prof. Rädler and all Lehrstuhl Rädlers. Our chair has an unique environment that I would never experience if not coming to Germany. The chair events such as winter school, hiking, and Christmas parties helped me to quickly integrate into German life. Thank you!

Thanks to BIOMOD 'DNA Diamonds' team members: Florian Schüder, Sebastian Huber, Marinus Huber, Florian Stehr, and Milena Mayer. Thanks for your great work and we can win the BIOMOD grand prize of 2013!

Thanks to Miao Li, Qi Hu, Lizhi Liu, Hsin-Yi Chiu. Thanks to all members in Munich DNA node labs and CeNS. I enjoyed the time we spent together and have learned a lot from you.

I sincerely thank my parents. Thanks for all your support and love so I can finish my

doctor studies.

Special thanks to my thesis committee members. Your discussion, ideas, and feedback will be absolutely invaluable.

List of Publications

Tao Zhang, Caroline Hartl, Stefan Fischer, Kilian Frank, Philipp Nickels, Amelie Heuer-Jungemann, Bert Nickel*, Tim Liedl*
Nanoparticles Co-Crystalization in 3D DNA Origami Lattices.
to be submitted.

Tao Zhang, Andre Neumann, Jessica Lindlau, Yuzhou Wu, Goutam Pramanik, Boris Naydenov, Fedor Jelezko, Florian Schüder, Sebastian Huber, Marinus Huber, Florian Stehr, Alexander Högele*, Tanja Weil*, Tim Liedl*
DNA-based self-assembly of fluorescent nanodiamonds.
J. Am. Chem. Soc. **2015**, *137*, 9776-9779.

Vivek V. Thacker†, Lars O. Herrmann†, Daniel O. Sigle, Tao Zhang, Tim Liedl, Jeremy J. Baumberg, Ulrich F. Keyser*
DNA origami based assembly of gold nanoparticle dimers for surface-enhanced Raman scattering.
Nature Commun. **2014**, *5*, Article number: 3448.

Robert Schreiber†, Jaekwon Do†, Eva-Maria Roller, Tao Zhang, Verena Schueller, Philipp Nickels, Jochen Feldmann, and Tim Liedl*
Hierarchical assembly of metal nanoparticles, quantum dots and organic dyes using DNA origami scaffolds.
Nature Nanotech. **2014**, *9*, 74-78.

Robert Schreiber, Ngoc Luong, Zhiyuan Fan, Anton Kuzyk, Philipp Nickels, Tao Zhang, David Smith, Bernard Yurke, Wan Kuang, Alexander Govorov, and Tim Liedl*
Chiral plasmonic DNA nanostructures with switchable circular dichroism.
Nature Commun. **2013**, *4*, Article number: 2948.

†These authors contributed equally to this work.